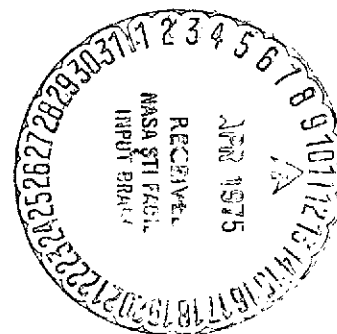MSC-05546

SKYLAB PROGRAM

EARTH RESOURCES EXPERIMENT PACKAGE

SENSOR PERFORMANCE EVALUATION
FINAL REPORT
VOLUME IV (S193 R/S)

JANUARY 2, 1975

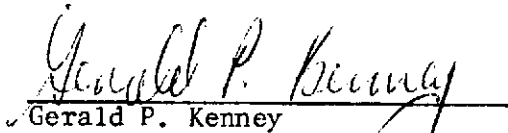CONTRACT NAS8-24000

AMENDMENT JSC-14S

National Aeronautics and Space Administration
LYNDON B. JOHNSON SPACE CENTER
Houston, Texas

MSC-05546
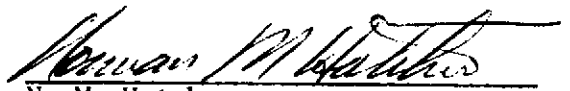
EARTH RESOURCES EXPERIMENT PACKAGE

SENSOR PERFORMANCE REPORT
VOL. IV (S193 R/S)
(SL2, SL3 AND SL4 EVALUATIONS)

January 2, 1975
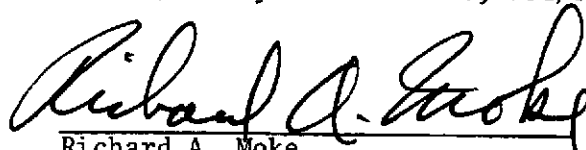
Submitted by: _____
　Gerald P. Kenney
Skylab/EREP Sensor Performance
Evaluation Manager, JSC/HC

Technical
Review By: _____
N. M. Hatcher
S193 R/S Project Scientist, JSC/TF

Approved: _____
Richard A. Moke
Manager, Systems Analysis and
Integration Office, JSC/HC

FOREWORD

This volume is Section IV of six sections of document MSC-05546, submitted by Martin Marietta Corporation, in accordance with the requirements of Annex I to Exhibit A, Statement of Work, Part I, Data Requirements List, of Contract NAS8-24000, Amendment JSC-14S, Line Item 295, and was prepared under WBS 02216.

CONTENTS

1. INTRODUCTION

1.1 Purpose

This document reports the final results of the sensor performance evaluation of the Skylab Earth Resources Experiment Package (EREP) S193 radiometer/scatterometer and is based on data and evaluations reported in the interim performance evaluation report (MSC-05528, Volume IV, dated October 30, 1974).

1.2 Scope

This document summarizes the results of the S193 radiometer/ scatterometer sensor performance evaluation based on data presented by Martin Marietta and the University of Kansas to the sensor performance evaluation interim reports, provides the results of additional analyses of S193 radiometer/scatterometer performance, and describes techniques used in sensor performance evaluation (Appendix A). The summarization includes significant performance degradation identified during the Skylab missions, and the performance achieved, in terms of pertinent S193 radiometer/scatterometer parameters. The additional analyses include final performance analyses completed after submittal of the SL4 interim sensor performance evaluation reports, including completion of detailed analyses of basic performance parameters initiated during the interim report periods. One item was added to this volume in an update to the format comments previously published in the SL4 interim report (MSC-05528, Appendix B). This paragraph was included because of its summary nature and its usefulness to users of the S193 radiometer/scatterometer sensor data.

1.3 Usage Guide

The basic task outline for the EREP sensor performance evaluation was specified EREP Mission Data Evaluation Requirements, JSC-05529, August 31, 1973. The results of these evaluations were subsequently reported in MSC-05528, Earth Resources Experiment Package, Sensor Performance Report, Volumes I through VII, as follows:

Volume I (S190A)	Multispectral Photographic Camera
Volume II (S191)	IR Spectrometer
Volume III (S192)	Multispectral Scanner
Volume IV (S193 R/S)	Radiometer/Scatterometer
Volume V (S193 Alt.)	Altimeter
Volume VI (S194)	L-Band Radiometer
Volume VII (S190B)	Earth Terrain Camera

Section 2 of this report is a list of reference documents used in the sensor performance evaluation (SPE). For reader convenience, reference citations in the body of the report are in the form of explicit footnotes.

Section 3 parallels the organization of the interim reports. Paragraphs 3.1 through 3.14 of this volume correspond, in sequence, to paragraphs 3 through 16 of MSC-05528, Volume IV. The number of the SPE task to which each paragraph responds is noted, and the contributors responsible for performance of each task are identified. The material in Section 3 summarizes the efforts described in the interim reports; therefore, frequent references direct the reader to paragraphs in the interim reports that are the sources of supplementary details.

Analyses of the three major radiometer/scatterometer anomalies, and the resulting effects on sensor performance, are presented in Section 4. Also reported in this section are the results of investigations conducted to supplement the basic efforts performed in accordance with the SPE task definitions, and analyses not completed in time for inclusion in the interim reports.

Section 5 is a summary of the results of the SPE investigations. Sensor characteristic values developed by the SPE efforts are tabulated in this section.

Conclusions drawn from the overall effort are presented in Section 6, and include those relating to the sensor design and performance, preflight calibration and testing, the SPE effort, and the provision of ground truth data.

Recommendations are listed in Section 7 for improving the usefulness of a next-generation radiometer/scatterometer. The recommendations flow logically from the conclusions stated in Section 6.

Appendix A reports details of analytical techniques developed specifically for application in the SPE tasks. The theoretical basis and application methods are described for each technique.

1.4 Abstract

This report presents the results of the sensor performance evaluation (SPE) of the 13.9 GHz radiometer/scatterometer, which

was part of the Earth Resources Experiment Package on Skylab. Agencies participating in the evaluation were the University of Kansas Space Technology Center, and the Denver Division of the Martin Marietta Corporation. Findings are presented in the areas of housekeeping parameters, antenna gain and scanning performance, dynamic range, linearity, precision, resolution, stability, integration time, and transmitter output. Supplementary analyses covering performance anomalies, data stream peculiarities, aircraft sensor data comparisons, scatterometer saturation characteristics, and RF heating effects are reported.

Results of the evaluation show that instrument performance was generally as expected, but capability degradations were observed to result from three major anomalies. Conclusions are drawn from the evaluation results, and recommendations for improving the effectiveness of a future program are offered. An addendum describes the special evaluation techniques developed and applied in the sensor performance evaluation tasks.

2.   APPLICABLE DOCUMENTS

MSC-05528   Earth Resources Experiment Package,
                                    Sensor Performance Report,
                                    (Engineering Baseline, SL2, SL3,   .
                                    and SL4 Evaluation), Volumes I
                                    through VII, July 1973 through
                                    October 1974. Volume IV, S193
                                    Radiometer/Scatterometer,
                                    30 October 1974; Volume V, S193
                                    Altimeter, 6 September 1974; Volume
                                    VI, S194 Radiometer, 6 September 1974,
                                    Lyndon B. Johnson Space Center,
                                    Houston, Texas.

72SD4234   S193 Historical Logbook, Volume 1A,
                                    Rev. A, S193 Vehicle 001, General
                                    Electric, 27 October 1972.

                                    Alternate Designation: 72SD4207,
                                    Rev. D, S193 Calibration Data
                                    Report, Flight Hardware - Prime
                                    Unit 1A, Volume 1A, General Electric -
                                    SSO, Contract NAS9-11195, 22 March
                                    1973.

MSC-07744   Skylab Instrumentation Calibration
                                    Data Book, Volume IV (EREP), Section
                                    5, Skylab Mission SL1, Rev. B, Lyndon
                                    B. Johnson Space Center, Houston,
                                    Texas, August 1973, Change Notice 3,
                                    November 1974.

                                    S193 Flight Hardware Operating
                                    Maintenance and Handling Procedures,
                                    Volume II, Mission Operational
                                    Procedures, General Electric – SSO,
                                    Contract NAS9-11195, S193-OMHP-002,
                                    Revision E, incorporating Change 1
                                    dated 14 March 1973.

72SD4234   S193 Historical Log Book, Volume 2,
                                    S193 Vehicle 001, General Electric-
                                    SSO, VSFC, 8 August 1972.

                                    Alternate Designation: Specification
                                    No. SVS7846, Rev. C, Flight Hardware
                                    Configuration Specification, Contract
                                    NAS9-11195, 27 April 1972.   .

Lee S. Miller and Donald L. Hammond,
"Objectives and Capabilities of the
Skylab S193 Altimeter Experiment",
IEEE TRANSACTIONS ON GEOSCIENCE
ELECTRONICS, Volume GE 10, Number 1,
January 1972, pp 73-79.

S193 Microwave Radiometer/Scatterometer
Altimeter Preliminary Design Review
Technical Reports, Volume V - Book 1
and Book 2, General Electric - SSO
Contract NAS9-11195 and 6, 7 October
1970.

TMX-64826   MSFC Skylab Contamination Control
Systems Mission Evaluation, Rev. B,
George C. Marshall Spaceflight
Center, May 1974.

PHO-TR524   Earth Resources Production Processing
Requirements for EREP Electronic
Sensors, Rev A, Change 2, Lyndon B.
Johnson Space Center, Houston, Texas,
18 October 1974.

A. Sobti, A Simulation Study of the
S193 Rad Scat in Orbit, The University
of Kansas Space Technology Laboratories,
CRES Tech. Report 190-2, May 1973.

3. SUMMARY OF SENSOR PERFORMANCE EVALUATION INTERIM REPORT

This section summarizes the results of baseline testing through the SL4 mission as reported in Volume IV of MSC-05528, (October 30, 1974, SL4 update).

The summary is organized at the major paragraph level to correspond with the sensor performance evaluation task identifications. Sections of MSC-05528 that contained redundant evaluations have been consolidated. To provide traceability, applicable paragraphs in MSC-05528 are referenced in the summary.

3.1 Function/Limit Verification (SPE-S193-001)

The general integrity of the S193 radiometer/scatterometer was evaluated by an analysis of mode sequencing, engineering parameters, gimbal position, internal calibration, and malfunction diagnostic data, as well as a review of comments made by the EREP control and display panel operator during the Skylab missions.

3.1.1 Malfunctions

There were several diagnostics monitors provided on the EREP control and display panel to allow the EREP operator to make a quick analysis of S193 operation. These monitors also appeared as bilevel (on-off) indicators in the S193 data. The diagnostic monitors were:

1) Radiometer ready;

2) Scatterometer ready;

3) Altimeter ready;

4) Transmitter overheat

5) Transmitter malfunction;

6) Receiver overheat;

7) Receiver malfunction;

8) Gimbal malfunction;

9) Altimeter unlock.

The monitors gave visual indications to the operator that
S193 was ready to take data or that there was a problem with the
instrument. For instance, the ready indicators would light up
when the power switch(s) were placed in the ON position for the
particular mode of operation desired (Rad, Scat, Rad/Scat, or
Alt) and the appropriate time delays in the S193 had elapsed.
The malfunction, overheat, and unlock indicators would light up
if there were abnormal operation. A malfunction was defined as
an unexpected indication on one of these monitors. Therefore,
if a ready indicator did not light up when the proper power
switch was turned on or a malfunction or overheat indicator did
light up, a malfunction was indicated. In addition to mal-
functions defined here, the S193 experienced anomalous operation
in which the data indicated performance that did not agree with
expectations. Anomalous operation is considered separately from
malfunction indication in this report.

In addition to the light displays, several S193 voltages
were displayed on control and display panel meters for performance
verification. All diagnostic monitors gave the indications that
were expected as a result of switch operation or known anomalous
Rad/Scat operation throughout the Skylab missions. During EREP
passes 1, 53, and 56, the transmitter malfunction light was on
because the scatterometer power switch was placed in the ON
position before the scatterometer timer had "timed out." This
timer was actuated by placing the power switch in the STANDBY
position, and its purpose was to prevent full power being applied
to the scatterometer transmitter before it had been allowed
sufficient time to warm up. Both the receiver and transmitter
malfunction lights were on after the anomaly occurred in EREP
pass 40 when the -10-volt reference power supply went to a very
low output voltage due to a short (See Paragraph 4.1) in the
pitch gimbal potentiometer and the gimbals went to approximately
+50 degrees in both the pitch and roll axes.

3.1.2 Sequencing

The Rad/Scat had several modes of operation that were
determined by the position of the mode and scan mode selector
switches on the EREP control and display panel. The modes were
Rad Only, Scat Only, and Rad/Scat. The scan modes were in-track
contiguous (ITC), in-track noncontiguous (ITNC), cross-track
noncontiguous left (CTNC-L), cross-track noncontiguous right
(CTNC-R), cross-track noncontiguous left and right (CTNC-L/R),
and cross-track contiguous (CTC). Although it was physically

possible to have the mode and scan mode selectors positioned
to obtain any of these mode and scan mode combinations, CTC
was the only scan mode that was valid in Rad Only or Scat Only.
All scan modes were valid in Rad/Scat. Each of these valid
mode and scan mode combinations had its own individual sequence
of operation. The prescribed sequencing for each valid mode
and scan mode is shown in detail in the G.E. Calibration Data
Report*.

The analysis to determine that the Rad/Scat was sequencing
according to the requirements of the particular mode and scan
mode during a data-taking period was accomplished in three
steps. The first step was to confirm that the Rad/Scat was
operating in the mode, scan mode, and polarization selected on
the EREP control and display panel for the specific flight
data-taking periods. The second step was to confirm that the
instrument was sequencing as specified* for the scan mode
selected. The third step was to check the Scat amplifier gain
and Scat bandpass filter/integrator readings to confirm their
operation. The Rad/Scat sequencing was in accordance with
the requirements specified* for all modes of operations through-
out the Skylab missions with the following exceptions.

1) There was a recurrent error at KSC and throughout the
Skylab missions in the Rad/Scat CTC mode of operation. The
first of a pair of readings in the CTC mode would give the
command angle and Scat gain readings of the previous pair.
Once a sequencing error occurred, an erroneous reading would
recur every 159 seconds thereafter during that data-taking run.
This recurrent erroneous reading for angle and gain was traced
to a logic race condition and the erroneous data can be
identified.

2) A recurrent logic race error was detected after the
SL4 mission, which caused an error in the CTNC mode sequencing
readout similar to that in the CTC mode. This is discussed in
paragraph 4.4. Processing of the S193 scatterometer data is

---

* S193 Historical Logbook, S193 Vehicle 001, Vol 1A, Document
No. 72 SD4234 Rev. A, 27 October 1972, General Electric
Company, p 1-1 through 1-12.

Alternate Designation: S193 Calibration Data Report, Flight
Hardware, Doc. No. 72 SD4207 Rev. D, 22 March 1973, Prime
Unit 1A Volume 1A, SSO Contract NAS9-11195, General Electric.

such that backscatter data that would be in error by the erroneous gain readout has been deleted from the processed output products. Because the gain error is in increments of 10 dB, the correct values can be retrieved from the raw S193 data.

3) There was a status bit error that gave the wrong command angle reading several times while in the CTC mode during the Skylab missions. However, this wrong command angle reading had no effect on the gimbals, as they continued to move in the proper manner.

3.1.3 Engineering Parameters

The Rad/Scat engineering parameter limit verification was performed for all Rad/Scat operations during SL2, SL3, and SL4 by analyzing each individual parameter to determine its minimum and maximum value for each run, determining if these minimum and maximum values were within established limit criteria, noting the operational characteristics of each parameter, and (where applicable) performing comparative analysis with other associated parameters.

The limit verification showed that, except for periods affected by the investigated S193 anomalies (paragraphs 4.1 and 4.2), voltage and current measurements, along with certain temperature measurements (i.e., reference temperatures T_1 and T_2 and RF oven temperatures) were very consistent in their output readings from pass to pass. The majority of temperature measurements susceptible to the variable operational environment (i.e., antenna reflector temperatures, pitch and roll shaft and housing temperatures) varied from pass to pass depending on the length of S193 operating period, length of time between operating periods, and sun angles.

When the S193 gimbal system anomaly occurred during EREP pass 40, several engineering parameter values changed immediately. These readings were instrumental in aiding diagnosis of the anomaly and the eventual modification that restored S193 to partial use. This anomaly was diagnosed as a mechanical short on the -10-volt reference power supply. The parameters that changed value in conjunction with anomaly were A050-193 00A pitch bias, A058-193 00A roll bias, A035-193 pitch command position, A036-193 roll command position, A037-193 pitch torquer supply, A038-193 roll torquer supply, and A008-193 Rad AGC integrator gain deviation. All of these parameters gave readings

that corresponded to a supply voltage of approximately -1 volt consistent with the short condition. They returned to normal readings when the short condition was partially repaired by the crew during a special EVA at the beginning of SL-4.

The gimbal anomaly that occurred during EREP pass 79 caused the failure of the A038-193 roll torquer current parameter to give readings above 0.25 amperes after the anomaly.

For more detailed results of the engineering parameter verification, including tables of evaluation criteria and parameter values, see MSC-05528, Volume IV, October 30, 1974, paragraph 3.3.

3.1.4 Gimbal Positions

In the Rad/Scat modes of operation, the antenna was scanned in the pitch or roll axis in two primary modes--contiguous and noncontiguous scans. The analysis of how well the gimbals performed in positioning the antenna in these two basic modes was based on the following criteria:

1) Contiguous modes - Attainment of the correct maximum and minimum gimbal scan angles, data acquisition initiation at the correct angles, and whether there was a linear scan from maximum for minimum gimbal angles;

2) Noncontiguous modes - Attainment of the correct gimbal angle, whether the gimbal maintained a nearly constant angle during each science measurement period, and whether the gimbal angle was repeatable.

This analysis was performed for all SL2 Rad/Scat operations, all SL3 Rad/Scat operations before EREP pass 40 when an anomaly occurred that prevented proper gimbal positioning (See paragraph 4.1) and for all SL4 Rad/Scat operations.

Throughout the Skylab missions, the gimbals were unable to attain the commanded position of plus or minus 48 degrees in any mode. This anomalous operation was attributed to the flex harness that connects the RF oven (on the antenna) to the integrated electronics package (IEP) within the S193 being stiffer than expected in the flight environment.

The following is a summary by mode of the gimbal performance during Skylab:

1) ITNC mode - The pitch gimbal angle did not attain the required 48-degree starting angle; the maximum angle ranged from 45 to 46 degrees. All CMD angles except 48 degrees were attained, and in all cases the angle attained remained constant throughout the science measurement period.

2) ITC mode - The 48-degree pitch angle was not attained by the antenna in this mode; the pitch gimbal actually drove the antenna to between 42 and 43 degrees. The expected linear scan from 48 down to 0 degrees was essentially limited to 40 down to 0 degrees.

3) CTNC mode - The roll gimbal did not attain either the plus or minus 48-degree starting angle. In addition, the negative 40.1-degree angle (right roll) was not attained because the flex harness had the most effect in this direction. In all cases, the angle achieved remained constant throughout the science measurement period.

4) CTC mode - The CTC gimbal operation was nominal during SL3 before EREP pass 40 and SL4 before EREP pass 79. However, during SL2, the right-to-left scan was more nonlinear than expected, and the maximum expected angles were not achieved. The deviation from linear motion was 0.2 degree and the maximum angles were approximately plus or minus 1 degree. Examples of the gimbal angles achieved are shown in Figures 3-1 through 3-5 with the tolerances imposed indicated. These tolerance bands are plus or minus 1.353 degrees in pitch and plus or minus 1.763 degrees in roll. Additional discussion of the gimbal positions, antenna scanning, and antenna anomalies are given in paragraphs 3.3, 4.1, and 4.2.

3.1.5 Scatterometer Internal Calibration

The scatterometer calibration (Scat Cal) parameter was a measurement of the transmitter pulse made by the Scat processor that appeared periodically in each scatterometer or Rad/Scat mode of operation and was used as a reference measurement of

SL3 ITNC
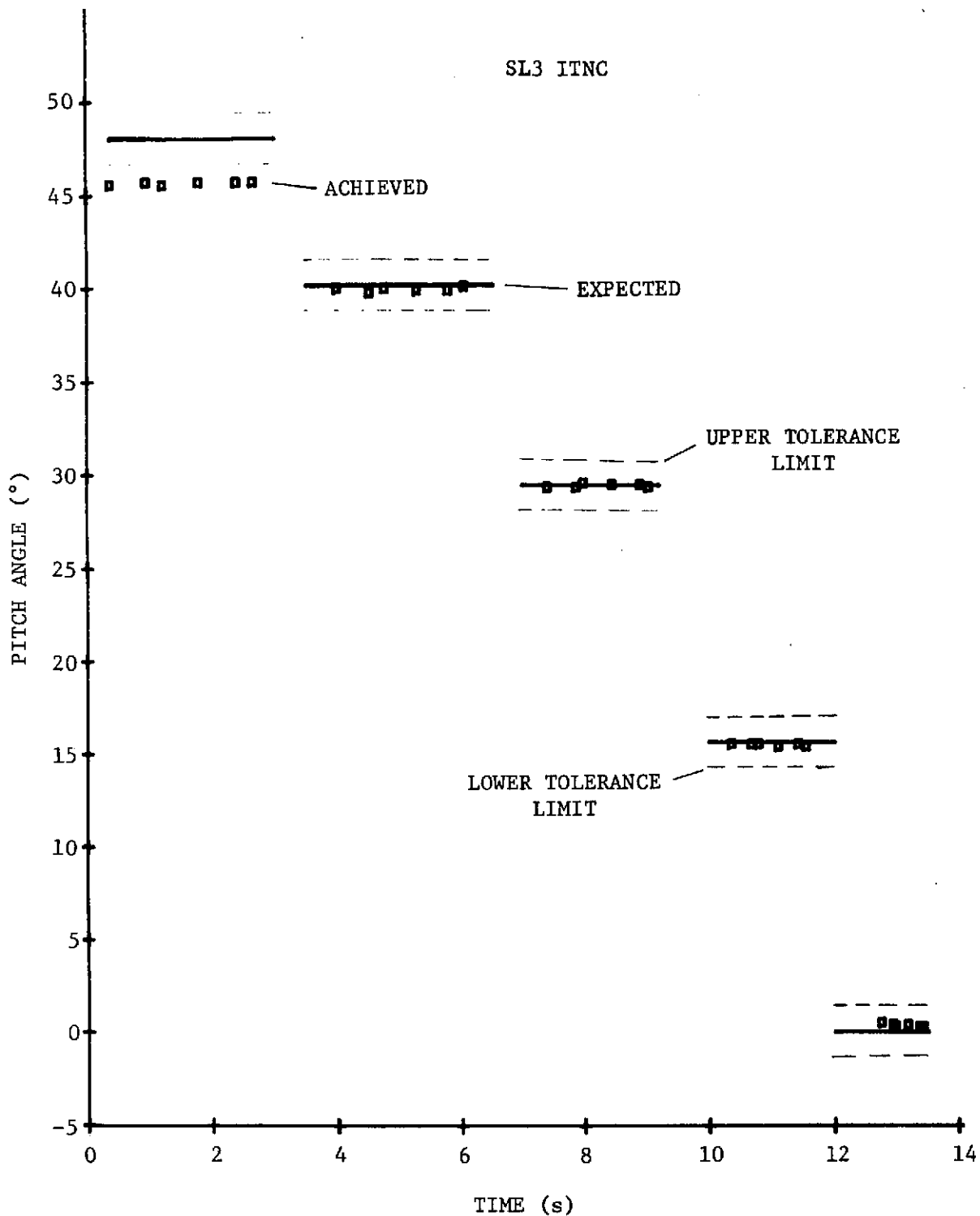
Figure 3-1   ITNC Pitch Angle versus Time (1 Cycle)
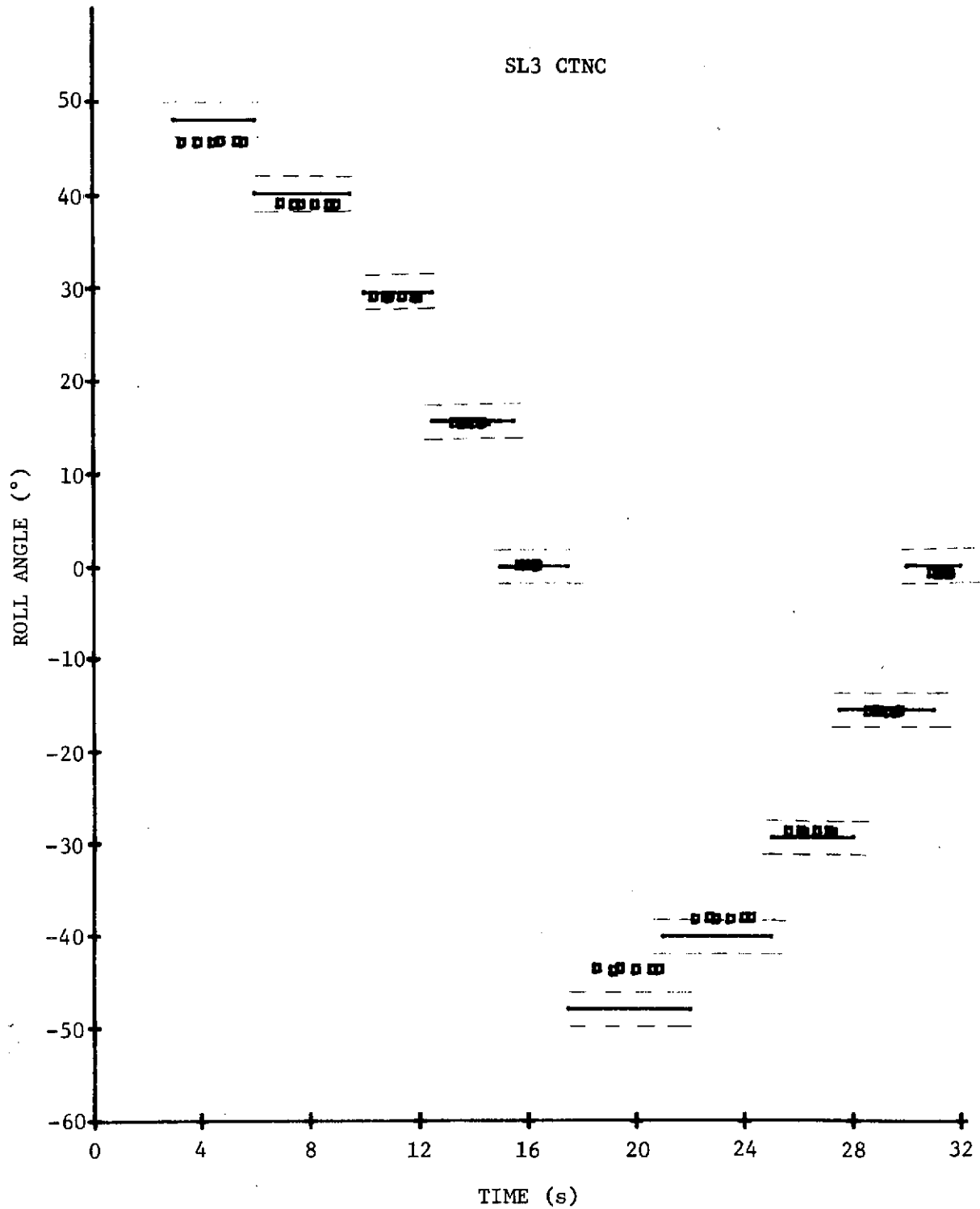
Figure 3-2 CTNC Roll Angle versus Time (1 Cycle)
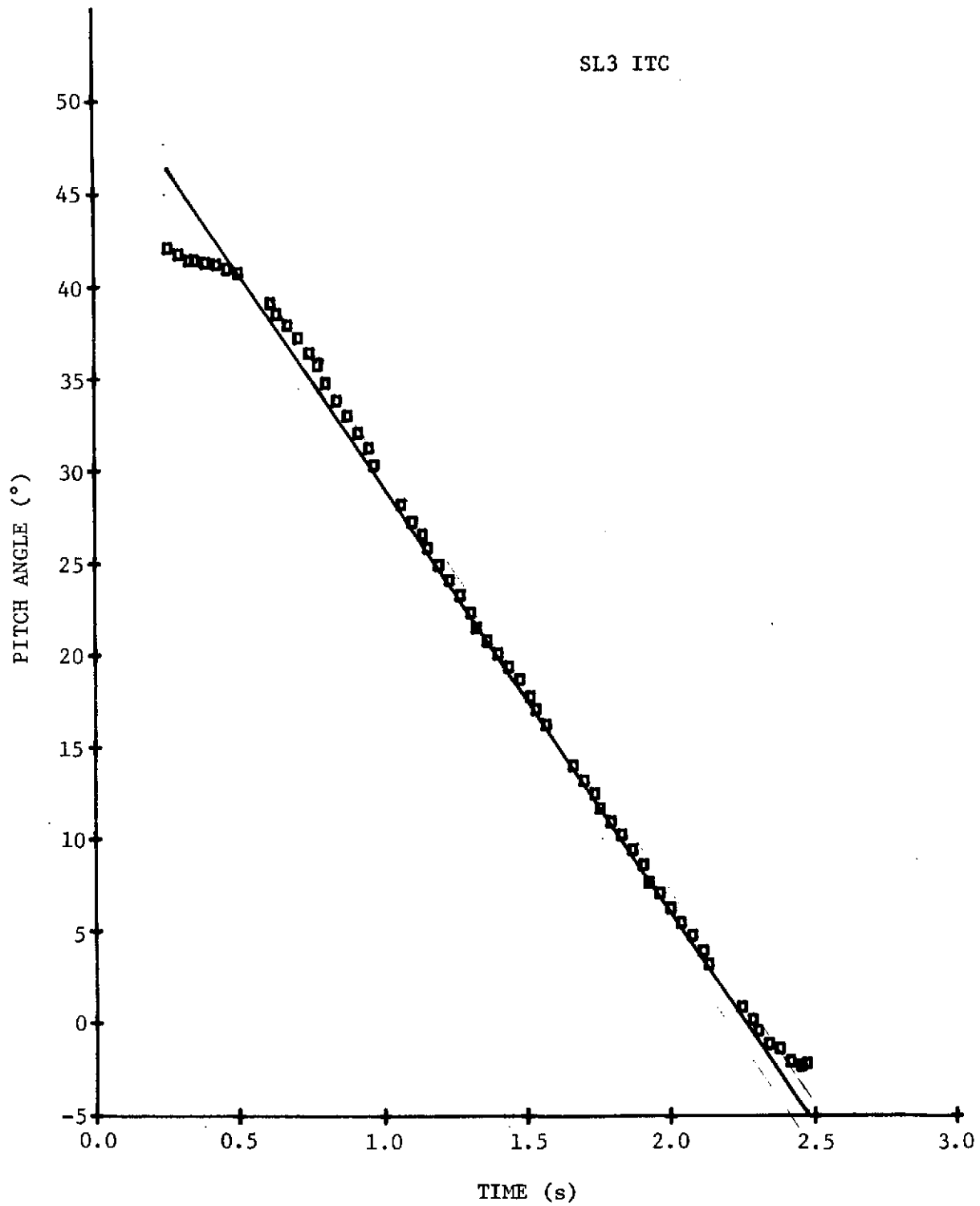
Figure 3-3 ITC Pitch Angle versus Time (1 Cycle)
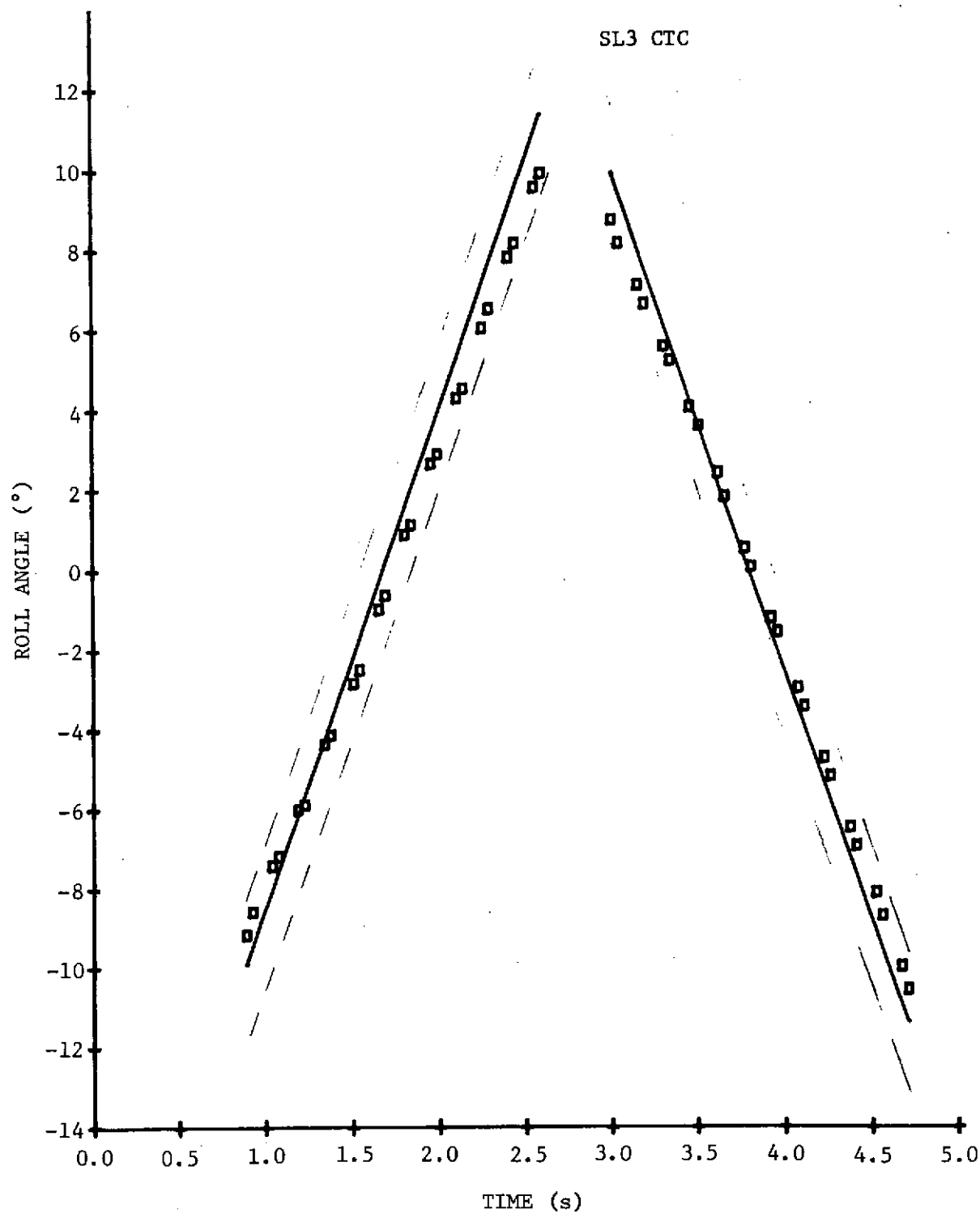
Figure 3-4 CTC Roll Angle versus Time (1 Cycle)
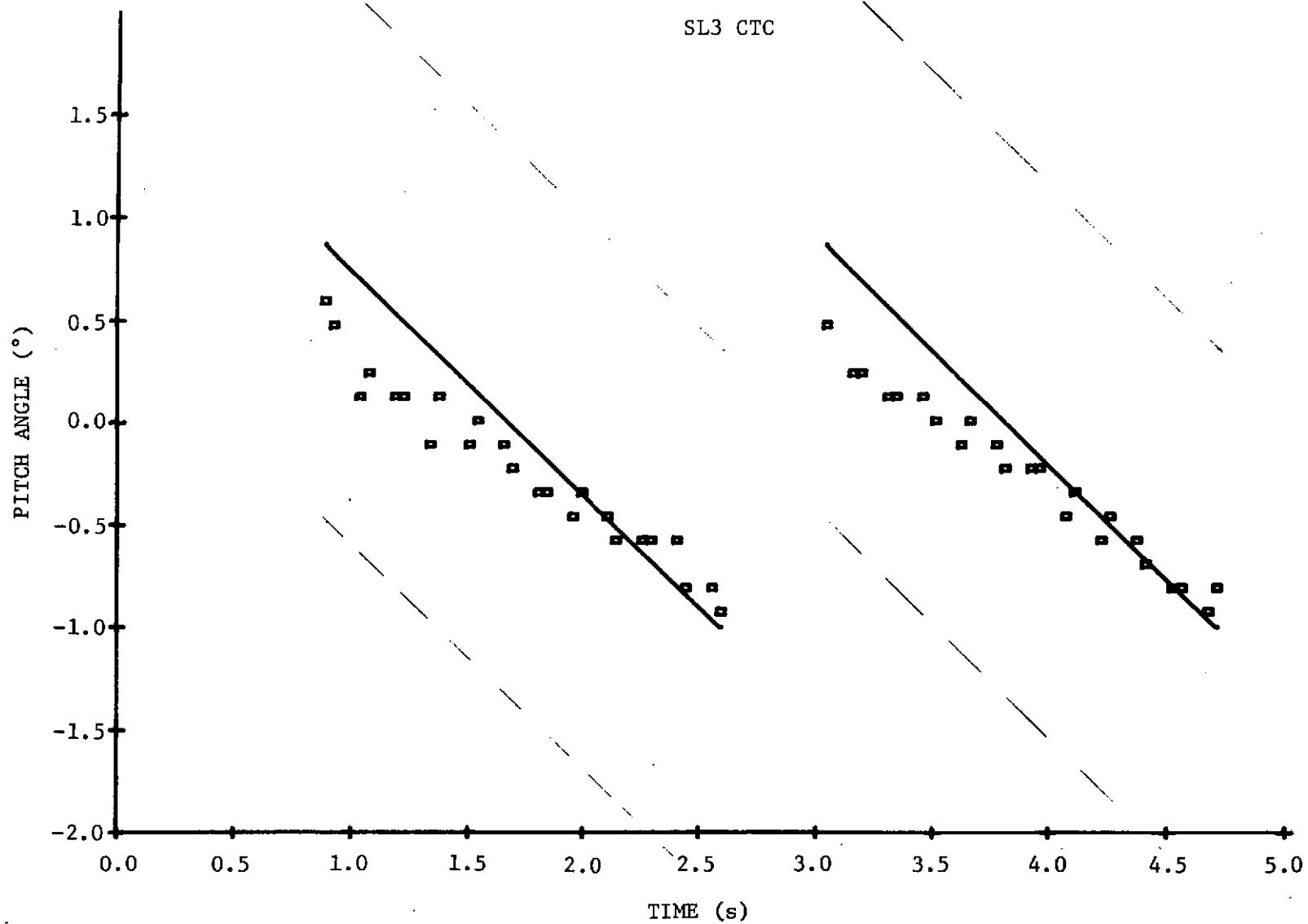
Figure 3-5   CTC Pitch Angle versus Time (1 Cycle)

the transmitted output power in processing the scatterometer data. The scatterometer processor received the transmitter pulse after it had been shunted through a fixed attenuation and then processed this signal through the 0-degree pitch filter/ integrator group. Two Scat Cal values were then provided with Scat Cal 1 being the output of the lower center-frequency filter/integrator (LCF) and Scat Cal 2 being the output of the middle center-frequency filter/integrator (MCF).

Evaluation and analysis performed under the scatterometer calibration limit verification throughout the Skylab missions consisted of evaluating 251 recorded Scat Cal values. This evaluation included analyzing both the raw Scat Cal voltage levels and Scat Cal values converted to equivalent power at the antenna against the following criteria:

1) Allowable range - 0.5 to 1.5 volts, raw PCM volts;

2) Repeatability - Determine the repeatability of Scat Cal throughout the Skylab missions;

3) Stability - Determine the stability of Scat Cal and whether any drift was correlatable to thermally induced gain changes.

The conclusions reached after analyzing all the Scat Cal data were:

1) Allowable range - All recorded raw Scat Cals (when the scatterometer transmitter was on) were within the specified allowable range;

2) Repeatability - The Scat Cal readings were repeatable within 0.81 dB after correction factors had been applied for scatterometer processor gain changes due to thermal variations;

3) Stability - The raw Scat Cal values appeared to be unstable, but, after correction factors had been applied for scatterometer processor gain changes due to thermal variation, the variation in Scat Cal values were reduced and the parameter appeared quite stable. A typical variation in a data pass would consist of approximately 0.4 dB over about 15 minutes or five Scat Cal readouts.

A catalog of all Scat Cals evaluated is in MSC-05528, Volume IV, Tables 3.4.2.2-1, 3.4.2.3-1, and 3.4.2.4-1, which contain a great deal of pertinent information including time of Scat Cal, raw Scat Cal value, corrected Scat Cal value, equivalent power at the antenna, scatterometer processor internal temperature, and TWTA temperatures. A discussion of the attempts made to correlate the variation in Scat Cal versus time with other S193 measured parameters accompanies the tables. This was done to improve the resolution of transmitter output power values for use in data processing during the long time span between Scat Cal samples. The only verifiable correlation was between Scat Cal data and the scatterometer processor temperature, which was subsequently used in correcting the raw scatterometer voltage. For Scat Cal values between Scat Cal samples, a straight-line interpolation between values was finally used.

3.1.6 Radiometer Internal Calibration Values

The S193 radiometer used two stabilized resistive loads at different temperatures as simulated radiometric sources (reference temperature T_1 = 393°K and reference temperature T_2 = 318°K). These reference sources were used to develop the system AGC reference, and to compute two points on the calibration curve of radiometric temperature versus voltage output. The system AGC was a demodulated error voltage proportional to $(T_1 - T_2)$. The two points on the calibration curve established from the resistive loads were Rad Cal $[$Rad Cal $\propto (T_1 - T_2)]$, and Rad baseline $($Rad baseline is a demodulated composite signal waveform $[f(T_1, T_2)]$ resulting in a zero-volt reference value (by definition) to the input of the integrator$)$.

The radiometer calibration limit verification criteria were derived from the measured KSC test data and applied to the mean values and standard deviations of the Rad Cal and Rad baseline measurements for the Skylab missions and are shown in Table 3-1.

There were a few violations of the these criteria noted during SL2 and SL3. No criteria violations were noted for SL4 data. Some of the violations were created by saturation of the Rad AGC as a result of the radiometer being turned on immediately after an altimeter operation or immediately after a CTC Scat Only mode. This was avoided in SL3 and SL4 by modifying the operational procedures. There were no explanations for some of the other criteria violations.

Table 3-1   Calibration Limit Verification Criteria

RAD CAL MEAN VALUE			
MODE-SCAN MODE	CMD ANGLE (°)	RAD CAL MEAN VALUE (mV)	ONE SIGMA LIMITS (mV)
ITNC-R/S	48 & 40.1	1145.6	15
	29.4 & 15.6	1118.8	15
	0.0	1136.9	15
CTNC-R/S	48 & 40.1	1145.6	15
	29.4 & 15.6	1118.8	15
	0.0	1136.9	15
ITC-R/S	NA	1133.4	15
CTC-R/S	NA	1142.2	15
CTC-R	NA	1144.7	15

RAD BASELINE MEAN VALUE			
MODE-SCAN MODE	CMD ANGLE (°)	RAD BASELINE MEAN VALUE (mV)	ONE SIGMA LIMITS (mV)
ITNC-R/S	48 & 40.1	352.9	10
	29.4 & 15.6	344.1	10
	0.0	350.9	10
CTNC-R/S	48 & 40.1	352.9	10
	29.4 & 15.6	344.1	10
	0.0	350.9	10
ITC-R/S	NA	337.7	10
CTC-R/S	NA	338.2	10
CTC-R	NA	344.6	10

Considerable analysis of the Rad Cal values was completed
and discussed in Volume IV of MSC-05528, paragraph 3.4.4.
Because the values result from a random variable, the technique
for determining the proper mean values for use in data reduction
was a problem. Review of the flight data indicated that the
sensor was only subject to small long-term variation, rather
than short-term instabilities. Thus, analysis of the Rad Cal
determined that a straight-line fit should be used when
processing radiometer data. This is the method employed by JSC
in processing the Skylab radiometer data.

3.1.7 Scatterometer Noise Level

The scatterometer noise measurement parameter was the total
noise equivalent power of receiver noise temperature and antenna
target temperature. This separate measurement provided a second
internal calibration measurement of the scatterometer referred
to as Scat Noise. The parameter was processed in the Scat
processor. An analysis was performed to determine the proper
method of correcting the raw Scat Noise data for processor
effects. One analysis of Scat Noise was a comparison with the
actual scatterometer data measurements. The lunar calibration
passes were used as the data source for this analysis because,
theoretically, none of the scatterometer transmitter power was
reflected from deep space and the only input to the scatterometer
processor was receiver noise and the antenna target temperature
of deep space. Therefore, data values of Scat and Scat Noise
should have been equal in all modes and at all look angles during
the lunar calibration runs. This was not always the case and,
as a result of this analysis, new integration times and a new
processing equation were developed that will be used on all JSC
processed data. The resulting equation for correcting the raw
Scat Noise voltage for drift, integrator bias, filter
characteristics, and new integration times is given in paragraph
3.8 Equation 1 and Table 3-2. See MSC-05528, Volume IV,
paragraphs 3.5.2, 3.5.3, 3.5.4, and 10.2.1.1 for a more detailed
analysis, including the processing equation and the new integration
times.

Table 3-2 Scat Noise Integration Time

MODE	ANGLE (°)	TIME CONSTANT (T.C.) (ms)	INTEGRATION TIME (I.T.) (ms)	
			Original	Improved
ITNC, CTNC	0	10.22	26.582	24.094
ITNC, CTNC	15.6, 29.4	33.00	61.532	57.990
CTC-R/S	NA	10.22	16.000	13.686
CTC-S (Only)	NA	4.00	6.813	6.544

3.2 Interference Check

There were three subtasks investigated under the primary task of interference check--contamination buildup on the S193 antenna, interaction between the radiometer and scatterometer due to the scatterometer transmitter, and electromagnetic/radio-frequency interference (EMI/RFI) from other sources.

Review of Rad/Scat data from all Skylab missions revealed no degradation attributable to contamination buildup, coupling of the scatterometer transmitter power into the radiometer, interference from other transmitters aboard Skylab, or conducted interference.

The contamination monitoring devices that most closely approximated S193 antenna temperatures were the Z-axis quartz-crystal microbalances (QCMs), which had an accumulated mass of 2.4×10^{-5} gm/cm^2 at the end of the SL4 mission. This is 0.1 percent of the amount estimated to produce 0.5-percent signal attenuation. The antenna pattern change (See paragraph 4.3.) for SL4 raised the possibility that, for the low-energy radiometric and Scat Noise measurements, the presence of the vehicle may have raised the effective antenna temperature a measurable amount. (See paragraph 4.3.4.)

Another item recorded under this task was the loss of sync created in S193 data by the activation of the S192 during an S193 data take. While this was not EMI, it did create data breaks that may affect some data applications. These data losses of sync were created by the tape recorder speed changes required for S192 data recording. The times of occurrances are recorded in MSC-05528, Volume IV.

3.3 Antenna Gain, Pattern, and Cross-Polarization,
     Pointing and Scan Performance

Except for discussion of the altimeter pulse shape
measurement and scan performance inserted by Martin Marietta in
MSC-05528, Volume IV, paragraph 5.0, reporting on this sensor
performance task, responsibility for completing this task was
assigned to the University of Kansas. MSC-05528, Volume IV
reports only the introduction to the Antenna Pattern Exercise
(APEX) evaluation of the in-flight antenna pattern, along with
samples of raw data and some discussion of the field operation
and planned data reduction. A description of APEX through the
stages reported is presented in Appendix A, Section III of this
volume. Obtaining a synthesized antenna pattern was complicated
by failures in gimbal performance and modification of the flight
antenna pattern during SL4 due to the missing feed cup. The
reader is referred to the final report to be published by the
University of Kansas in the late spring or early summer of 1975.
Inputs based on APEX were submitted to the reprocessing of
S193 flight data so that final data releases from NASA/JSC
incorporate the best antenna parameter values. A brief
description of the antenna parameters is given in paragraph 4.3.
Scan performance is summarized below and further covered under
the antenna gimbal performance discussion in paragraph 3.1.4 and
the anomaly discussions in paragraphs 4.1 and 4.2.

In-flight scan motion of the antenna throughout the Skylab
missions was considerably different than planned. Fortunately,
however, the gimbal position potentiometers continued to read
gimbal position so that the achieved antenna pointing of the S193
antenna relative to the S193 mounting could be determined from
the S193 data stream.

During review of the SL2 scan motion, it was noted that the
large-scan-angle positions were not achieved. This was
believed to be caused by the flex cable harness between the
electronics box and the gimbaled antenna being colder and hence
stiffer than expected. The planned 48-degree scan position in
pitch was thus replaced by an actual 46-degree limit on pointing
in ITNC and 43 degrees in ITC throughout all three Skylab
missions. The planned 48-degree scan position in CTNC was
limited to -44 degrees and +46 degrees. There were two primary
effects on the data. The first was that the forward-pitched
ITC and ITNC data from the commanded 48-degree scan position
did not experience the expected Doppler shift. Thus, when the
scatterometer measured return signal at less than about 43 degrees

it was affected by the preprogrammed Doppler filter group skirt attenuation. Data processing of the S193 data at JSC attempted to remove these extra Doppler filter attenuations. The second effect was that the desired ground-spot overlap to provide radiometric and scatterometer data from the same terrain sample at different aspect angles was not achieved. An example of the achieved overlap for the ITNC mode five-angle samples is shown in Figure 3-6.

Late in SL3, DOY 256, Pass 40, the pitch gimbal-position potentiometer shorted, causing loss of control of the gimbals until the antenna repair EVA by the astronauts before S193 operation during SL4. The roll scan operation then returned to the SL2 performance. However, total scan motion was limited to roll motion only, because the pitch gimbal was pinned at 0 degree (pitch)   to establish a partial gimbal-system recovery.

On DOY 009 (Pass 79) during SL4, a component failure in the electronics of the roll gimbal drive again caused a change in antenna scan motion. Data during the remainder of SL4 were taken with a limited roll-motion scan. The roll motion after pass 79 was essentially limited to angle scans to the right of the track, with only slight excursions to the left. The scan motion for the remainder of the mission was also not repeatable after the failure, which requires even closer attention to the measured position sensor output for each individual data point.

Additional discussions of antenna position and gimbal failures are in paragraphs 3.1, 4.1, and 4.2. Some analysis of antenna pointing and scan motion was attempted using land-sea interfaces and other discontinuities. However, these added to the need for improvement in determining vehicle orbital and altitude parameters, and timing errors in the data reduction needed to be corrected.

3.4 Left Blank Intentionally
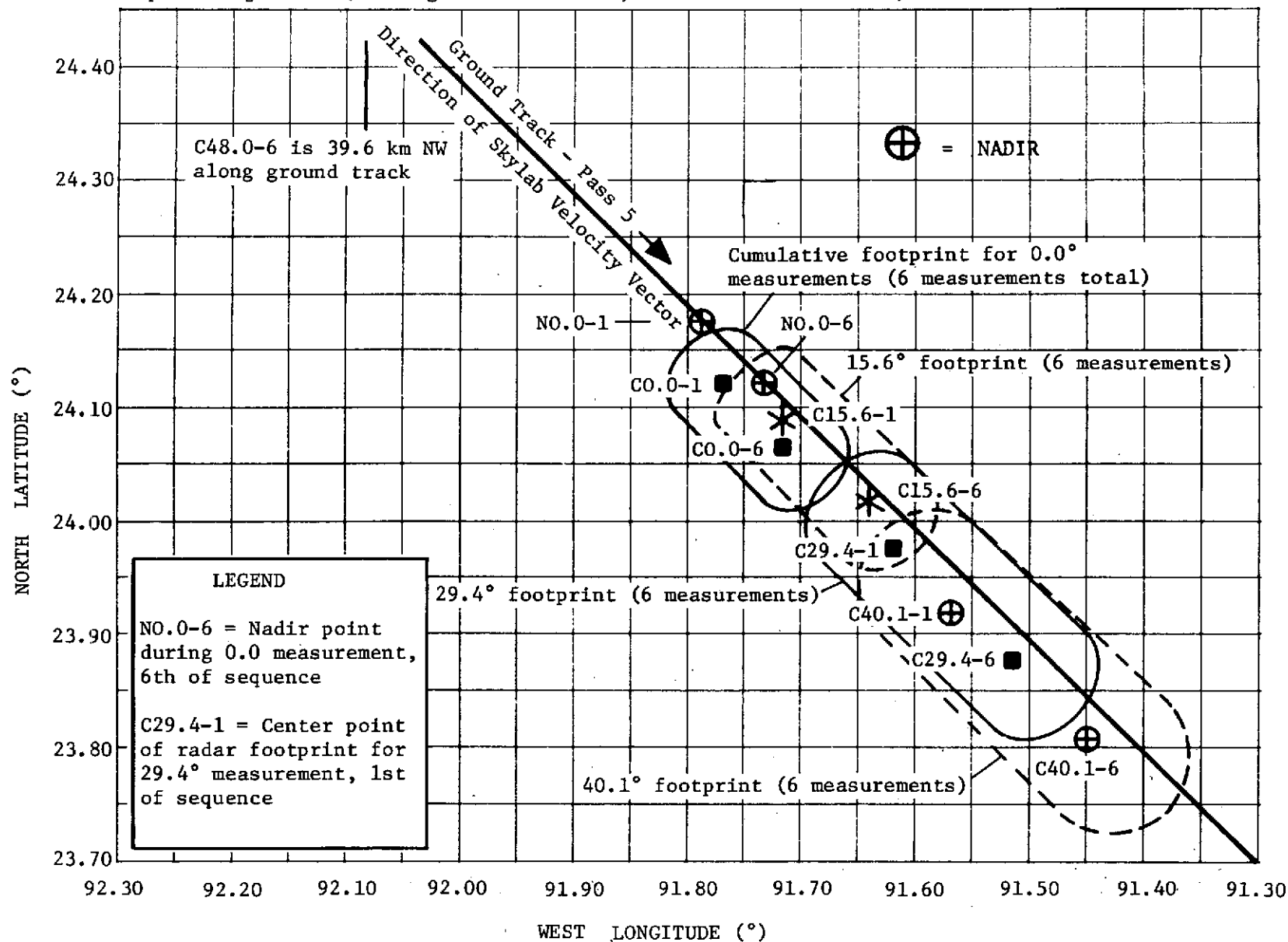
Figure 3-6 Sample Ground Coverage for SL2 Pass 5 ITNC Mode

THIS PAGE LEFT BLANK INTENTIONALLY

THIS PAGE LEFT BLANK INTENTIONALLY.

for EREP Passes 6 and 10 on DOY 160 and 164. Data were
also taken during SL4, but have not been
reduced or published. Pulse period and duty cycle were found
to be within 1.7 percent of specfication values. Recorder
bandwidth limitations prevented precise measurement of pulse
rise and fall times; a value of 41.5 microseconds for each of
these intervals was estimated. A discussion of the data
analysis, including oscilloscope photographs, was presented
in Section 9 and test results were tabulated in paragraph
5.3.1 of MSC-05528, Volume IV.

3.8 Scatterometer Measurement Time

The objective of this task was to determine the
validity of theoretical (preflight design)
integration time values for the scatterometer processor by
analyzing lunar calibration data acquired during SL2 and SL3.
For correction of raw Scat and Scat Noise voltages to
equivalent values at the integrator input, the following
equation was used.

$$V_i(\text{corrected}) = \frac{V_i(\text{raw}) - (\text{I.T.}) \left[\text{Drift}_{TC} + \frac{DC_{TC}}{T.C.} \right]}{\frac{\text{I.T.}}{\text{T.C.}} F_{PA}} \qquad [3\text{-}1]$$

where

V_i(corrected)   =   corrected voltage at processor input
                          (directly proportional to input power)
                          i = both Scat and Scat Noise

V_i(raw)   =   raw voltage recorded directly on tape
                          (function of scatterometer processor
                          variables)
                          i = both Scat and Scat Noise

I.T.   =   integration time (function of mode,
                          angle, and measurement)

T.C.   =   time constant of integrator (function
                          of mode and angle)

Drift_{TC} = integrator drift voltage (function of T.C.)

DC_{TC} = dc offset voltage (function of T.C. and gain)

F_{PA} = filter noise gain (function of pitch gimbal angle)

In lunar calibration modes, the antenna was directed away from the earth and there were thus no scatterometer return signals. Scatterometer data acquired during these periods would be equivalent to radiometric measurements of a uniform 4°K target ("deep space") and were expected to be equal to the Scat Noise readings. When the scatterometer and Scat Noise measurements were processed using Equation 3-1, the expected equality was not found. It was thus concluded that the theoretical integration times as obtained from the G.E. calibration data report* were incorrect.

Improved values for Scat Noise integration time were calculated by setting corrected scatterometer equal to corrected Scat Noise and using Equation 3-1 to obtain the relation between the raw voltages and the respective integration times:

$$\text{I.T.}_N = \left(\frac{V_{NR}}{V_{SR}}\right) \text{I.T.}_S \qquad [3\text{-}2]$$

where

I.T._N = integration time of Scat Noise

I.T._S = integration time of Scat

---

* S193 Historical Logbook, S193 Vehicle 001, Vol 1A, Document No. 72 SD4234 Rev. A, 27 October 1972, General Electric Company, p 1-1 through 1-12.

Alternate Designation: S193 Calibration Data Report, Flight Hardware, Doc. No. 72 SD4207 Rev. D, 22 March 1973, Prime Unit 1A, SSO Contract NAS9-11195, General Electric.

V_{NR} = raw (uncorrected) Scat Noise voltage recorded

V_{SR} = raw (uncorrected) Scat voltage recorded

which, for several different data sets became

$$I.T._N = \frac{I.T._S}{N} \sum_{i=1}^{N} \left(\frac{V_{NR}}{V_{SR}} \right)_i \qquad [3\text{-}3]$$

where N = number of data sets.

Table 3-3 lists the results obtained by this process. The improved Scat Noise integration times were incorporated in the production data processing system in September 1974.

Table 3-3 Scat Noise Integration Time

MODE	ANGLE (°)	TIME CONSTANT (T.C.) (ms)	INTEGRATION TIME (I.T.) (ms)	
			Original	Improved
ITNC, CTNC	0	10.22	26.582	24.094
ITNC, CTNC	15.6, 29.4	33.00	61.532	57.990
CTC-R/S	NA	10.22	16.000	13.686
CTC-S(Only)	NA	4.00	6.813	6.544

3.9 Radiometer Combined Insertion Loss

The S193 radiometer was specified to be a relative radiometer with no absolute value requirements. The absolute value determination was performed to evaluate the receiver "front-end" insertion loss constants required for conversion of recorded radiometric readings into absolute antenna temperature values. The relative radiometric data from a given pass was not significantly influenced by the

"front-end" loss terms because their physical (kinetic) temperature and loss constants could be assumed to remain constant over short time spans, particularly because most were located in a stable-temperature oven. However, from pass to pass, some component physical temperatures changed and hence, their contribution to the radiometric data varied. If the loss values were assumed to remain constant, the physical temperature measurements could be used to transfer the measured relative data into absolute antenna temperatures. The specific objective of this task was to determine the loss between the antenna and the tunnel diode amplifier (TDA) from radiometer data acquired while scanning targets of known temperature. After this objective was achieved, improved values were developed for the integrator gain constant, which was found to be mode dependent. Details of the analyses were reported in paragraphs 11 and 12.3.1 of MSC-05528, Volume IV.

3.9.1 Measurement Approach

Within the instrument, the radiometer measurement was performed by comparing antenna temperature, T_A, with a reference temperature, T_R. Figure 3-7 is a schematic of the circuitry used for this comparison. Data stream measurement numbers indicate the sources of physical temperature data for the circuit components. While the insertion loss of each component was either measured or accurately estimated before flight, the combined insertion loss could not be assumed to be simply the sum of the component losses, for the following reasons:

1) Imperfect physical mating of components could produce an increase in VSWR and hence additional loss;

2) Imperfect impedance match between mated components could increase VSWR and contribute additional loss;

3) Temperature gradients along the RF path in the flight environment could significantly affect end-to-end loss;

4) Scatterometer transmitter operation could increase the temperature of some of the components, and thus change the combined insertion loss during Rad/Scat modes.
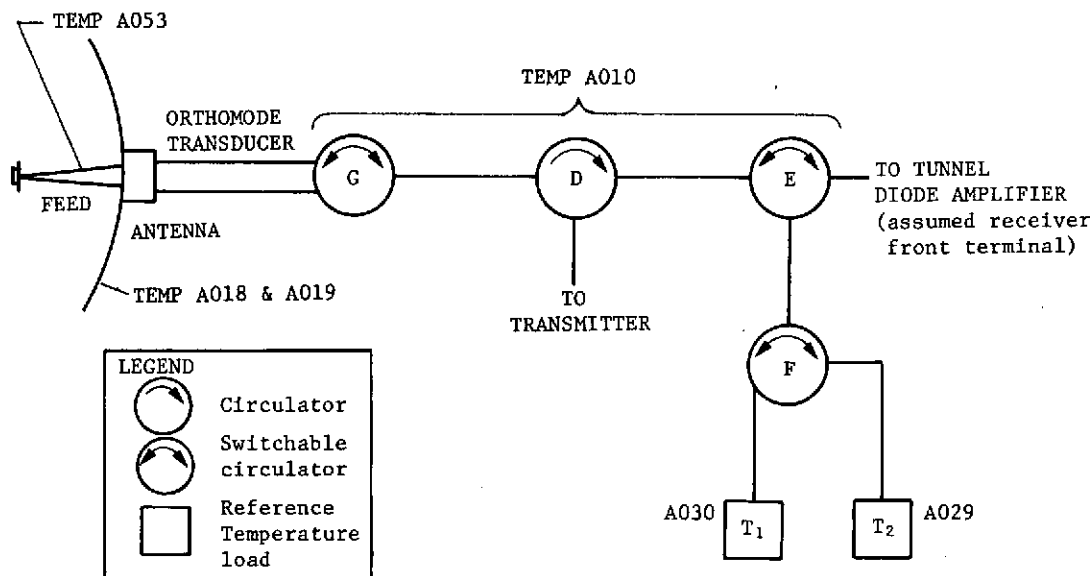
Figure 3-7 Radiometer RF Circuit Schematic

These considerations defined the need for on-orbit calibration of the insertion loss. A known radiometric input was required, obtainable by causing the antenna to scan a homogeneous target of known temperature. Deep space was the selected target. Although its temperature is below the specified nominal operating range of the radiometer, it satisfies the requirement for homogeneity, its temperature is well established, and the radiometer output range had been extended to indicate its temperature.

Before proceding, the effect of scatterometer transmitter operation on the radiometric measurements was investigated by using the experiment developer's heat-up algorithm.* This algorithm predicted the temperature rise of a circulator above the ambient temperature when the transmitter was operated. A nominal RF oven temperature of 20°C was assumed, and measured values of component losses were used. Results indicated that, in all modes, the temperatures of all circulators would be within 1°K of the temperature of circulator G. The maximum heat-up effect on measured radiometric temperatures was calculated to be 0.16°K. This value is an order of magnitude smaller than the theoretical resolution of the radiometer, and the transmitter heating effect could therefore be ignored. (Also see paragraph 4.6.)

---

* S193 Historical Logbook, S193 Vehicle 001, Vol 1A, Document No. 72 SD4234 Rev. A, 27 October 1972, General Electric Company, p 3-8B.

Alternate Designation: S193 Calibration Data Report, Flight Hardware, Doc. No. 72 SD4207 Rev. D, 22 March 1973, Prime Unit 1A, SSO Contract NAS9-11195, General Electric.

3.9.2 Insertion Loss Calculations

The equivalent circuit for the radiometer RF path is shown in Figure 3-8. Definitions of the losses, their nominal values, and the temperature measurements associated with each loss are listed below the circuit diagram. Some of the loss temperatures were defined to be the weighted average of two or more measurements. To make it possible to calculate an unknown loss with one set of radiometer data, it was necessary to lump the losses into two losses, one of which was considered "known" by recourse to preflight measured values. Weighted average temperatures were assigned to each of the two lumped losses. Through application of standard expressions relating true and effective radiometric temperatures, and with the equations defining the operation of the instrument, it was possible to express the unknown loss in terms of measured temperatures, known losses, data voltages, and the target temperature.

T_A antenna circuit: L_D, T_D — L_F, T_F — L_T, T_T — L_G, T_G — L_A, T_O — REFERENCE POINT AT WGSA OUTPUT (T'_A, T'_R); reference leg L_R, T_O with T_R.
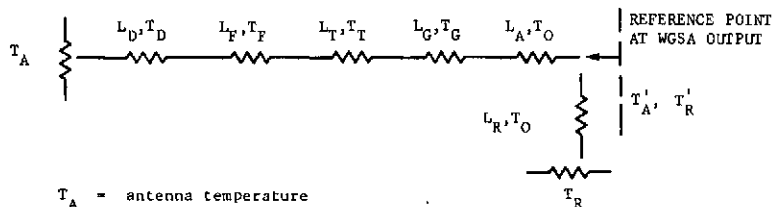
T_A = antenna temperature

T'_A = effective antenna temperature seen through the antenna path

T_R = reference temperature = $\left(T_1 + T_2\right)/2$

T'_R = effective reference temperature seen through the antenna path

LOSS SYMBOL	LOSS REPRESENTED	LOSS SPECIFIED BY VENDOR (Vert pol) (dB)	LOSS SPECIFIED BY VENDOR (Horiz pol) (dB)	ASSOCIATED TEMPERATURE
L_D	parabolic dish	0.013	0.013	$T_D = \dfrac{A018 + A019}{2}$
L_F	feed assembly	0.112	0.112	$T_F = A053$
L_T	ortho-mode transducer	0.032	0.076	$T_T = \dfrac{A018+A019+A053+3A054}{6}$
L_G	input waveguide	0.107	0.095	$T_G = A054$
L_A	WGSA (ant. path)	0.66	0.65	$T_O = A010$
L_R	WGSA (ref path)	0.44*	0.41	$T_O = A010$

* high reference temperature $\left(T_1\right)$ path

low reference temperature $\left(T_2\right)$ path

Figure 3-8 Definition of Radiometer Insertion Losses

Data from the lunar calibration pass of DOY 165 were used, with the assumption that the deep space target was at 4°K. Calculations of the unknown loss were made separately from ITC and CTC data. Three methods of lumping the losses were applied. In one of these cases, all losses were combined into a single equivalent loss.

Results of these calculations are listed in Table 3-4. For comparison, the total insertion loss based on preflight measurements and predicted temperatures is also given. Use of this last value in the system equations gave calculated deep-space temperatures of 8.0°K and 9.6°K for the ITC and CTC modes, respectively. To check insertion loss values, each was applied to radiometer data taken over the Gulf of Mexico during EREP Pass 11. This yielded corrected T_A values ranging from 123.7 to 127.0°K; aircraft data for the same location on the same day indicated 128 ± 3°K. See Appendix A for details of comparison technique.

Table 3-4 Radiometer Insertion Loss

KNOWN LOSS		UNKNOWN LOSS				
Components	Assumed Value, (dB)	Components	Calculated Value (dB)		Total Insertion Loss (dB)	
			ITC	CTC	ITC	CTC
L_T, L_G, L_A	0.610	L_D, L_F	0.484	0.503	1.094	1.113
L_A	0.655	L_D, L_F, L_T, L_G	0.360	0.386	1.015	1.041
--	--	L_D, L_F, L_T, L_G, L_A	1.004	1.028	1.004	1.028
L_D, L_F, L_T, L_G, L_A	*	--	--	--	0.924	0.946

* Preflight predictions of operational values

The first algorithm listed in Table 3-4 showed the least difference between modes for deep-space data, and produced the closest agreement with aircraft data for the pass over the Gulf of Mexico. Production data processing used the method of lumping all losses into a single loss, but assigned temperature weighting factors.

3.9.3 Integrator Equalization Constants

In the previous paragraph, it was noted that the calculated insertion loss was not the same for all modes. When the algorithms were applied to deep-space data from SL3 and SL4 lunar calibration modes, similar differences were seen. Studies were conducted to determine whether these differences could be resolved.

The G.E. calibration data report*, page 3-5 described how switching-transient effects were avoided by interrupting the input to the radiometer integrator for 21.531 microseconds at the time each circulator was switched. The theoretical correction factor to account for the resulting net loss of integration time was shown to be 0.978, but a better fit to preflight data was produced by the empirical value 0.844. Integrator gain was assumed to be constant.

To make deep-space data from different modes agree, an optimum value of insertion loss was selected and a mode-dependent integrator equalization constant, K_i, was calculated from deep-space data. The optimum insertion loss was chosen by using the first algorithm of Table 3-4 and assigning an average of the values obtained in the various modes to the unknown portion. Values of K_i were found to be inversely proportional to integration time, consistent with the thought that the 21.5-microsecond time segment was a greater influence on the shorter total integration time, and all were larger than the empirical K value of 0.844.

---

* S193 Historical Logbook, S193 Vehicle 001, Vol 1A, Document No. 72 SD4234 Rev. A, 27 October 1972, General Electric Company.

Alternate Designation: S193 Calibration Data Report, Flight Hardware, Doc. No. 72 SD4207 Rev. D, 22 March 1973, Prime Unit 1A Volume 1A, SSO Contract NAS9-11195, General Electric.

Values of K_i were further refined using SL3 and SL4 deep-space data. Final values are listed in Table 3-5. These new values of K were used as inputs to JSC data processing of S193 flight data.*

Table 3-5 Optimum Integrator Equalization Constants

MODE	INTEGRATION TIME (ms)	K_i
ITC	32	0.83965
CTC-R/S	32	0.8595
CTC-R/O	58	0.8377
NC 0°	58	0.8386
NC 15°/29°	128	0.8381
NC 40°/48°	256	0.8325

3.10 Radiometer Receiver Performance Baseline and Gain Stability

This task included evaluation of radiometer gain stability, relative accuracy, precision, linearity, and dynamic range. Results were reported in MSC-05528, Volume IV, Section 12. Some of the results were included in the summary in paragraph 3.9 because they were directly related to the insertion loss evaluation.

3.10.1 Receiver Gain

Radiometer receiver gain was shown in the G.E. calibration data report[†] to be proportional to the difference between Rad

---

* Earth Resources Production Processing Requirements for EREP Electronic Sensors, Document PHO-TR524 Rev. A, Ch 2, JSC, 18 October 1974.

[†] S193 Historical Logbook, S193 Vehicle 001, Vol 1A, Document No. 72 SD4234 Rev. A, 27 October 1972, General Electric Company.

Alternate Designation: S193 Calibration Data Report, Flight Hardware, Doc. No. 72 SD4207 Rev. D. 22 March 1973, Prime Unit 1A Volume 1A, SSO Contract NAS9-11195, General Electric.

Cal, R_C, and Rad Baseline, R_{BL}, data voltages, and inversely proportional to the difference of the reference temperatures. Theoretical and empirical expressions for the gain were distinguished by the choice of proportionality constants. It was found that a corrected value of L_R, the loss in the reference temperature path, made the two expressions identical. The corrected value of L_R, used in all subsequent work, was 1.10281.

An automatic gain control (AGC) was used in the radiometer receiver to stabilize the transfer function. However, individual values of R_C were observed to scatter about the mean value in a noise-like manner, verifying that the AGC time constant was large compared to the time between samples. Use of the variable instantaneous values of R_C and R_{BL} to establish the gain produced large variations in the calculated antenna temperature, T_A. Tests of data smoothing techniques were therefore made. R_C and R_{BL} data from a 1-minute slice of pass LC-1 on DOY 165 were processed by the use of a 10-point running average and then by a least-squares straight-line fit.

T_A values calculated with the 10-point running-average gain had much less scatter than the values calculated from "instantaneous" gain, but the radiometric temperature trend with time was biased by the shape of the gain curve. Application of the least-squares straight-line technique yielded a T_A population with smaller scatter about a mean that did not vary with time. This was not surprising because the straight-line fit agreed with the assumption that the instrument fluctuations and variations would be long term compared to the data-taking periods. As a result of this finding, least-squares straight-line fits to Rad Cal and Rad Baseline data were incorporated in the JSC production data processing in June 1974.*

Least-squares straight-line fits were used to evaluate gain stability in selected modes from SL2, SL3, and SL4. The maximum rate of change of gain observed was 0.03 percent per second. Even this small value was suspect because, for the duration of every mode analyzed, the total change of $R_C - R_{BL}$ described by the least-squares fit was less than two standard deviations. In addition, both positive and negative slopes

---

* Earth Resources Production Processing Requirements for EREP Electronic Sensors, Document PHO-TR524, Rev A, CH 2, JSC, 18 October 1974.

occurred. The evidence of low magnitude and random sign for the least-squares straight-line slopes suggested that the slopes might be insignificant.

A significance test was derived and reported in MSC-05528, Volume IV, paragraph 12.5.1.4. It was concluded that the slope is insignificant if, during the operating period, the least-squares slope defines a change that is less than one standard deviation of the raw data. In such a case, use of the mean value of R_C or R_{BL} from a data pass would be fully as precise as use of the straight-line function for R_C or R_{BL} during that data pass. Of 26 modes analyzed, only four were found to have significant slopes. Even in those four cases, the gain stability was considered excellent.

3.10.2 Relative Radiometric Accuracy

This performance quality was evaluated for cases in which data from two or more targets of known temperature were acquired. The first opportunity arose during KSC testing, where data were recorded with the radiometer alternately sensing the temperatures of a single-point temperature reference (SPTR) connected to the vertical port of the antenna and a dummy load connected to the horizontal port. The radiometric temperatures of the SPTR and dummy load were calculated to be 318.20°K and 297.04°K, respectively. For the difference in temperature of 21.16°K, radiometer data indicated a difference of 21.40°K. The error was thus only 0.24°K, or 1.1 percent.

Aircraft data for in-flight evaluation of relative radiometric accuracy was available for relatively few targets measured by the radiometer. However, two reasonably homogeneous targets were measured by S193 and an aircraft sensor at times not too far separated to invalidate a comparison. Data from lunar calibration 5 were also used in the comparison because the deep-space target was also of known temperature. To minimize the effects of terrain variations, long-term average values were calculated.

Table 3-6 presents the data used in the evaluation, and Table 3-7 shows the resulting relative radiometric accuracy. Calculated errors were of the same order of magnitude as the uncertainty in the aircraft data, indicating that the relative accuracy was good. The 1°K relative accuracy sought during flight could not be shown with the ground truth data available. However, there is no indication that it did not exist.

Table 3-6   Data Used to Evaluate Relative
Radiometric Accuracy

TARGET	THEORETICAL OR MEASURED TEMPERATURE, MEAN $\pm\sigma$ (°K)	S193 INDICATED TEMPERATURE, MEAN $\pm\sigma$ (°K)
Deep Space	4.0	4.4 ± 1.08
Gulf of Mexico	130 ± 5	137 ± 3
White Sands	238 ± 5	243 ± 1

Table 3-7   Relative Radiometric Accuracy

TARGETS	EXPECTED TEMPERATURE DIFFERENTIAL (°K)	S193 INDICATED TEMPERATURE DIFFERENTIAL (°K)	Δ (°K)
Gulf of Mexico/ Deep Space	126	132.6	+6.6
White Sands/ Gulf of Mexico	108	106.0	-2.0
White Sands/ Deep Space	234	238.6	+4.6

3.10.3 Radiometric Precision

Lunar calibration data from all three missions were used to evaluate radiometric precision. Because of the scarcity of suitable ground truth data, deep space represented the only target of known characteristics that was observed in all missions. Thus, it was used in spite of the fact that the temperature was below the specified operating range. Precision was evaluated by calculating the standard deviation of antenna temperature data sorted according to mode and integration time. Before calculation of standard deviations, raw measurements were corrected to account for insertion-loss temperatures and internal calibrations.

Ten combinations of mode and integration time were analyzed for evaluation of SL2 precision. An average standard deviation of 1.62°K was found, and the largest standard deviation was 3.95°K. Radiometric precision at the lower limit (50°K) of the nominal operating range was extrapolated to be approximately 1°K as desired by preflight design, with poorer precision expected at lower target temperatures. SL2 precision therefore confirmed preflight predictions.

SL3 deep-space data were processed with an improved insertion loss algorithm and mode-dependent integrator equalization constants (described in paragraph 3.9 of this volume). This resulted in lower values for both antenna temperature and standard deviation. These results indicated maintenance of the satisfactory performance measured for SL2.

Standard deviations calculated from SL4 lunar calibration passes were found to be approximately twice the SL3 values. This result was ascribed to a degraded antenna pattern caused by damage to the antenna feed. (See paragraph 4.3.)

3.10.4 Radiometer Linearity and Dynamic Range

Data from the three targets listed in Table 3-6 were used to make a first-order estimate of linearity and dynamic range of the radiometer. When the known target temperatures were plotted against radiometer output voltage, a least-squares straight-line fit to the three points yielded the following equation:

$$T_A = 383.672 - 86.557 \ R \qquad\qquad [3\text{-}4]$$

where

T_A = target temperature, °K

R = radiometer output, volts

Maximum departure of any of the three points from this straight line was found to be 4.3°K.

It can be seen from the Equation 3-4 that radiometer output voltage decreased with increasing **data cell temperature**. The lowest usable output voltage would be the Rad Baseline voltage, which was the minimum output producible by the radiometer processor. Rad Baseline was consistently near 0.35 volt throughout the missions. In accordance with Equation 3-4 this would correspond to a **data cell temperature of 353°K**, which would be the upper limit of the dynamic range. This exactly agrees with the preflight prediction.

3.11 Left Blank Intentionally

3.12 Left Blank Intentionally

3.13 Radiometer Receiver Dynamic Range and Linearity

Baseline values of dynamic range and linearity were established during acceptance testing of the instrument. It was intended that operational values be determined by analysis of radiometer data from targets of precisely known radiometric temperature. Sufficient aircraft data of adequate precision from suitable targets were not available to support a precise analysis. Gross estimates, based on a very limited number of data points, were found as follows:

Dynamic Range - 4 to 353°K

Linearity - within 4.3°K of best straight line over 350°K

3.14 Radiometer Receiver Integration Time

This task included evaluation and analysis of radiometer stability, circulator switching time, antenna loss factor, L_{ANT}, and calibration times. Results were reported in MSC-05528, Volume IV, Section 16.

A preliminary analysis was performed to calculate a value for an insertion loss term for the antenna path to correct computed antenna temperatures, T_A. The calculations used SL2 lunar calibration data. The computed antenna loss term, L_{ANT}, corrected calculated antenna temperatures from a previous mean value of 22°K to a mean of near 4°K. However, a spread of 8 to 12°K remained in T_A values between modes. There was a difference in integration times between modes that could be

attributed to the spread in T_A values. It was also discovered that in the calibration mode during each data sync demodulation signal, a 21.531-microsecond period to allow for proper circulator switching was not removed in the system timing waveforms. This additional period lengthened the integration time during calibration and led to a correction term of 0.844 to be incorporated in the system transfer equation.* However, the 21.531-microsecond period is a difference percentage of each integration period and a blanket 0.844 correction term factor resulted in a wide spread in T_A values calculated between modes. To correct the spread in T_A values, the correction term, 0.844, was recalculated and made mode dependent. The mode (integration-time) dependent correction terms which were calculated using SL-2 and SL-3 data are given in table 3-5.

---

* S193 Historical Logbook, S193 Vehicle 001, Vol 1A, Document No. 72 SD4234 Rev. A, 27 October 1972, General Electric Company, p 3-5.

  Alternate Designation: S193 Calibration Data Report, Flight Hardware, Doc. No. 72 SD4207 Rev. D, 22 March 1973, Prime Unit 1A Volume 1A, SSO Contract NAS9-11195, General Electric.

The use of these correction terms reduced the spread of calculated T_A data to $\pm 2°K$, which was considered acceptable. In addition, the correction terms eliminated the need to correct the integration times as they affected the system transfer equation. Due to this analysis, transfer Equation 3-5 resulted:

$$T_A = 1.11613 \left[T_R + (0.10281)\, T_0 - K \left[\frac{E_{OA}-E_{OB}}{E_{OC}-E_{OB}} \right] \left[T_1 - T_2 \right] \right]$$
$$- (0.07)\, T_{ANT} - (0.1613)\, T_K. \qquad\qquad [3\text{-}5]$$

where

$$T_R = \frac{T_1 + T_2}{2}$$

T_0 = sensor temperature A010

K = correction factor

T_1 = reference load temperature (393.16°K)

T_2 = reference load temperature (318.16°K)

$$T_{ANT} = \frac{A018 + A019 + A053}{3}$$

T_K = 0.177 (A054) + 0.823 (A010)

T_A = antenna radiometric temperature

Equation 3-5 was based on several simplifying assumptions; namely, that all cross-polarization coupling terms are one and all leakage terms are zero. The current PHO-TR524* data processing equation incorporates these cross-polarization coupling and leakage terms. However, if the simplifications are made, the two equations agree.

---

* Earth Resources Production Processing Requirements for EREP Electronic Sensors, Document PHO-TR524 Rev A, Ch 2, JSC, 18 October 1974.

4. SUPPLEMENTARY ANALYSES

This section presents the results of analyses conducted to supplement the basic evaluation effort summarized in Section 3. Analyses of major anomalies, their probable causes, and their effects on sensor performance are reported. Also included are a compilation of anomalous characteristics of the Radiometer/ Scatterometer (Rad/Scat) data, a comparison of S193 scatterometer data with aircraft underflight data, a determination of scatterometer saturation levels, and an evaluation of circulator heating produced by dissipation of transmitter power.

4.1 Pitch Anomaly

An anomaly in antenna gimbaling performance occurred during SL3 at 17:17:10 GMT on DOY 257. Symptoms of the problem were a significant offset of the antenna axis from the intended pointing direction, a grossly degraded scan pattern, and out-of-limits readings from eight housekeeping measurements. One of these measurements (A040) indicated that the -10 Vdc excitation power supply voltage had decreased to -0.98 Vdc. The other seven measurements with anomalous readings (A008, A035, A036, A037, A038, A050, and A058) were found to depend on the -10 Vdc excitation voltage.

Assuming an excitation voltage of -0.98 Vdc for the dependent measurements, circuit analyses produced calculated outputs in close agreement with the postanomaly readings. Further analysis disclosed that the excitation voltage for the gimbal potentiometers was buffered by an operational amplifier, and that a short circuit at the output of this device would bring the power supply voltage to approximately -0.9 Vdc.

The gimbal potentiometers were not in sealed enclosures, and a short occurred in this area during preflight operations when particles of aluminized mylar from an insulation blanket entered one of the potentiometers. The same mechanism was concluded to have caused the in-flight anomaly. Ground tests on the backup S193 instrument were also conducted. Because the instrument was in the ITC mode at the time of the anomaly, with only the pitch gimbal active, the pitch potentiometer was suspected to be shorted.

It was recommended that an extra vehicular activity (EVA) be scheduled early in SL4 to effect a repair. An EVA was conducted on DOY 326. The pitch potentiometer was found to be shorted, and could not be cleared. Preflight planning had allowed for several contingencies. Therefore, the crew cut the excitation lead to this

potentiometer and locked the pitch gimbal at 0 degrees. All measurements that had been anomalous returned to normal values. The repair precluded subsequent operation of in-track modes, eliminated pitch compensation and operation of nadir-align, and prohibited the selection of pitch offsets in cross-track contiguous modes. Thus, for the SL4 mission, the S193 pitch orientation became that of Skylab to within the ±0.5 degrees mounting alignment accuracy of the S193.

4.2   Roll Gimbal Anomaly

During SL4, mission day 009, EREP pass 79, the S193 Rad/Scat antenna roll gimbal drive failed and would not respond normally when commanded to positive (left-of-ground-track) roll angles.

Before day 009, during SL4, the S193 antenna performed several cross-track contiguous (CTC) and cross-track non-contiguous (CTNC) scan maneuvers. Figures 4.2-1 and 4.2-2 present antenna roll-angle position-sensor readings for several scans from a CTC and CTNC S193 maneuver. The antenna was positioned to the proper roll angles within acceptable tolerances. Figures 4.2-3 and 4.2-4 present antenna roll-angle position-sensor readings for CTC and CTNC maneuvers after the gimbal failure. Figures 4.2-3 and 4.2-4 show that the antenna did not scan properly to the left of the track. Analysis of S193 Rad/Scat housekeeping data revealed that during attempted left-of-track scans, no positive roll torquer current was sensed and suggested a component failure in the positive roll-torquer current electronics. Two components were identified that would, if failed, give the observed response.

Analysis of other Rad/Scat maneuvers, than those of day 030, has shown that the antenna positioning was random for positive roll angles. Figures 4.2-5 and 4.2-6 are plots of antenna roll positioning for CTC and CTNC maneuvers on DOY 011, pass 81. Comparison of these points with the points in Figures 4.2-3 and 4.2-4 shows the randomness with which the roll angles were attained during any given pass. The antenna positioning anomalies of SL3 and SL4 have in no manner affected the quality of the Rad/Scat science data, only the angle at which the data were acquired.
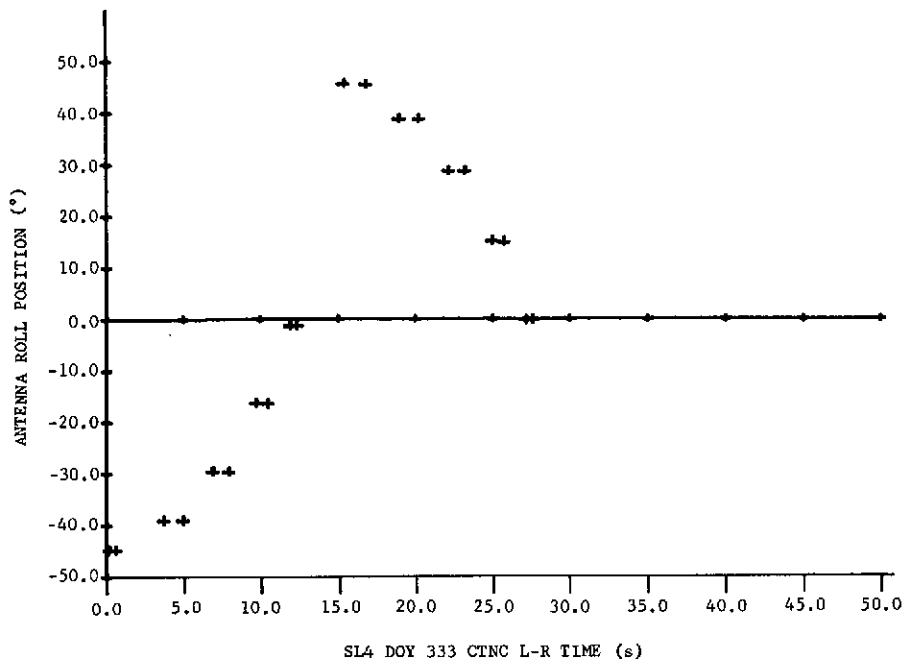
Figure 4.2-1 CTNC Left-Right Mode with Normal Left-Right
Scan Motion
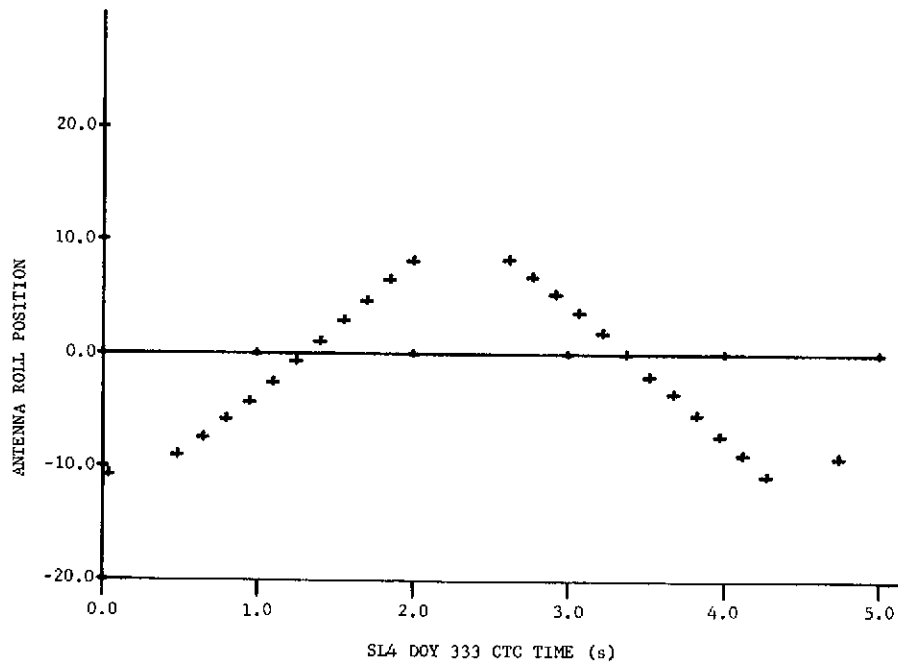
Figure 4.2-2 CTC Mode with Normal 0° Roll Centered Motion
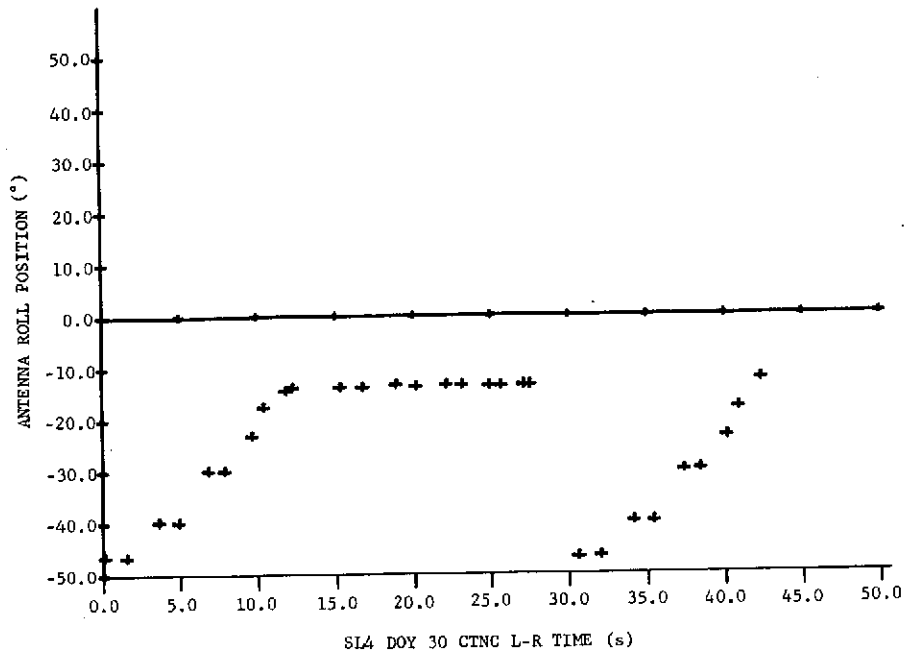
Figure 4.2-3   CTNC Mode with Anomalous Left-Right Scan
                Motion
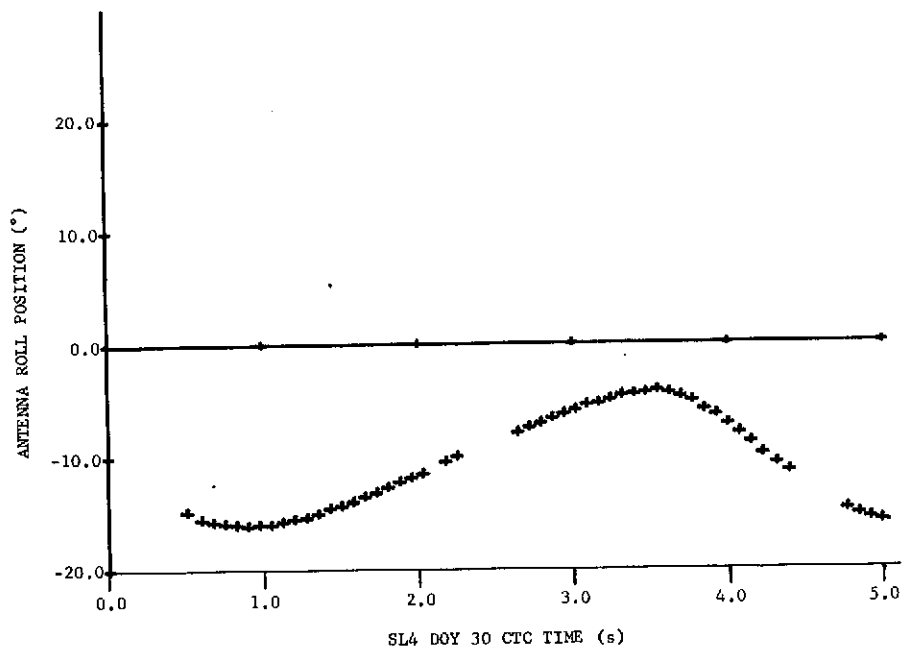
Figure 4.2-4   CTC Mode with Anomalous Scan Operation about
                a Commanded 0° Roll Bias
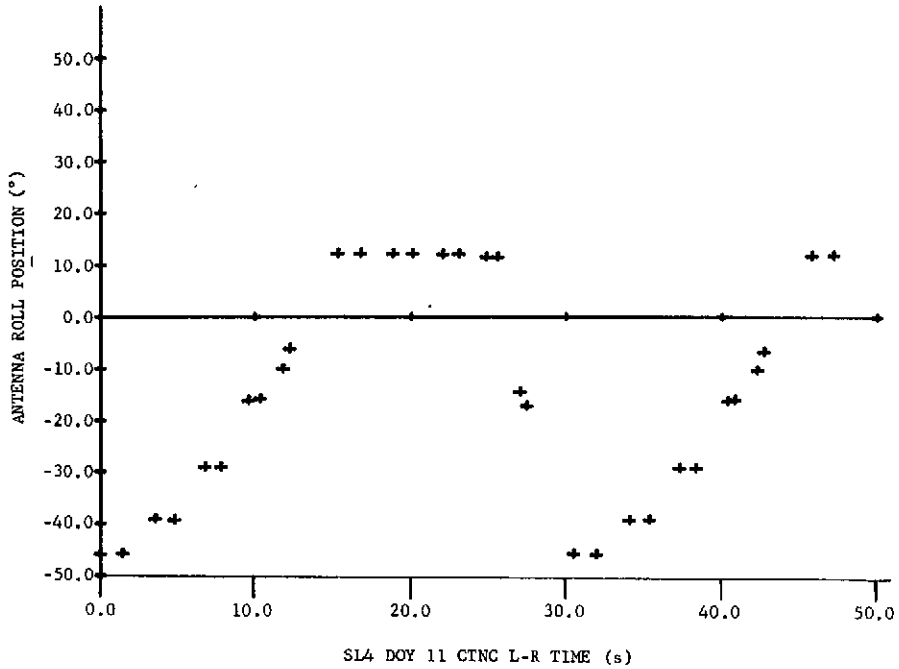
Figure 4.2-5 CTNC Mode with Anomalous Left-Right Scan Motion
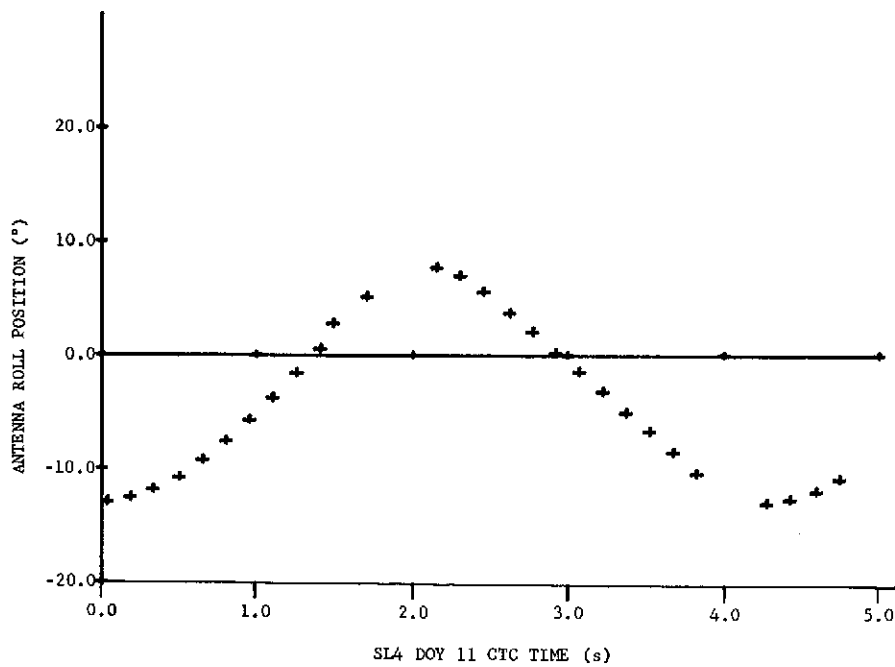
Figure 4.2-6 CTC Mode with Anomalous Scan Operation about
a Commanded 0° Roll Bias

4.3 Antenna Pattern Variation

4.3.1 Antenna Pattern Measurements

Antenna pattern cuts were measured by G.E.* before SL2 and by JSC after SL4, using the backup antenna. G.E. measured both the flight and backup antennas. The JSC patterns were made using the backup antenna adjusted to represent both the SL2 and SL4 configurations of the flight antenna. In-flight measurements of the antenna pattern by the University of Kansas APEX (See MSC-05546, Volume IV, Appendix A, Section III.) were used to guide the postflight antenna measurements by JSC.

Table 4.3-1 Antenna-Pattern Principal-Axis Cuts, Vertical Polarization

	G.E. (w feed cup)		JSC (w feed cup)		JSC (w/o feed cup)	
	E plane	H plane	E plane	H plane	E plane	H plane
3 dB BW	1.5	2.0	1.5	2.0	2.7	2.0
10 dB BW	2.5	3.5	2.5	3.8	4.2	4.5
1st SL	-20 dB	-27 dB	-25 dB	-28 dB	-16 dB	-16 dB
Residual Sidelobes	-38 dB	-38 dB	-37 dB	-37 dB	See plots.	

Figures 4.3-1 through 4.3-6 are 360-degree plots of the principal-plane cuts for the G.E. and JSC measurements. There are some differences, as shown in Table 4.3-1, which lists some characteristics of the principal-plane cuts. The major differences appear to be in sidelobe levels, with the main beam shape matching closely down to the 10-dB points. For the first sidelobe levels, a difference of about 5 dB was noted in the E-plane cut and only about 1 dB in the H-plane cut. These differences can be accounted for by the new feed applied to the

---

* S193 Microwave Radiometer/Scatterometer/Altimeter, Calibration Data Report, Flight Hardware, Vol II, Revision B, General Electric, 31 July 1972.

Skylab S193 Radiometer/Scatterometer/Altimeter Sensor Antenna Testing Results, Job Order 16-604, Lockheed Electronics Company, Inc. Aerospace Systems Division, Houston, Texas, Contract NAS9-12200.
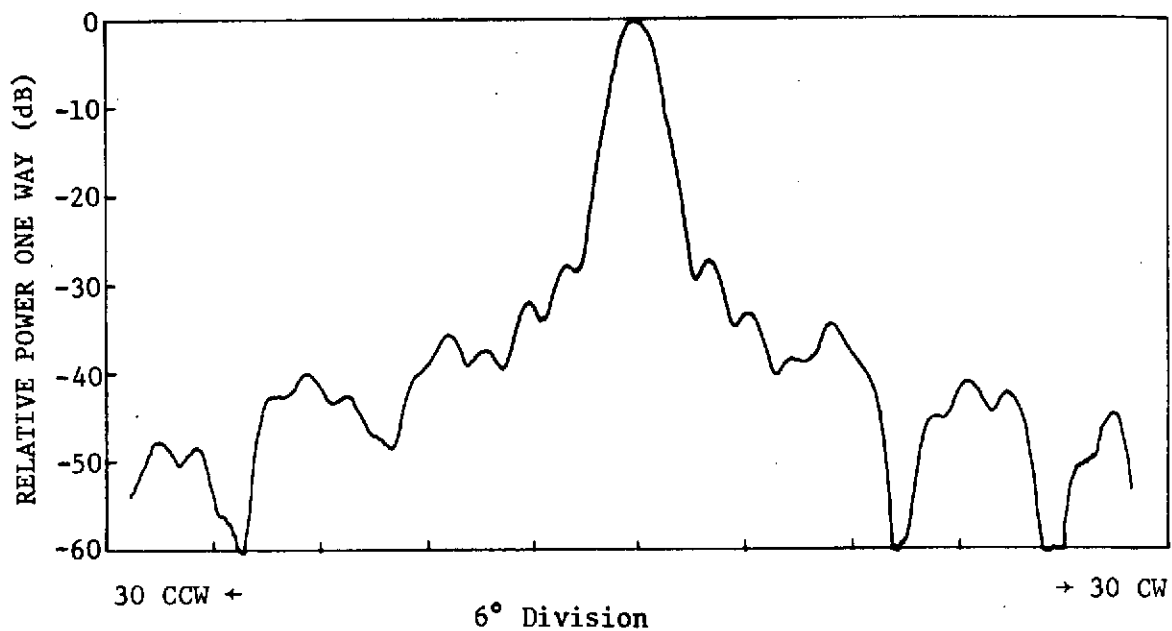
4.3-1 H-Plane Cut, GE
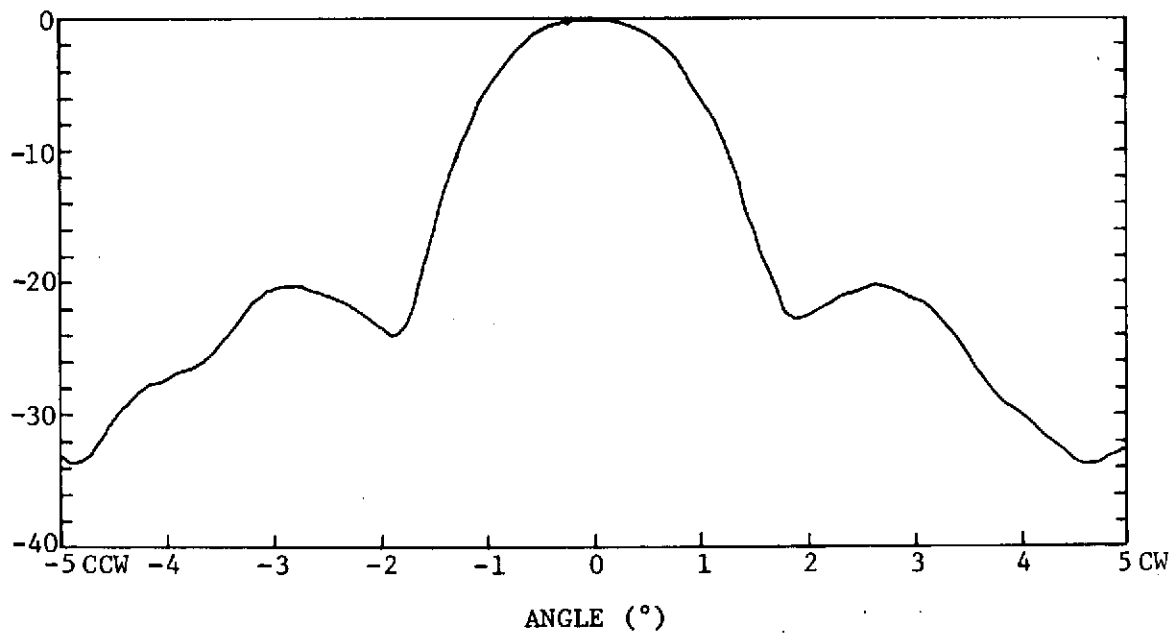
Figure 4.3-2 E-Plane Cut, GE
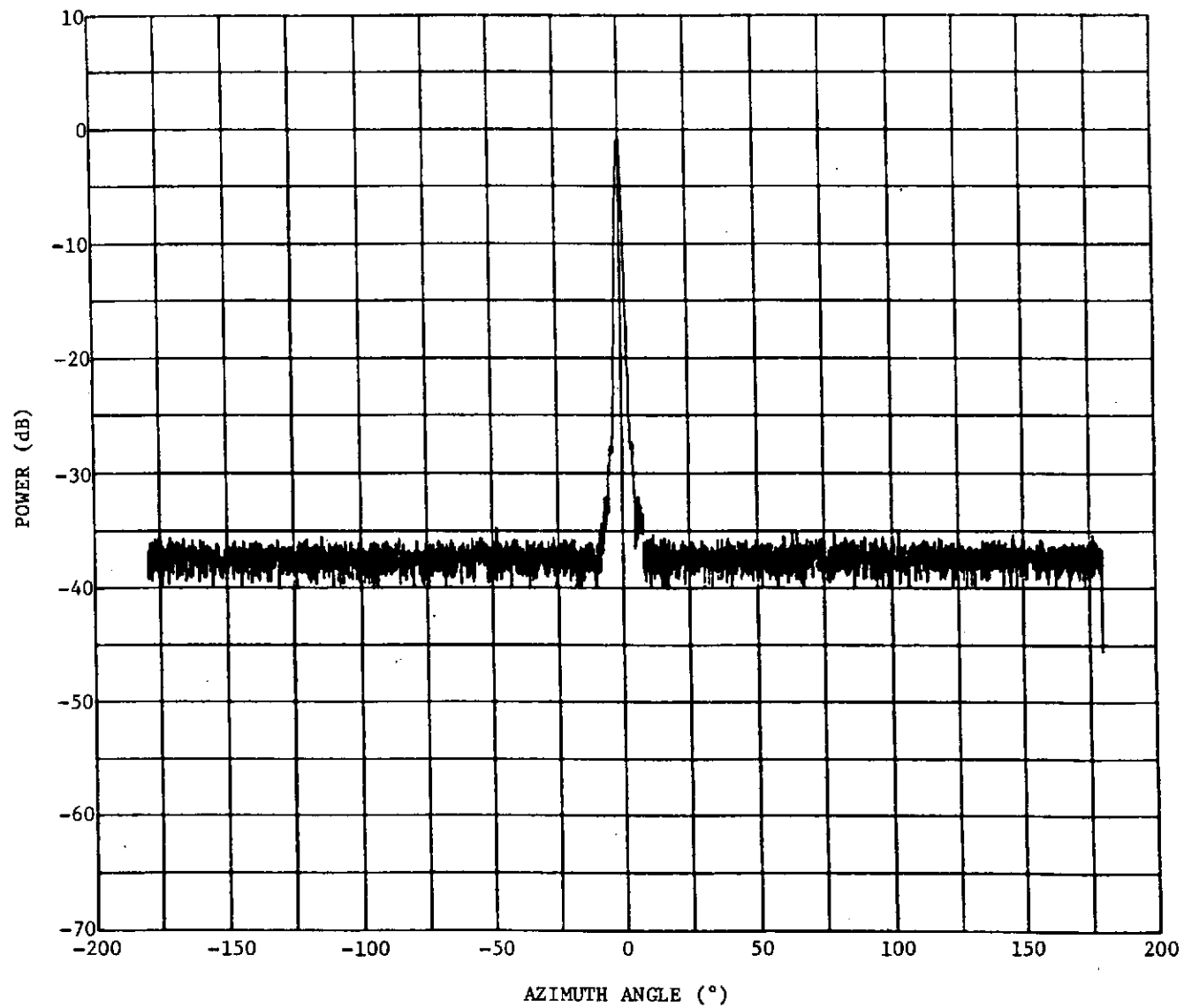
Figure 4.3-3 H-Plane Cut, JSC Feed Cup On
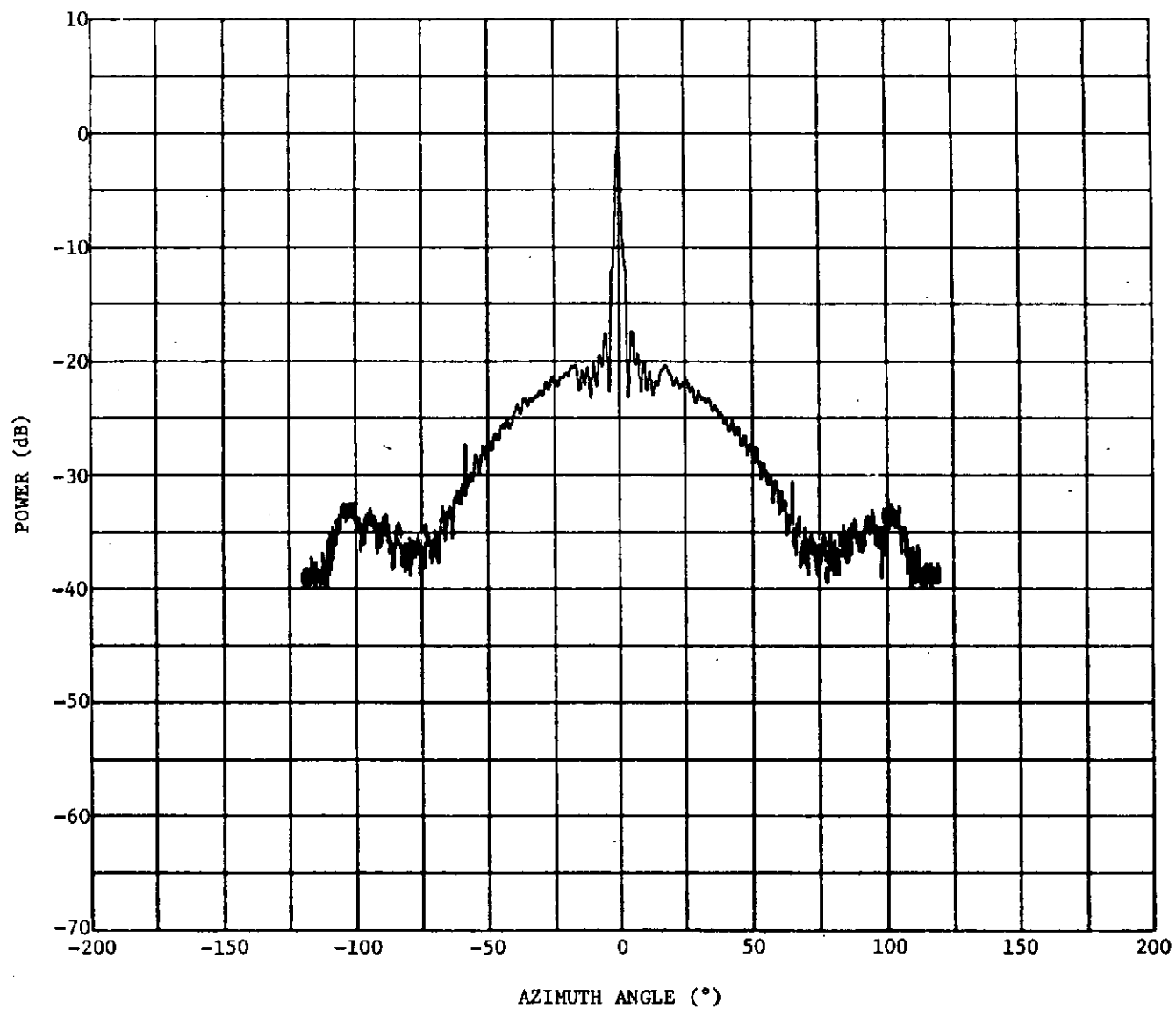
Figure 4.3-4 E-Plane Cut, JSC Feed Cup Off
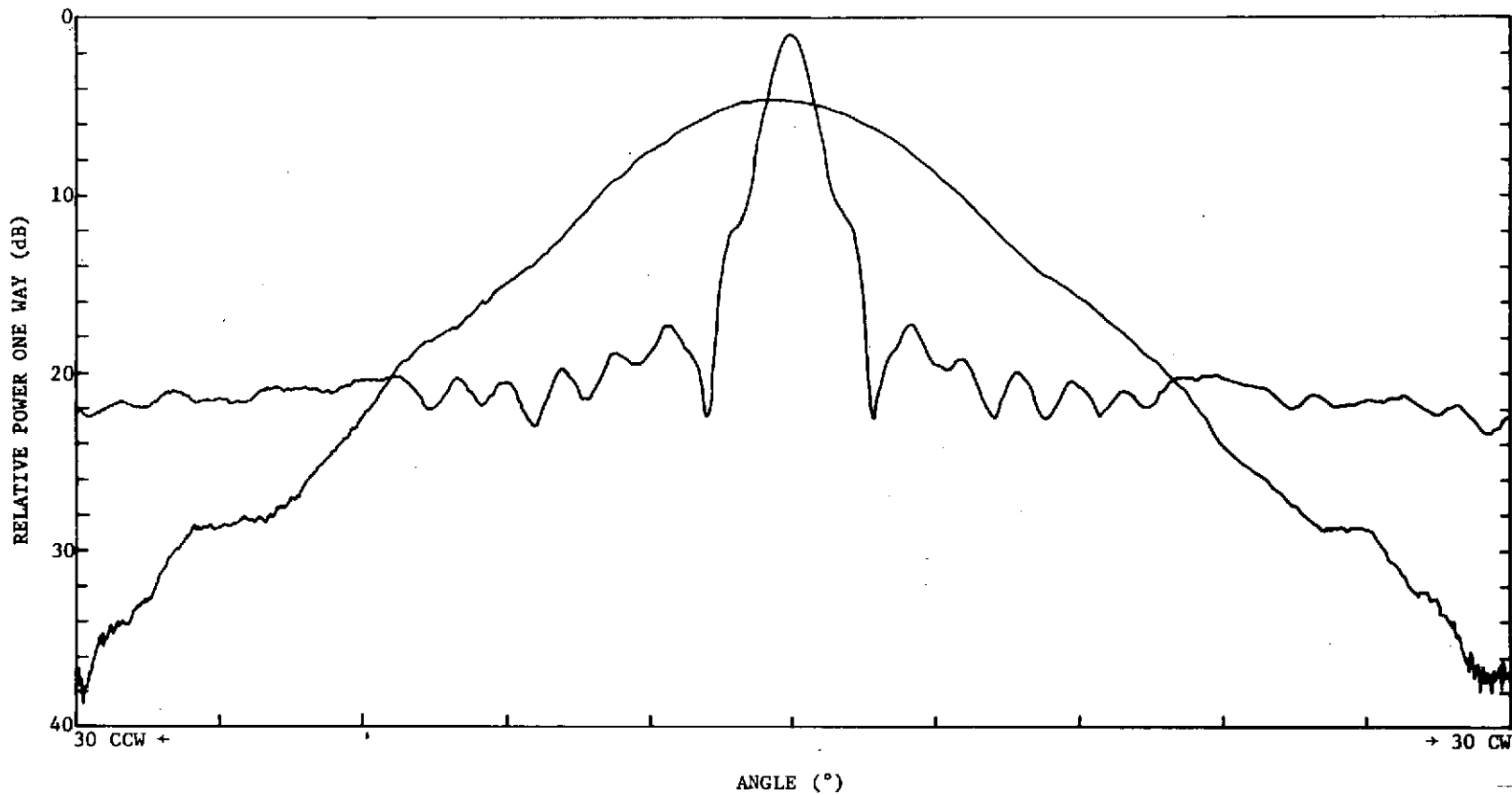
6° Division

Figure 4.3-5 H-Plane Cut, JSC Comparison with Standard-Gain Horn, Feed Cup Removed
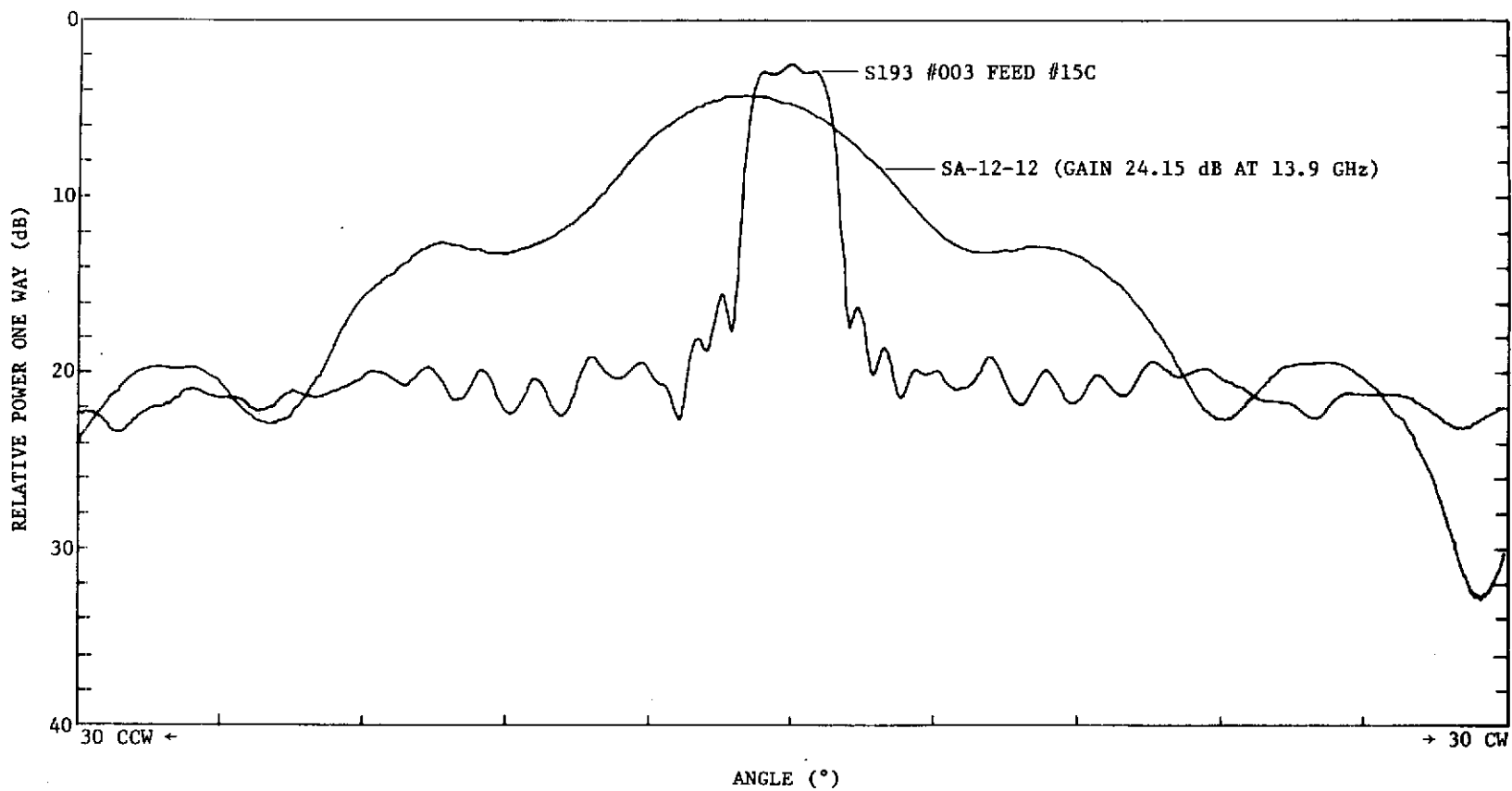
6° Division
Figure 4.3-6   E-Plane Cut, JSC Comparison with Standard Gain Horn, Feed Cup Removed

IV-54

MSC-05546

antenna before testing at JSC and possibly to some range differences. To simulate antenna conditions for SL4, patterns were also cut at JSC with the feed cup removed. In this case, the main beam was widened somewhat, as shown in Figure 4.3-4 compared to 4.3-3, but the major difference is again in the higher sidelobes.

Gain measurements were taken on the antenna boresight (pattern peak gain) by G.E. with the feed cup in place and by JSC with the cup removed. Gain loss due to the missing feed cup, assuming the two measurements were comparable to the flight antenna, was 13.1 dB when driving the vertical port and 15.3 dB when the horizontal port was driven. (See Table 4.3-2.) In-flight measurements with APEX had given a preliminary indication of a gain loss on the order of 13 dB. The JSC cuts were taken every 22.5 degrees, rotating the antenna for each cut around the boresight axis of the antenna so that each cut ran through the peak gain point on the antenna. G.E. cuts were taken in azimuth for various elevation angles in elevation steps of 0.1 degree. In both antenna tests, cross-polarization plots and dominant-polarization plots were developed. Both vertical and horizontal ports were driven. Complete patterns are given in the reports cited.

Table 4.3-2 Antenna Peak Gain with and without Feed Cup

	G.E. (w feed cup) (dB)	JSC (w/o feed cup) (dB)	Gain Loss in SL4 (dB)
Vertical Feed	41.1	28.0	13.1
Horizontal Feed	41.3	26.0	15.3

4.3.2 Brightness Temperature Variation with Aspect Angle

During SL4, the signal power of the altimeter and scatterometer experienced a drop of about 24 dB. It was concluded that this drop of power was due to the loss of the feed cup on the S193 antenna during SL4. Also, during SL4, it was noted that the separation of the radiometric temperatures from the two polarizations (radiometric temperatures T_{AV} and T_{AH}) decreased at large scan (look) angles for SL4 data compared to SL2 and SL3. Figure 4.3-7 shows T_A versus look angle for a nominal data sweep of the S193 radiometer for a pass in SL3 (before antenna failure) and a pass in SL4 (after antenna failure). Both data takes were
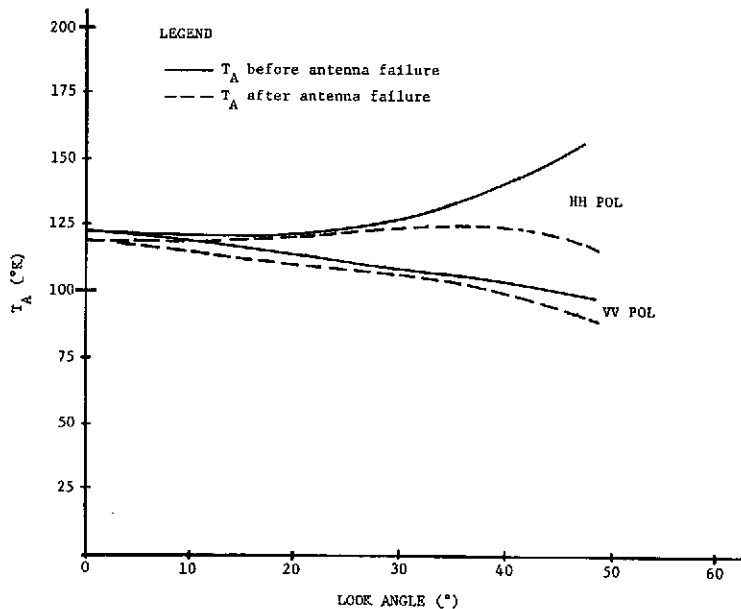
Figure 4.3-7 T_A versus Look Angle before and after
Antenna Failure, S193 Measured Data

over sea targets that were assumed to be uniform and similarly smooth. This variation in the polarization separation of T_A at large scan angles was not seen in either the SL2 or SL3 missions. Therefore, an effort was made to verify that the difference in T_A for SL4 was due to the degraded antenna pattern caused by the missing feed cup during SL4. The high sidelobes from the SL4 broken feed antenna would have a dominant contribution to T_A, whereas before, the sidelobes were sufficiently down to conclude that they made little contribution to T_A. However, before concluding that the antenna pattern change caused the temperature thermal change, there were questions to be answered. Three of these were:

1) If the cause for the reduced separation between the values was due to the increased large "bulbous" sidelobes, why were not both polarizations affected and tend toward the T_A value of the nadir orientation because a significant portion of the

antenna pattern would always view the nadir point and be independent of view angle?

2) Could the apparent polarization-sensitive change have been due to leakage or some failure of the polarization circulator? (The existence of the separation itself was taken to indicate that the polarization circulator was switching properly.)

3) Did the analysis properly account for polarization mixing contributing to the measured temperatures at angles off nadir?

Because of these questions, a computer program, using the antenna patterns before antenna failure and after antenna failure, was developed to determine whether the resulting simulated T_A curves would behave like those seen in the SL3 and SL4 missions (Figure 4.3-7). The antenna pattern itself is discussed in paragraph 4.3.1.

The computer program developed assumed a uniform flat-earth sea target. The results of this program are given in Figure 4.3-8. The computed curves in Figure 4.3-8 have the same relative shape and trends for the two different polarization values of T_A as those in Figure 4.3-7 which were measured by S193. One of the major differences between the measured and computed curves is the look angles at which the H polarization data turns down. This was believed to be a result of the round-earth measurement versus the flat-earth computation. Comparing the measured and the simulated brightness temperatures from the preliminary model, it was concluded that the T_A perturbation in SL4 was caused solely by the antenna failure, and that the H polarized downturn of T_A during SL4 must be due to the higher sidelobes. [1]/

The equations and geometry used in the calculation of T_A were taken from Claasson and Fung.* The assumed target brightness temperature curves used were taken from Swift†, using the polarized data at a frequency of 8.4 GHz based on Hollinger's smooth-water

---

* John P. Claasson and Adrian K. Fung: "The Recovery of Polarized Apparent Temperature Distributions of Flat Scenes from Antenna Temperature Measurements," IEEE Transactions on Antenna and Propagation, Vol Ap-22, No. 3, May 1974, p 433-441.

† C. T. Swift: "Multifrequency Radiometric Measurement of a Rough Water Surface," presented at the 1973 USNC/URSI Meeting and IEEE/G-AP International Symposium, Boulder, Colorado, August 21-23, 1973.

[1]/ A degraded impedence match was measured for the broken-feed antenna at JSC. This degraded impedence match plus any asymmetry in the broken-feed quartz-to-space boundary would introduce additional polarization mixing. It is very likely that antenna mismatch and/or asymmetry contributed to the decreased separation between vertically and horizontally polarized data.
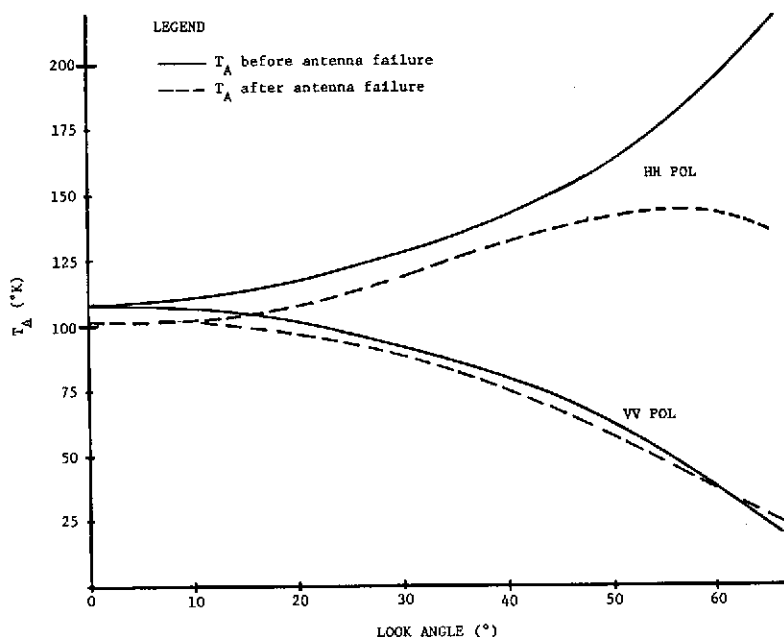
Figure 4.3-8 T_A versus Look Angle, Computer-Predicted
T_As for before and after Antenna Failure
Patterns

data.   The preliminary model was believed sufficient for the task,
and thus no improvement of the simulation was attempted to more
exactly match the data obtained during SL4.

4.3.3   Rad/Scat Interaction

To determine whether energy from the scatterometer transmitter
was coupled into the radiometer measurements, radiometer measurements
of deep space during consecutive CTC Rad Only and CTC Rad/Scat
operation were compared.   Table 4.3-3 lists comparison data of average
antenna temperatures and standard deviations for CTC Rad Only and CTC
Rad/Scat runs from SL2 lunar cal #1 and SL3 lunar cal #3.   The data
presented are averaged over an entire data run for each mode listed.
Analysis of the data in Table 4.3-3 indicated that there was no effect
on Rad data attributable to the Scat transmitter.   It should be noted
that data from SL4 lunar cal #4 was inconclusive in determining Rad/
Scat interaction.   The unexpected problem encountered was that T_A

calculated from CTC Rad/Scat data during SL4 was considerably lower
in temperature, with larger standard deviations than any previously

encountered. It is believed that the antenna anomalies discussed
in paragraphs 4.3.1 and 4.3.2 produced these effects.

Table 4.3-3 Rad Only to Rad/Scat
Performance Comparison

	DOY	MODE	T_A (°K)	σ
SL2	165	CTC R/O	3.7	1.1
	165	CTC R/S	3.5	1.1
SL3	254	CTC R/O	3.3	0.91
	254	CTC R/S	4.4	0.94

4.4 Format and Parameter Comments

Many anomalous characteristics in the Rad/Scat data were
discovered during system test and sensor performance evaluation.
Some of these were found to be caused by malfunctions, some were
due to design peculiarities, and some were the result of performance
deficiencies. All these characteristics, together with some
documented before the Skylab missions, were compiled for the
guidance of S193 data users.

In the following list, qualities and characteristics are listed
in the form of comments under affected parameters. These items may
repeat some of the cautionary data notes in the calibration data
report.* However, this listing is supplementary to that report for
inclusion of items identified after its publication. Each parameter
is identified by measurement number, title, and format location, and
pertinent paragraphs in MSC-05528, Volume IV, are cited.

---

* S193 Historical Logbook, S193 Vehicle 001, Vol 1A, Document
No. 72 SD4234 Rev. A, 27 October 1972, General Electric
Company.

Alternate Designation: S193 Calibration Data Report, Flight
Hardware, Doc. No. 72 SD4207 Rev. D, 22 March 1973, Prime
Unit 1A Volume 1A, SSO Contract NAS9-11195, General Electric.

A008 - Rad AGC - Subframe 1, word 24 - para 3.4.4.2

1. Saturates when Rad is operated immediately after altimeter or CTC Scat mode; recovers in about 30 seconds; problem alleviated in SL3 and SL4 by procedure change.

2. Not a sensitive indication of gain state of radiometer.

3. Invalid readings from 257:17:17:10 to 263:14:31:30 because of shorted -10 V excitation bus.

A046 - Scat TWTA Collector Current - Subframe 3, word 42 - para 3.3.4

1. Undersampled; usable for instantaneous values, not for waveform reconstruction.

A061 - Pitch Gimbal Angle - All subframes, words 7, 17, 27, 37, 47 - para 3.4.1
A062 - Roll Gimbal Angle - All subframes, words 8, 18, 28, 38, 48 - para 3.4.1

1. Maximum angles are 2 to 6 degrees less than commanded angles because of flex harness stiffness, i.e., commanded 48 degrees resulted in 42 to 46 degrees.

2. Data invalid at times of Rad Cal, Rad Baseline, and Scat Cal.

3. Subtract on-orbit-alignment biases (A050 and A058) from readings to obtain angles with respect to nadir following a nadir align mode.

4. In ITC mode, pitch motion is nonlinear during initial and final portions of each scan cycle (approximately 48 to 41 degrees and 2 to 0 degrees).

5. Pitch locked near 0 degrees for SL4 following malfunction at 257:17:17:10 in SL3; eliminated use of in-track modes in SL4, and prevented operation of pitch compensation in CTC modes.

6. Roll malfunction at 009:15:55:48 restricted scan to right of track (negative roll angles) for balance of SL4.

7. Time tagged to these data may be as much as 18.75 ms later than the time the measurements were sampled.

8. Pitch and roll values recorded in this S193 R/S data stream corresponded to the gimbal positions at the time of the pitch and roll buffer updates. The pitch and roll positions were updated after each science measurement. The pitch and roll readouts were corrected by TR524 production data processing to represent the gimbal positions at the time of the science measurement.

A035 - Pitch Command Position - Subframe 3, word 13 - para 3.3.4
A036 - Roll Command Position - Subframe 3, word 14 - para 3.3.4
A037 - Pitch Torquer Current - Subframe 3, word 21 - para 3.3.4
A038 - Roll Torquer Current - Subframe 3, word 22 - para 3.3.4
A050 - OOA Pitch Bias - Subframe 4, word 12 - para 3.3.4
A058 - OOA Roll Bias - Subframe 4, word 32 - para 3.3.4

1. Invalid readings from 257:17:17:10 to 263:14:31:30 because of shorted -10 V excitation bus.

A002-A060 - All housekeeping measurements - para 3.3

1. May erroneously indicate either 0 or 2.5 V when a science word takes priority at A-to-D converter.

B003E - Gimbal Malfunction - Subframe 4, word 43, bit 5 - para 3.1

1. Often indicated malfunction when attempting to overcome resistance due to excessive flex harness stiffness near extremes of gimbal travel.

D005A,B - Scat Gain - All subframes, words 5, 15, 25, 35, 45 -
          bits 1, 2 - para 3.2.1

1. Erroneous values may be indicated when repeated-status-word anomalies occur. (Values will be in error by increments of approximately 10 dB.)

2. When Scat and Scat Noise appear in consecutive words (CTC-S mode), indicates gain during Scat measurement.

3. Maximum gain always used for Scat Noise.

4. Minimum gain always used for Scat Cal.

D005C,D,E,F - Command Angle - All subframes, words 5, 15, 25, 35, 45 - bits 3, 4, 5, 6 - para 3.2

1. In CTC-R/S mode, may erroneously repeat previous sample values. When present, this error tends to occur at 159-second intervals.

2. At time of Scat Cal, indicates:

   a. 0000 in all NC modes and ITC

   b. 1000 in CTC modes

3. In ITC-R/S modes, incorrect values can occur.

4. Starts at 0000 in all CTC modes regardless of whether a scan is to the right or to the left. Use roll gimbal angle (A062) to determine direction of scan.

5. In ITC-R/S modes, the command angle is just a measurement counter. Use pitch gimbal angle (A061) to determine angle for Scat doppler filter gain corrections. The number of Rad measurements can vary because of logic circuitry design.

6. In CTNC-R/S modes, command angle does not indicate whether the scan is to the right or to the left; use roll gimbal (A062) to determine direction of scan.

D006A,B - Filter/Integrator - All subframes, words 6, 16, 26, 36, 46 - bits 1, 2 - para 3.5

1. Scat Noise measurement uses the same Filter/Integrator setting as the last previous Scat measurement.

2. When Scat Noise and Rad appear in consecutive words (all NC modes and CTC-R/S) the Filter/Integrator is set for the Scat Noise measurement.

3. In ITNC and CTNC-R/S modes using sequencing polarization (#5), because of data sequence, the Filter/Integrator for Scat Noise may not be the same as for the Scat with the same receive polarization.

4. Only indicates which of the three filters (LCF, MCF, HCF) was automatically selected on the basis of strongest signal from the filter bank selected by pitch gimbal angle.

5. During Rad, Rad Baseline and Rad Cal measurements, reads the setting from the last Scat, Scat Noise, or Scat Cal measurement.

6. Always reads 00 in CTC-R mode.

7. Reads 00 at time of Scat Cal.

D006I,J – Polarization – All subframes, words 6, 16, 26, 36, 46 – bits 9, 10 – para 3.2.4

1. In CTC-R mode, at time of Rad Cal and Rad Baseline, indicates C&D panel polarization selection.

2. Order of polarization:

   D006I – Receive polarization
   D006J – Transmit polarization

3. The science data polarization could be changed during a pass by selecting the desired polarization on the C&D panel without placing the sensor power switches in STANDBY and then back to ON. Invalid data may be recorded during time of polarization change.

4. The polarization readout in the data for nonsequencing polarization operations reflects the C&D panel switch position and does not indicate the condition of the polarization circulator. In sequencing polarization modes, readout reflects polarization logic commands and does not indicate the condition of the polarization circulator. If proper switching procedures were followed, however, the circulator polarization agrees with the switch and logic commands.

5. The polarization readout identifies the receive/transmit polarization with respect to the S193 antenna; V and H are the identifications of the paths in the instrument and are orthogonal to each other. The true polarization with respect to the surface of the earth must be determined from pointing information (pitch, roll, and SKYBET). In CTNC, and CTC with zero pitch offset, the true polarization is approximately the reverse of the indicated polarization. In in-track modes, the indicated polarization is approximately correct. In CTC with pitch offset, the relationship between indicated and true polarizations is complex.

Rad Cal - Any subframe, words 10, 20, 30, 40 or 50 - para 3.4.4

1. Indicates radiometer gain (proportional to T1 minus T2).

2. No Rad AGC hold during Altimeter and Scat Only modes, causing Rad AGC to saturate. When Rad AGC is driven to saturation, the Rad and Rad Cal values track the gain state. Rad data are recoverable by proper use of calibration data.

3. Erroneous values may be produced by turn-off switching transients.

4. Instantaneous values are random samples from a gaussian population. Statistical techniques must be employed to predict the best value of Rad Cal for determination of gain. Mean values or straight-line fit trend values have been shown to be the best to use.

5. Insensitive to processor temperature.

D005, 006 - Status Words - All subframes, words 5-6, 15-16, 25-26, 35-36, 45-46 - para 3.2.4

1. Logic race problem can cause the status word, or some portion of it, to repeat a previous value thereby incorrectly identifying the status of the new science measurement. When present, the problem occurs at beat frequencies between telemetry and science acquisition rates. The period of occurrence is mode dependent:

    a. CTC-R/S - 15 scan cycles (31.8 seconds)
       75 scan cycles (159 seconds)

    b. ITC-R/S - 3 scan cycles (12 seconds)
       6 scan cycles (24 seconds)

    c. ITNC-R/S   - 3 scan cycles (45.75 seconds)
       or CTNC-R/S

    When any of these anomalies occur, the roll angle readout will show the previous value instead of the proper value for the science data point for which the status word is in error.

Scat Cal 1 - Any subframe, word 9, 19, 29, 39, or 49 - para 3.4.2, 3.4.3

Scat Cal 2 – Any subframe, word 10, 20, 30, 40, or 50 – para
3.4.2, 3.4.3

1. First occurrence in a mode is in the first scan cycle;
   subsequent occurrences are as follows:

   a. All NC modes – Next 0-degree sequence occurring after
      256 seconds have elapsed since first Scat Cal; each 17th
      scan cycle.

   b. ITC mode – Next 15.6-degree sequence occurring after
      239 seconds have elapsed since first Scat Cal; each 60th
      scan cycle.

   c. CTC modes – Next 9th through 11th command angle occurring
      after 201 seconds have elapsed since first Scat Cal; each
      96th scan cycle.

2. Scat Cal 1 uses lower center frequency filter; Scat Cal 2
   uses middle center frequency filter.

3. Strong correlation indicated between Scat Cal and Scat
   processor temperature (A012).

Rad Science Data – All subframes, words 10, 20, 30, 40, 50 – para
12, 13

1. Rad processor gain is proportional to difference of reference
   temperatures (A030 minus A029).

2. Rad Cal is also proportional to this difference of temperatures
   and, thus, is used to establish the gain of the radiometer.

3. Rad AGC (A008) is not a sensitive indication of radiometer
   gain.

4. Rad processor gain is insensitive to processor temperature
   changes.

5. Rad Cal is a radiometric measurement and thus exhibits random
   variations. Least-squares straight lines fit to the Rad Cal
   samples recorded during an operation time slice are the
   preferred estimate of gain.

6. Measures relative temperature difference between antenna
   temperature and reference temperature as seen at the input to
   the receiver (TDA). Data correctable to the antenna aperture
   using insertion loss and data-stream front-end component-
   temperature values.

using insertion loss and data-stream front-end component-temperature values.

7. Rad AGC(A008) saturates during Altimeter and Scat Only modes because there is no AGC hold signal during these modes. Radiometer operation following AGC saturation records Rad Cal and Rad values which track the saturation. The Radiometer recovers from AGC saturation in approximately 30 seconds in an exponential fashion. To recover Rad data recorded during saturation recovery, a curve (rather than a straight line) should be fit to Rad Cal data.

8. Invalid data may be recorded while polarization selection is being changed at the C&D panel.

9. The antenna feed cup was found to be missing for the entire SL4 mission. The antenna pattern was altered; in particular, there was a significant increase in the sidelobes. This causes radiometric temperature to be integrated over a much larger solid angle, and special processing techniques must be used to recover SL4 Rad data.

10. K-factors have been derived to reconcile mean values recorded in different modes while a homogeneous target was observed. The K-factors are integrator-time-constant dependent.

11. Time tagged to these data may be as much as 18.75 ms later than the time the measurements were sampled.

12. Time correlation with gimbal angle data is described in comment 8 under pitch and roll gimbal angles.

Scat Science Data - All subframes, words 9, 19, 29, 39, 49

1. Scat processor gain appears to vary as a function of Scat Processor Temperature (A012). Scat, Scat Noise, and Scat Cal have demonstrated high correlation with processor temperature.

2. In noncontiguous Rad/Scat modes using sequencing polarization, the filter/integrator setting for Scat Noise may be different from the setting for the Scat measurement having the same receive polarization.

3. Invalid data may be recorded while polarization selection is being changed at the C&D panel.

4. Invalid data may be recorded during the first scan cycle prior to Scat Cal.

5. During Lunar Cal modes, Scat is the same as Scat Noise because there are no return signals.

6. Scat measurements are the integrated return of a series of pulses, the number of pulses depending on the mode and angle. The gain state of the Scatterometer is set by comparison of the integrated voltage of each of the first three return pulses to a reference voltage. Gain is initialized at the highest state for each measurement and is reduced in 10-dB steps until the correct gain is selected. Certain changes in target characteristics after gain selection can cause either saturation or an incorrect value to be recorded for that measurement.

7. In CTC Scat Only modes, Scat readout is delayed until Scat Noise is developed and both are read out together. Pitch, roll, and time values are those corresponding to scat noise buffer update (this has been corrected in JSC data processing).

8. The pitch gimbal did not attain the maximum commanded angle (48 degrees) in the ITC-R/S mode because of excessive stiffness of the flex harness in the flight environment. The doppler-shifted return signal is on the skirt of the LCF filter for the Scat measurement at that angle. A change in data processing to correct this error has been implemented by JSC. However, the change is not completely effective.

9. The antenna feed cup was found to be missing for the entire SL4 mission. The antenna pattern was significantly altered and main beam gain was reduced approximately 12 dB. To recover normalized backscatter from the SL4 Scat data, the antenna pattern measured for the backup antenna with feed cup removed should be incorporated.

10. It has been shown by analyses of Lunar Cal data that to make the Scat and Scat Noise data reflect the same calibration base, certain Scat Noise integration times must be changed. These appear in this report (paragraph 3.8) and are incorporated in the JSC production data processing.

11. The transfer function for correcting the recorded Scat data to the integrator input was improved during the in-flight performance analysis. See paragraph 3.8 of this volume.

12. Time tagged to these data may be as much as 18.75 ms later than the time the measurements were sampled.

13. Time correlation with gimbal angle data is described in comment 8 under pitch and roll gimbal angles.

4.5 Scatterometer Backscatter Analysis

4.5.1 Aircraft Data Comparison

EREP pass 5 (DOY 156) of SL2 over the Great Salt Lake Desert (site 116) was selected as one of the "known" targets for this analysis. The aircraft underflight was made the day after the Skylab pass (Skylab on DOY 156, aircraft on DOY 157). A summary of the aircraft data is in Appendix A of MSC-05528, Volume IV and in Table 4.5-1. The aircraft backscatter data in the table were taken with a 13.3-GHz scatterometer that had a wide beam (±60 degrees) fore and aft and a narrow beam (approximately 3 degrees) across the flight path. Backscatter values as a function of incidence angle were derived by sorting the total return by doppler frequency. The aircraft altitude remained relatively constant throughout the flight (See Table 4.5-1.) at 3000 to 3100 feet. Figure 4.5-1 is a map of the Great Salt Lake Desert (site 116) that also shows the aircraft underflight path and the Skylab path with the S193 scatterometer footprints. (The aircraft flight path was directly over the Skylab flight path but in the opposite direction.) The footprint of the aircraft scatterometer antenna pattern (3 degrees) was approximately 158 feet wide on the ground. The S193 footprint was approximately 6 nautical miles wide, as seen in Figure 4.5-1. With this large difference in footprint size, caution should be taken in comparing an aircraft to a Skylab backscatter cell. Because of the homogenous area required by Skylab S193 scanning, the footprint locations were much more critical on land than they were on the sea.

A plot of the Skylab S193 backscatter versus time (GMT) over the Great Salt Lake Desert (site 116) is shown in Figure 4.5-2. Table 4.5-2 shows S193 backscatter versus angle of incidence, and Figure 4.5-3 is a plot of the S193 backscatter versus incidence angle over the site for all data taken over that site. The S193 Rad/Scat was in the CTC mode over the site. Therefore, the maximum incidence angle obtained was less than 10 degrees, whereas the aircraft data start at ±5 degrees and go to ±60 degrees in 5-degree increments. No aircraft data were processed between 0 and ±5 degrees, which meant that only incidence angles at 5 and 10 degrees could be used in this comparison. With Skylab at a nominal altitude of 238.6 nautical miles (442.14 km) over the ground sites, actual ground footprint locations of the S193 for incidence angles between 5 and 10 degrees

Table 4.5-1 Aircraft Support Data for Great Salt Lake Desert, DOY 157

| START TIME 20-s Int | Incidence Angle (°) (σ_o dB) | | | | | | | | | | | | NUMBER OF POINTS | APPROX. AIRCRAFT ALTITUDE (ft) |
| | 5° | | 10° | | 20° | | 30° | | 40° | | 50° | | | |
	σ_o	Std Dev	σ_o	Std Dev	σ_o	Std Dev	σ_o	Std Dev	σ_o	Std Dev	σ_o	Std Dev		
15:21:45	-0.73	1.99	-3.72	1.29	-2.22	1.26	-8.89	0.95	-7.75	0.93	-12.62	0.80	3	3060
22:05	-2.91	2.10	-3.81	2.41	-3.34	1.72	-9.00	2.29	-8.03	1.59	-12.51	2.46	11	3065
22:25	-4.30	0.99	-4.14	1.59	-2.41	1.49	-7.49	2.21	-5.14	2.87	-10.74	3.52	16	3065
22:45	-4.15	1.33	-4.67	1.58	-3.29	1.92	-8.13	2.14	-6.32	2.63	-10.70	1.80	15	3070
23:05	-5.99	1.93	-6.15	1.32	-3.50	1.24	-7.94	1.57	-6.58	1.70	-11.66	1.69	15	3070
23:25	-10.46	1.63	-8.77	0.71	-2.48	1.40	-5.84	1.99	-3.63	1.49	-6.55	2.69	10	3000
23:45	-11.28	0.20	-8.03	0.09	-1.08	0.53	-2.58	0.18	-1.84	0.77	-2.81	0.27	2	2400
24:25	-4.81	1.89	-4.26	1.03	-3.45	2.91	-10.71	2.33	-11.72	2.95	-14.69	1.26	9	3075
24:45	-9.11	3.00	-6.17	2.19	-2.72	0.89	-6.19	1.26	-4.73	1.07	-7.48	0.67	6	3085
25:05	-3.36	0.99	-4.43	1.13	-2.31	1.30	-7.49	0.99	-6.93	0.74	-11.16	1.28	12	3080
25:25	-1.51	0.78	-2.98	1.45	-1.39	1.03	-7.26	1.24	-5.46	1.51	-9.81	1.13	16	3080
25:45	-1.97	1.04	-3.30	0.83	-1.10	0.98	-6.25	1.61	-5.02	0.97	-9.53	1.23	15	3095
26:05	-1.91	0.92	-2.83	1.56	-0.67	0.68	-6.16	1.27	-4.66	1.15	-9.77	1.19	15	3090
26:25	-4.02	1.16	-3.75	2.00	-0.98	1.49	-6.09	2.05	-4.47	2.17	-8.85	2.02	15	3095
26:45	-3.52	1.69	-4.94	2.71	-2.40	2.47	-7.72	1.91	-5.27	1.50	-10.84	2.38	15	3095
27:05	-3.12	0.90	-2.75	1.07	+0.14	1.24	-5.32	1.75	-3.96	1.35	-8.76	1.59	15	3100
27:25	-3.08	2.63	-2.75	1.93	-0.30	1.36	-4.98	1.02	-3.66	1.18	-8.23	1.42	15	3110
15:28:05	-9.71	1.66	-8.66	0.52	-2.23	0.60	-6.55	0.91	-2.94	0.80	-6.83	0.45	2	3105
28:25	-1.70	1.94	-3.56	2.29	-2.57	2.16	-7.24	2.28	-6.33	1.63	-10.52	2.68	14	3100
28:45	-7.22	3.19	-7.50	3.75	-6.07	1.13	-9.59	1.55	-8.66	1.25	-12.61	0.80	9	3105
29:05	-4.66	2.15	-4.36	2.24	-2.29	1.63	-6.17	1.83	-5.31	2.25	-9.74	1.58	15	3110
29:25	-8.10	2.28	-8.62	2.78	-5.92	3.23	-11.08	2.84	-8.74	2.54	-13.53	2.41	15	3100
29:45	-4.20	3.09	-3.74	3.34	-1.28	3.96	-4.74	5.19	-4.17	4.84	-9.74	4.41	15	3100
30:05	-5.93	3.81	-2.83	4.94	+1.46	5.37	-3.24	4.88	-2.13	4.12	-6.60	3.79	13	3100
30:25	-7.35	4.82	-4.71	5.82	-0.64	5.12	-5.34	5.57	-4.52	4.40	-9.79	4.09	12	3110

Aircraft Mission 235

Flight 16

Test Site 116

Great Salt Lake Desert

Experiment Date 6/6/73 (DOY 157)

GMT start 15:21:25.0

GMT stop 15:34:45.0

Target conditions clear
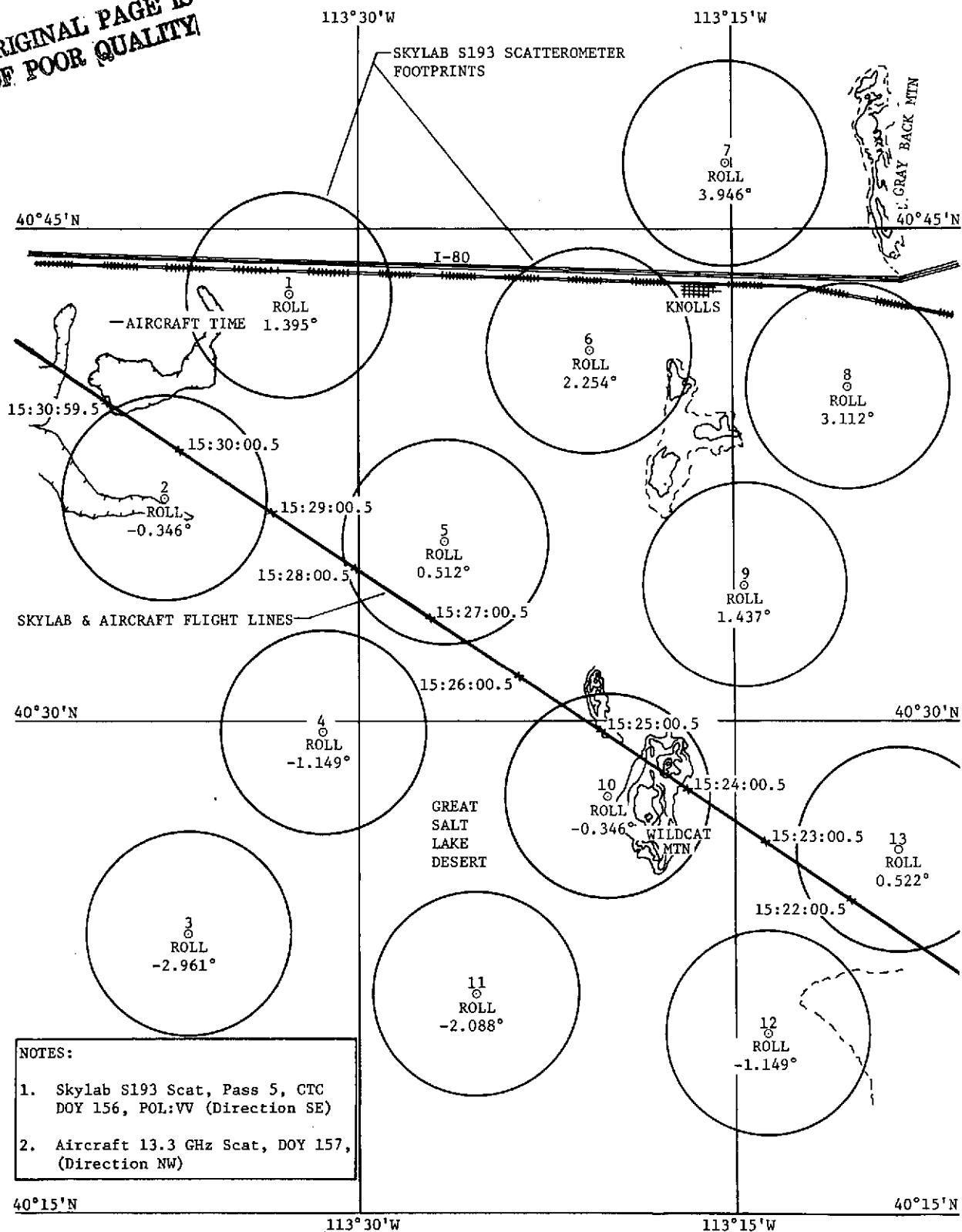
Figure 4.5-1   Great Salt Lake Desert (Site 116)
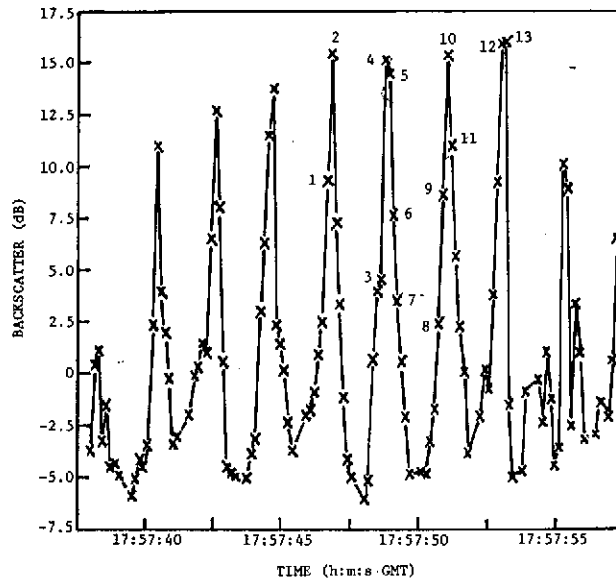
Figure 4.5-2 S193 Backscatter versus Time
for SL2, Pass 5, CTC, Rad/
Scat, VV Polarization over
Great Salt Lake Desert
(Site 116)
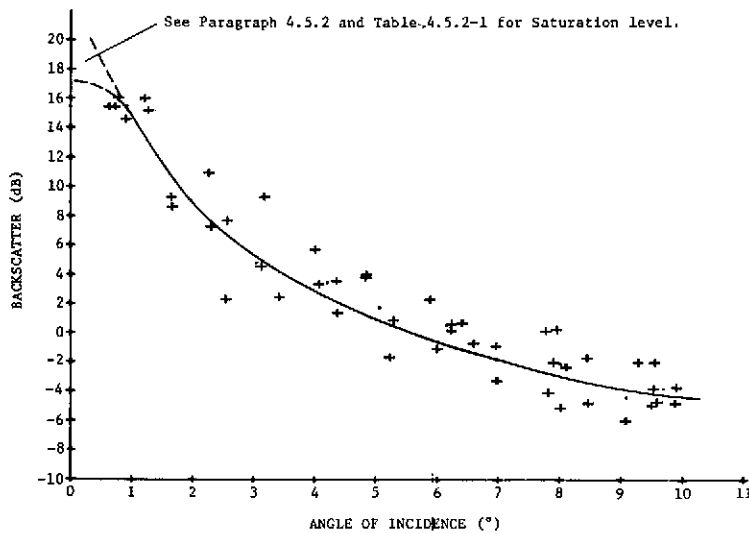
Figure 4.5-3 S193 Backscatter versus Incidence
Angle for SL2, Pass 5, CTC Rad/Scat,
VV Polarization over the Great Salt
Lake Desert (Site 116) DOY 156

Table 4.5-2   Skylab S193 Backscatter Data
for Great Salt Lake Desert, DOY 156

INCIDENCE ANGLE ± 0.5 (deg)	AVERAGE σ_0 (dB)	STANDARD DEVIATION	AVERAGE INCIDENCE ANGLE ACTUAL (deg)	STANDARD DEVIATION	NUMBER OF POINTS
0	--	--	--	--	0
1	15.5	0.5	0.92	0.27	6
2	9.2	1.3	1.97	0.36	4
3	5.7	2.4	3.05	0.40	6
4	3.8	1.5	4.21	0.19	4
5	2.3	0.9	5.05	0.24	4
6	0.6	1.1	6.15	0.21	5
7	-1.5	1.1	6.85	0.22	3
8	-1.8	1.5	8.01	0.22	7
9	-4.2	1.6	9.08	0.44	4
10	-3.7	1.1	9.68	0.19	5

NOTES:

1. Data taken over Great Salt Lake Desert
    with 17:57:45 GMT start time, 17:57:53
    GMT stop time.

2. Nominal Skylab altitude = 238.6 n mi (442.14 km)

ranged between 20 and 42 nautical miles off the aircraft flight path and the aircraft sensor footprints. This large offset, along with the size of the S193 footprint and relatively small size of the homogenous target, made the validity of comparison between aircraft data and Skylab S193 data conjectural. A better target would have been a large homogeneous area of water; however, there were no concurrent aircraft and Skylab S193 scatterometer data available.

Figure 4.5-4 is a plot of aircraft 13.3-GHz backscatter versus incidence angle over a selected area of the Great Salt Lake Desert (data taken from Table 4.5-1). The selected area, west of Wildcat Mountain, was assumed to be homogeneous. Figure 4.5-4 indicates that the homogeneity assumption may not be true; the data have large spreads and do not exhibit a smooth trend. However, the S193 backscatter (Figure 4.5-3) has the definite smooth trend that was expected. At the two points that could be compared, 5 and 10 degrees, results were as follows:

Incidence	Aircraft Backscatter		Skylab S193 Backscatter	
Angle (degrees)	Average σ_o (dB)	Range of σ_o (dB)	Average σ_o (dB)	Range of σ_o (dB)
5	-4.3	-1.8 to -8.0	2.0	+4.2 to -1.8
10	-4.4	-3.0 to -9.0	-3.4	-1.8 to -4.2

The backscatter data at 5 degrees have very little correlation, but at 10 degrees the data are within 1 dB. The data spread at 5 and 10 degrees is large for the aircraft backscatter, which makes comparison of aircraft and Skylab data unreliable.

The backscatter data obtained by aircraft over the Great Salt Lake Desert on DOY 157 indicates that this site is not an adequately homogeneous target. (See Figure 4.5-4.) Data taken by Skylab S193 has a good trend. (See Figure 4.5-3.) However, the footprints (between 5 and 10 degrees) are very large and are more than 20 nautical miles from the aircraft footprints, which may or may not contain similar terrain. A large homogeneous target, such as the Gulf of Mexico, would be a preferable target over which to make a comparison.

4.5.2 Backscatter $\left(\sigma_o\right)$ Saturation

The strong return signals when the S193 scatterometer antenna was pointed near nadir could drive the instrument into saturation. Determination of conditions resulting in saturation was required.
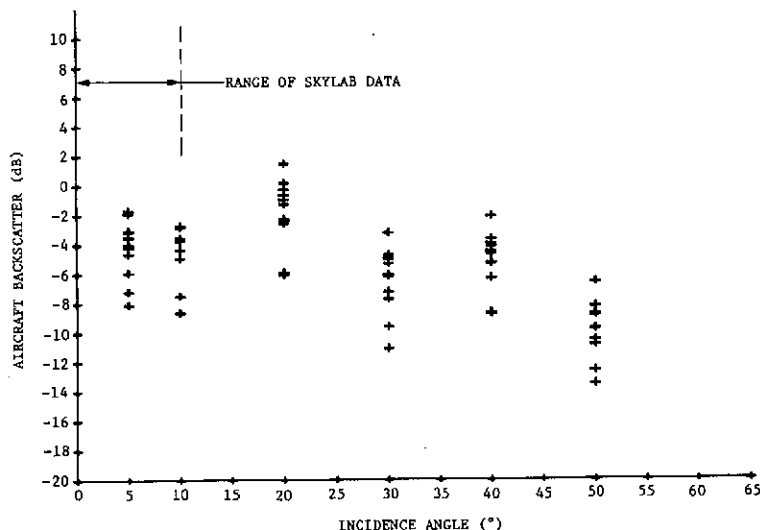
Figure 4.5-4   Aircraft 13.3-GHz Backscatter versus
               Incidence Angle over Great Salt Lake
               Desert, DOY 157

There were two sections of the scatterometer data processor
susceptible to saturation--the RF detector and the integrator with
analog-to-digital converter.

The output of the RF detector (referenced to integrator input)
saturated at approximately 1.5 volts. Figure 4.5-5, taken from the
calibration data report,* Volume I, is a plot of integrator input
voltage versus power received at the antenna (valid for the zero
middle center frequency filter). This figure indicates that any
received signal stronger than -70 dBm would drive the RF detector
into saturation (indicated by integrator input voltages ≧1.5 volts).

---

* S193 Historical Logbook, S193 Vehicle 001, Vol 1A, Document
  No. 72 SD4234 Rev. A, 27 October 1972, General Electric
  Company.

  Alternate Designation: S193 Calibration Data Report, Flight
  Hardware, Doc. No. 72 SD4207 Rev. D, 22 March 1973, Prime
  Unit 1A Volume 1A, SSO Contract NAS9-11195, General Electric.
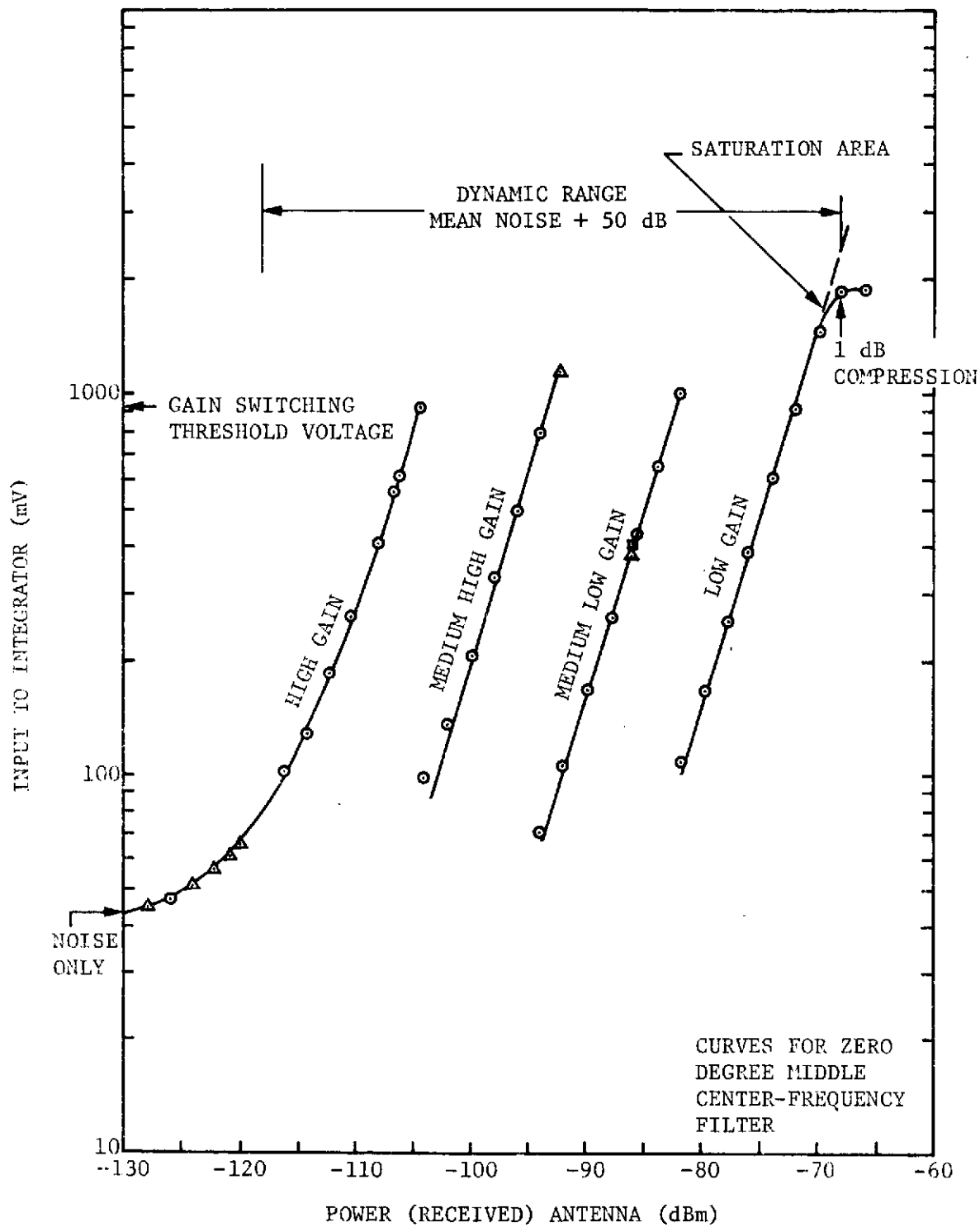
Figure 4.5-5   Scatterometer Integrator Input versus Power at Antenna $\left(P_R\right)$

The integrator/converter section saturated when the output from the integrator exceeded the 5-volt maximum signal that the analog-to-digital converter could accept for digitization. The integrator transfer function depended on the instrument mode and antenna look angle due to differing integration time requirements.

The output from the integrator was a function of the product of the required signal integration time and the input signal to the integrator from the RF detector and could result in a saturation level input to the analog-to-digital converter (i.e., >5 volts) even though the RF detector output was below its saturation level ($\geq$1.5 volts).

Considering these facts, it was clear that the scatterometer could be saturated in two ways—too much return power at the antenna, or a voltage at the input of the integrator that drove the output to voltages greater than 5 volts. To calculate the above limits, the following equations were used: (See Figure 4.5-6 for a functional block diagram.)

$$V_S \ (\text{raw}) = V_S \ (\text{raw})_{PCM} \frac{5.0 \ V}{1023} \qquad [4.5.1]$$

$$V_S \ (\text{corrected}) = V_S \ (\text{raw}) - \left[DC_S \times \frac{IT_S}{TC_S} + IT_S \times \text{Drift}_S \right] \qquad [4.5.2]$$

$$V'_{S_I} \ (\text{corrected}) = \frac{V_S \ (\text{corrected})}{\dfrac{IT_S}{TC_S}} \qquad [4.5.3]$$

$$V'_{S_P} \ (\text{corrected}) = \frac{V'_{S_I} \ (\text{corrected})}{F_S \times G_r} = \frac{V_S \ (\text{corrected})}{\dfrac{IT_S}{TC_S} \times F_S \times G_r} \qquad [4.5.4]$$

$$V''_{S_P} \ (\text{corrected}) = \frac{V'_{S_I} \ (\text{corrected})}{G_r} = \frac{V_S \ (\text{corrected})}{\dfrac{IT_S}{TC_S} \times G_r} \qquad [4.5.5]$$

$\left(\text{which is a JSC TR524 PDP* output product} \left(V''_S \right) \text{S062-15 of S062-A} \right)$.

---

* Earth Resources Production Processing Requirements for EREP Electronic Sensors, Document PHO-TR524 Rev A, Ch 2, Equation 21, p 6-22c, Lyndon B. Johnson Space Center, Houston, Texas, 18 October 1974.
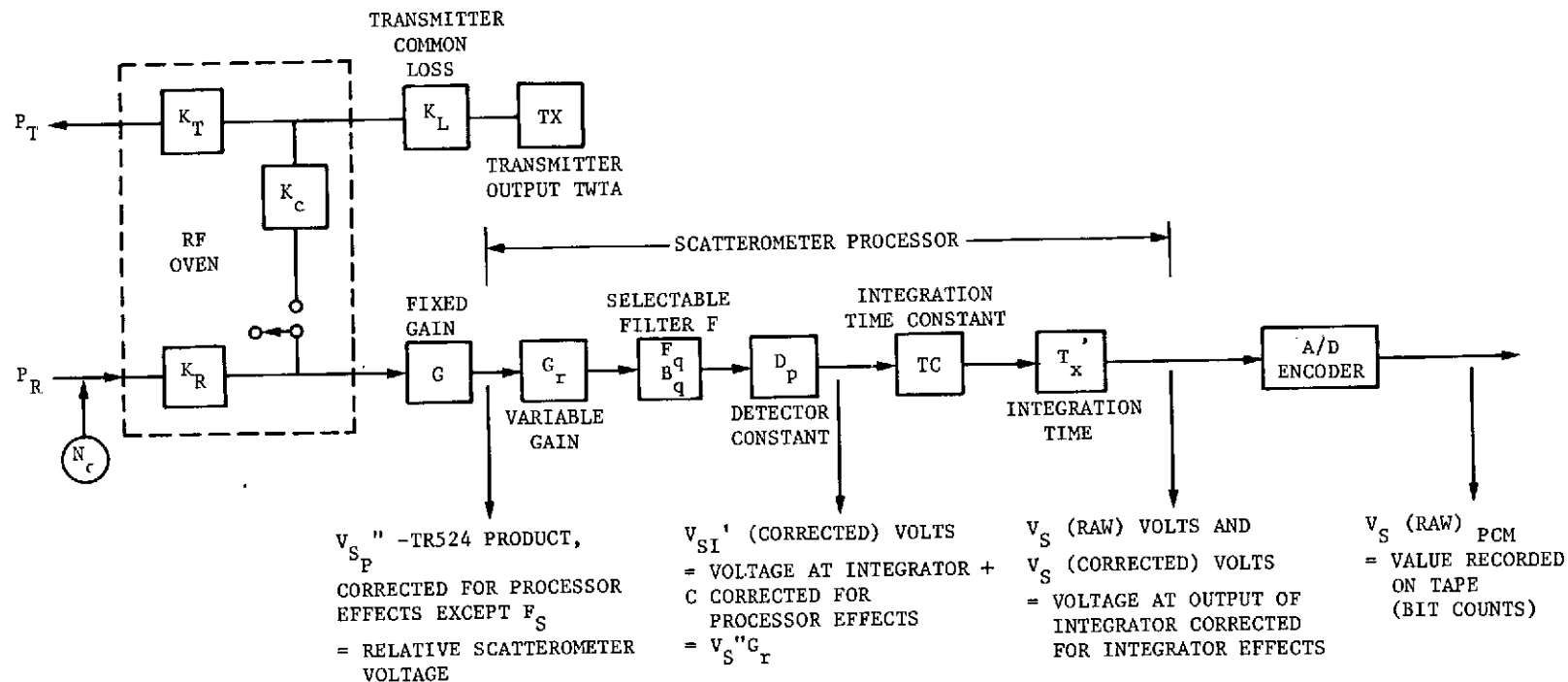
Figure 4.5-6   Functional Block Diagram for Scatterometer Receiver/Transmitter Unit

$$V'_{S_I} \text{ (corrected)} = V''_{S_P} \text{ (corrected)} \times G_r \qquad\qquad [4.5.6]$$

(equation relating signal voltage at integrator and relative signal voltage)

where

$V_S \text{ (raw)}_{PCM}$ = signal value recorded on tape (binary coded value)

$V_S \text{ (raw)}$ = signal voltage at output of integrator

$V_S \text{ (corrected)}$ = signal voltage at output of integrator corrected for integrator effects (dc offset and drift rate)

$V'_{S_I} \text{ (corrected)}$ = signal voltage referenced at input of integrator (taking out integration time and time constant of integrator)

$V'_{S_P} \text{ (corrected)}$ = signal voltage referenced at input of processor (taking out processor effects; integration time, time constant, filter gain, and variable gain stage, which are a function of mode, antenna angle position, and temperature)

$V''_{S_P} \text{ (corrected)}$ = relative scatterometer signal voltage (taking out processor effects, except the filter term, F_S. (This is a JSC TR524 PDP* output product $\left(V''_S \right)$ in S062-15 of S062-A product)

IT_S = integration time for scatterometer measurement

TC_S = time constant for scatterometer measurement

$Drift_S$ = drift rate correction for the integrator

DC_S = dc voltage offset bias of the integrator

F_S = average noise gain of the filter

---

* Earth Resources Production Processing Requirements for EREP Electronic Sensors, Document PHO-TR524 Rev A, Ch 2, Equation 21, p 6-22c, Lyndon B. Johnson Space Center, Houston, Texas, 18 October 1974.

G_r = programmable gain (four curves in Figure 4.5-5) provided by the step attenuator in the scat processor.

To relate saturation voltage and power to the backscatter coefficient, σ_o, the following relation was used:

$$\sigma_o = P_R + K \qquad\qquad [4.5.7]$$

where

σ_o = backscatter coefficient from the calculation procedure in the JSC TR524 PDP* to include system and link parameters.

P_R = return power at antenna terminals (See Figure 4.5-5.)

K = constant relating backscatter to return power.

The maximum signal voltage at the input to the integrator that will cause saturation at the output was calculated from Equations 4.5.1, 4.5.2, and 4.5.3. However, if a worst-case approach were used, the signal voltage at the output of the integrator should not be corrected as in Equation 4.5.2, but should be left in its raw form and related to the integrator input by Equation 4.5.3 modified as follows:

$$V'_{S_I} \text{ (raw)} = \frac{V_S \text{ (raw)}}{\dfrac{IT_S}{TC_S}} \quad \begin{array}{l}\text{(signal voltage at input of} \\ \text{integrator for worst-case} \\ \text{saturation level)}\end{array} \qquad [4.5.8]$$

where

V_S (raw) from Equation 4.5.1 is, in the worst case, 5 volts

V_S (raw) = V_S (corrected) for worst case.

The values and solutions to these equations are given in Table 4.5-3 for all modes (only for 0-degree filter). The value of V'_{S_I} (raw)

was also related to power received at antenna by Figure 4.5-5 and

---

* Earth Resources Production Processing Requirements for EREP Electronic Sensors, Document PHO-TR524 Rev A, Ch 2, Equation 8, p 6-14, Lyndon B. Johnson Space Center, Houston, Texas, 18 October 1974.

Table 4.5-3 Backscatter σ_0 Saturation Levels versus Mode

Mode	V_S(raw) (PCN counts)	V_S(raw) (mV)	IT_S (ms)	TC_S (ms)	DC_S worst-case MCF (10°C)	Drift $\frac{mV}{ms}$	F_S (MCF)	V_{SI}'(raw) worst-case (mV)	P_R Power at Antenna (dBm)	K	σ_0 sat.
CTC S only	1023	5000	10.935	4.0	4.8	0.210	1.02	1828.99	-69.11 (sat.)	Note 2	Note 2
CTC R/S	1023	5000	24.057	10.22	4.9	0.083	1.02	2124.12	-68.46 (sat.)	89.75	19.78 (Due to RF sec)
ITC 0°	1023	5000	13.122	4.0	4.8	0.210	1.02	1524.84	-69.90	89.59	19.59 (Due to RF sec)
ITNC 0°	1023	5000	43.740	10.22	4.9	0.083	1.02	1168.27	-71.06	89.76	18.58 (Due to Int)
CTNC 0°	1023	5000	43.740	10.22	4.9	0.083	1.02	1168.27	-71.06	89.76	18.58 (Due to Int)

NOTE 1: All calculations are for points near nadir where maximum return signal is expected.

NOTE 2: Values not completed before publication due to the small number of target measurements made.

V_S(raw)PCM = 1023 bits, which indicates saturation

V_S(raw) = 5000 mV signal voltage at output of integrator, which indicates saturation

IT_S, TC_S, DC_S, Drift, F_S as defined after Equation 6 and taken from calibration data report*

V_{SI}'(raw) = maximum signal voltage at input of integrator, that would dause saturation at output

P_R = Power received at antenna terminals (Figure 4.5.2-1), 1.5V = saturation or -69.97 dBm at antenna terminal

K = Used in Equation 7

σ_0 sat. = Backscatter level that could cause saturation.

---

* S193 Historical Logbook, S193 Vehicle 001, Vol 1A, Document No. 72 SD4234 Rev. A, 27 October 1972, General Electric Company, p 1-1 through 1-12.

Alternate Designation: S193 Calibration Data Report, Flight Hardware, Doc. No. 72 SD4207 Rev. D, 22 March 1973, Prime Unit 1A Volume 1A, SSO Contract NAS9-11195, General Electric.

given as P_R. The voltages for V_{S_I}' (raw) show that, in the ITNC 0-degree and CTNC 0-degree modes, the signal at the output of the integrator could saturate at voltages lower than 1.5 volts at the input to the integrator. Therefore, in the ITNC 0-degree and CTNC 0-degree modes, the output of the integrator would saturate before the RF detector and would determine the limiting value of σ_0.

To calculate the saturation value of σ_0, the value of K in Equation 4.5.7 must be determined. Taking data from the JSC TR524 PDP outputs, which have values of σ_0 and V_S'', the value of K can be obtained. Table 4.5-3 lists K versus mode (at ~0 degree incidence) and values of σ_0 that would saturate the processor. After a value of K has been calculated for a particular mode by use of Equation 4.5.7, Equation 4.5.7 is used again but with the maximum return

power (-70 dBm) in place of P_R and then calculating a new σ_0 (saturation). However, in the ITNC 0-degree and CTNC 0-degree modes, the value for P_R (saturation) is -71.14 dBm, which reduces the σ_0 (saturation) level. An example of how K was calculated is shown for two samples:

Data taken from TR524 products for CTC R/S mode, DOY 156, pass 5 over Great Salt Lake Desert (site 116)

Sample	Time	σ_0 (dB)	V (raw)$_{PCM}$	Gain	V_S'' (mv)	Incidence Angle (°)
A	17:57:46.779	15.43	268	3	685.25	0.726
B	17:57:48.898	14.58	221	3	563.94	0.903

Gain 3 = low gain curve for which G_r = 0.0008044.

Using Equation 4.5.6:

$$V_{S_I}' \text{ (corrected)} = V_{S_P}'' \text{ (corrected)} \times G_r$$

Sample A

$$V_{S_I}' \text{ (corrected)} = 685.25 \times 0.0008044 = 551.21 \text{ mV}$$

Sample B

$$V_{S_I}' \text{ (corrected)} = 563.94 \times 0.0008044 = 453.63 \text{ mV.}$$

Using Figure 4.5-5 and correcting V_{S_I}' (corrected) mV to P_R dBm.

P_R of A 551.21 mV → -74.32 dBm

P_R of B 453.63 mV → -75.16 dBm

Substituting in Equation 4.5.7 and solving for K

$$\sigma_0 = P_R + K \qquad\qquad [4.5.9]$$

$$K = \sigma_0 - P_R$$

Sample A = 15.43 - (-74.32) = 89.75

Sample B = 14.58 - (-75.16) = 89.74

Therefore, $K_{avg} = 89.745$

Now to calculate σ_0 saturation

$$\sigma_0 \text{ (sat)} = P_R \text{ (sat)} + K$$

$$= -69.97 \text{ dBm} + 89.745 \cong 19.78 \text{ dB}$$

where P_R (sat) = −69.97 dBm at antenna or 1.5 V at input of integrator.

Thus, target backscatter values of approximately 18 dB or greater should be reviewed to determine whether instrument saturation has affected the validity of the data.

4.6 Heat-Up Algorithm

Due to the injection of RF power into the circulator and antenna systems of the S193 Rad/Scat instrument by the scatterometer transmitter during Rad/Scat operations, heat-up of circulators can occur from RF dissipation and switching inefficiency. An algorithm to calculate the instantaneous temperature of a body experiencing a transient heat-up or cool-down was formulated to account for circulator temperature changes.* Subsequent analysis using Skylab science data for Rad/Scat operation has suggested that the contribution to circulator heat-up by RF power dissipation is negligible. (See paragraph 3.9.) Further, worst-case analysis of the radiometer transfer equation has shown that for circulator temperature rises of 4°K, approximately twice that normally seen, the change in calculated antenna temperature is small, amounting to less than 0.5 °K, which is shown by the following:

The equation for antenna brightness is (based on the G.E. cal data report†)

$$T_A = \frac{1}{K_3} \left[K_1 \left(\frac{T_1 + T_2}{2} \right) + K_2 T_F - K_4 T_G - K_5 T_D \right] + \frac{E_{OB} - E_A}{K_3 G} \quad [4.5.10]$$

---

* S193 Calibration Data Report, Flight Hardware, Doc. No. 72 SD4207, Rev. D, Prime Unit 1A Volume 1A, Contract NAS9-11195, General Electric Company-SSθ, 27 March,1973, p 3-8b.

† S193 Historical Logbook, S193 Vehicle 001, Vol 1A, Document No. 72 SD4234 Rev A, General Electric Company, 27 October 1972, p 3-6.6

where temperatures T_G and T_D are circulator "G" and circulator "D" temperatures and are subject to heatup.*

Then:

$$\Delta T = \frac{1}{K_3} \left[-K_4 \Delta T_G - K_5 \Delta T_D \right] \qquad [4.5.11]$$

which reduces to:

$$\Delta T = -\left(L_G - 1 \right) \Delta T_G - \left(L_D - 4 \right) L_G \Delta T_D \qquad [4.5.12]$$

substituting:

$$\Delta T = -(0.02186)4 - (0.0817)(1.02186)4$$

$$= 0.4214°K.$$

---

* An improved equation for T_A, incorporating polarization-dependent terms and accounting for leakage in circulator "G", is used in production data processing. The simplified expression is adequate for the worst-case analysis described here.

5. FINAL RESULTS

Operating characteristics of the radiometer/scatterometer were found to be in close agreement with preflight predicted values. Table 5-1 shows the values observed in the in-flight performance evaluation. The only consistent discrepancy throughout all three missions was in the antenna gimbaling, where electrical harness stiffness due to low temperatures prevented full achievement of maximum commanded angles. Three major anomalies produced degradations in experiment capabilities, but did not result in complete failure. The very complex operations of sequencing and data processing functions were executed with minimal faults in all operational periods.

Engineering parameters indicated consistent values that, in general, were within limits established before launch. These measurements proved extremely useful in establishing the causes of the three major anomalies.

Analyses of flight data yielded refined values for some internal constants of the instrument. In addition, detailed inspection of the data disclosed a number of data-stream peculiarities that were documented to guide data users. Calibration signals generated in the instrument provided means for evaluating radiometer receiver and scatterometer transmitter stability, which were found to be excellent. Statistical smoothing techniques were developed to process data in which random fluctuations tended to obscure the values of interest.

Lunar calibration passes were the only opportunities to acquire data from a target of truly "known" temperature and homogeneity. Measurements of the deep-space target were used to determine radiometer insertion loss and to develop improved values for Scat Noise integration time. Aircraft underflights produced a limited amount of reference data on selected earth scenes. Within the range of uncertainty of aircraft sensor data, the radiometer accuracy and linearity were substantiated and the predicted dynamic range was confirmed.

Table 5-1   Radiometer/Scatterometer Operating Characteristics

CHARACTERISTIC	OBSERVED VALUE	REFERENCE PARAGRAPH MSC-05528, Volume IV
Scat Transmitter		
Peak power (tube output)	14.1 W min (at antenna)	3.4.2
Pulse width	4.98 ±0.02 ms	5.3
Rise & fall time	41.5 μs	9.4
Pulse repetition frequency	123.3 pps	5.3
Scat Receiver		.
Noise temperature	962 ±357°K	15.4.1
Noise integration times	57.990 ms	
	24.094 ms	10.2.1
	13.686 ms	
	6.544 ms	
Saturation return signal	-70 dBm	4.5.2 (MSC-05546, Volume IV)
Rad Receiver		
Resolution	1.06°K (150°K target)	13.5.1
Dynamic range	4 to 353°K	12.8

Table 5-1 (Concluded)

CHARACTERISTIC (°)	OBSERVED VALUE (°)	REFERENCE PARAGRAPH MSC-05528, Volume IV
Antenna Gimbaling (before gimbal anomaly of pass 79)		
Pitch precision (before gimbal anomaly of pass 40)		
48	+0 , -5.92	
40.1	+0.065 , -1.457	
29.4	+0.111 , -1.294	3.4.1
15.6	+0.096 , -1.777	
0	+0.593 , -0	
Roll precision		
48	+0 , -4.45	
40.1	+0 , -2.04	
29.4	+0.454 , -0.690	3.4.1
15.6	+1.024 , -0.029	
0	+1.404 , -0	
Engineering Parameters		
All parameters were within criteria limits throughout Skylab missions except:		
A002 A003 A004 A005 A006 A007 A018 A019 A033 A047 A052 A053 A054		3.3

6. CONCLUSIONS

The conclusions that follow were drawn at the end of the sensor performance evaluation task. Being made after the fact, these conclusions are not constrained by the budget and schedule concerns that greatly affected the development of this sensor. They are intended to be a reference checklist for future development of remote sensing devices and programs.

6.1 Sensor Design and Performance

The S193 radiometer/scatterometer demonstrated the feasibility of a remote sensing instrument of this type to acquire radiometric and backscatter data, even during periods when darkness or cloud cover obscured the earth's surface. The data collected during SL2 and SL3 are good and only degraded by the failure of the antenna scan to achieve the 48-degree scan position. The data collected during SL4 are valid for the scatterometer, although at lower signal-to-noise ratios, while the spatial resolution of the radiometer was grossly degraded during SL4.

The radiometer dynamic range exceeded the design requirement of 50 to 350°K and was often evaluated at deep-space temperatures. The radiometer, although intended to be a relative-reading instrument, demonstrated good absolute-reading capability. The reference load temperatures and controlled oven temperatures were very stable. Radiometer calibration measurements (Rad Cal and Rad Baseline data readouts) were adequate for establishing radiometer system gain. However, in postflight data processing, special handling of these data had to be developed. Use of the Rad AGC had been desired as an aid to the calibration parameters, but it was determined that this measurement was at such a point in the circuit that it was an insensitive indicator of Rad gain. No evidence of either EMI or radiometer/scatterometer interaction was observed except radiometer saturation during scat only modes.

Scat cals were measured at time intervals too large to determine short-term transmitter power variations, thereby increasing the uncertainty of the transmitter output power values used in evaluating the terrain backscatter coefficients.

The scatterometer processor exhibited gain variations with changes in temperature, although it was in a partially controlled temperature environment. However, the transmitter was relatively stable throughout the mission when corrections for the scatterometer processor temperature changes were made.

The scatterometer transfer function developed during the sensor performance evaluation effort was an improvement on the version developed before the mission. This included re-evaluation of integration times for scatterometer noise measurements.

Engineering parameter measurements were generally adequate for sensor performance evaluation and for use in analysis of anomalies. Some TWTA parameters were undersampled and, consequently, were of little use in data analysis. Inclusion of a TWT cathode current measurements would have been helpful.

Flex harness stiffness prevented achievement of the full range of commanded pitch and roll angles by the antenna gimbaling system during all three missions. The sensor capability was greatly diminished by three anomalies--the gimbal potentiometer short at the end of SL3, the roll torquer drive failure during SL4, and the missing antenna feed cup for all of SL4. The pitch anomaly probably would not have occurred had the gimbal potentiometers been protected by suitable enclosures.

Polarization selection and switching logic did not guarantee operation in the intended polarization modes, and undetectable errors were possible. However, it is believed that these were avoided by special switching constraints. In operations checked by the ground receiver arrays, and in data examined for the power polarization split as a function of incidence angle, no polarization errors were seen. The relation between earth-referenced polarization and instrument-referenced polarization is complex in certain modes. Data processing does not perform the required coordinate transform, and data users must be aware that all polarization labels are instrument referenced.

The highly complex nature of the instrument and its operating sequences caused associated complexity in data processing software.

Error analyses of the data output from the instrument and the data processing conversion of it into terrain characteristics has not been completed due primarily to a lack of adequate ground truth data and computer models for the system.

6.2 Preflight Calibration

Adequate preflight calibration data for engineering parameter measurements were available. However, a preflight calibration of the complete S193 system was not performed. In retrospect, a more comprehensive preflight calibration of certain system characteristics was needed. Specifically, the thermal response of scatterometer filters, antenna patterns, scatterometer processor integration time, drift, offset, and end-to-end insertion loss.

6.3 Mission Operations

The usefulness of the astronaut crew for repairing equipment was demonstrated when the SL3 crew rectified the pitch gimbal problem. Provision of handholds near the S193 antenna would have made this operation easier.

Design of the experiment operation mode logic permitted inadvertent selection of invalid operating modes, which were not detectable before the return of the EREP tape and analysis of data. There were numerous switching sequence and position constraints for proper operation of the S193.

The real-time down-link (EREP diagnostic downlink unit) was useful for assessing anomalies during a mission.

Simultaneous operation of the altimeter and scatterometer, not possible in S193, would have permitted acquisition of uniquely valuable sea-state data.

Many useful analyses were made possible by the availability of deep space (lunar calibration) data. The radiometer was not intended to be used for targets of such low temperature (approximately 4°K), but the homogeneity and known temperature of the deep-space target outweighed the performance degradation. There was not an adequate quantity of aircraft underflight and ground truth data of adequate quality available to support S193 performance evaluation as originally planned.

6.4 Data Processing

Production data processing software development was completed too late to provide processed data for sensor performance evaluation. Most of the analyses were conducted using raw data

or data partially processed by the use of programs developed
for system test evaluation at Kennedy Space Center. This resulted
in a considerable increase in the time and effort required for
the evaluations accomplished and resulted in several tasks not
being completed.

6.5 Postflight Evaluations

Postflight evaluation concentrated on the engineering
performance of the instrument, rather than on determining the
significance and application of the scientific data acquired.

7. RECOMMENDATIONS

Derived from selected conclusions of the sensor performance evaluation effort, the following recommendations are offered for consideration in future programs. They relate to instrument design and development, calibration, crew interface, mission operations and support, and data return.

1) An end-to-end sensor calibration should be performed on the flight unit during preflight operations.

2) Gimbal potentiometers should be protected from the entry of foreign matter.

3) Increased use of a down-link should be preferred as the primary method of data return and is recommended so that postflight data processing is not delayed. If this is not feasible, a down link should be available on a part-time basis for near-real-time performance checking.

4) Sensor operations and aircraft underflights should be coordinated to make concurrent observations of large, homogeneous targets, such as ocean areas or large deserts. The use of lunar calibrations should be incorporated in sensor operations planning. To simplify the hardware, preflight calibration, crew operations, and data processing, modes and capabilities should be reduced. When astronaut operators are available, operational features for acquiring data from targets of opportunity should be incorporated in the sensor design.

5) During instrument development, a simulation model should be established for studies of sequencing logic and analysis of measurement errors; instrument design should be responsive to the results of simulation. The model should be comprehensive enough to guide the selection of engineering measurements and their sampling rates.

6) Consideration should be given to extending the antenna gimbal travel to reach the Brewster angle. At any angle, data should be identified with the achieved gimbal position rather than with a commanded angle.

8. NOTES

8.1 Acknowledgements

The effort covered by this report was sponsored by the Lyndon B. Johnson Space Center Earth Resources Program Office. It is based on the results of a concerted effort by numerous individuals in NASA, industry, and academic organizations. These results primarily reflect the contributions of the University of Kansas, Remote Sensing Laboratory, Lawrence, Kansas, in addition to those of the Martin Marietta Corporation.

Particular acknowledgement is due the late Mr. Charles K. Williams of the Skylab Program Office of JSC for his conception and implementation of the EREP sensor performance evaluation. His dedication and leadership were essential to the successful completion of these evaluation studies.

Acknowledgement is also made to R. Eisenberg of the General Electric Space Systems Organization for his assistance relative to sensor design and calibration.

This volume of the final report was prepared by R. J. Plugge, W. B. Cox, W. E. Smull, G. R. Proctor, and D. Walker of the Martin Marietta Corporation, Denver, Division.

8.2 Abbreviations

Abbreviations in common usage have been used for English units of measure. International Units (SI) have been abbreviated in accordance with E. A. Mechtly's NASA SP-7012, The International System of Units, 2nd Rev, National Aeronautics and Space Administration, Washington, D.C., 1973--except for steradian, which has been abbreviated to ster.

AGC	Automatic gain control
AM	Amplitude modulation
AMT	Airlock module time
Ant	Antenna
APEX	Antenna pattern exercise
avg	Average
BW	Bandwidth
Cal(s)	Calibration(s)
C&D	Control and display

CMD	Command
CTC	Cross-track contiguous
CTC R/S	Cross-track contiguous Rad/Scat
CTC-R or CTC R/O	Cross-track contiguous radiometer (only)
CTC-S	Cross-track contiguous scatterometer (only)
CTNC	Cross-track noncontiguous
CTNC-R	Cross-track noncontiguous right
CTNC-L	Cross-track noncontiguous left
CTNC-L/R	Cross-track noncontiguous left/right
CW	Continuous wave
DOY	Day of year
EMI	Electromagnetic interference
EREP	Earth Resources Experiment Package
EVA	Extra-Vehicular Activity
FM	Frequency modulation
G.E.	General Electric
GMT	Greenwich Mean Time
HCF	Higher center frequency
H/K	Housekeeping
HPBW	Half-power bandwidth
IEP	Integrated Electronics Package
IF	Intermediate frequency
Int	Internal
IRIG	Inter-Range Instrumentation Group
I.T., IT	Integration Time
ITC	In-track contiguous
ITNC	In-track noncontiguous
JSC	Lyndon B. Johnson Space Center
KSC	Kennedy Space Center
LCF	Lower center frequency
LO	Local oscillator
MCF	Middle center frequency
MSC	Manned Spacecraft Center (now JSC)

MMC	Martin Marietta Corporation
NASA	National Aeronautics and Space Administration
N/A	Not applicable
NC	Noncontiguous
OOA	On-orbit alignment (nadir alignment of antenna)
OWS	Orbital Workshop
P	Page
Para	Paragraph
PCM	Pulse Code Modulation
PDP	Production Data Processing
QCM	Quartz Crystal Microbalance
R, RAD, Rad	Radiometer, radiometer output data
Rcvr	Receiver
Ref	Reference
Rev	Revision
RF	Radio frequency
RFI	Radio frequency interference
R_C	Radiometer calibration
R_{BL}	Radiometer baseline
R/S	Radiometer/scatterometer
Scat	Scatterometer
S&AD	Science and Applications Directorate
SKYBET	Skylab Best Estimate Trajectory (computer program)
SL	Skylab
SPE	Sensor performance evaluation
SPTR	Single-point temperature reference
STAPE	Surface Test for Altimeter Performance Evaluation
Sync	Synchronization
S/N	Signal-to-noise ratio

T, Temp	Temperature
T_A	Antenna temperature (radiometric)
T_B	Brightness temperature
TC, T.C.	Time constant
TDA	Tunnel diode amplifier
TWT	Traveling wave tube
TWTA	Traveling wave tube amplifier
VHF-FM	Very high frequency-frequency modulation
Vol	Volume
VSWR	Voltage Standing Wave Ratio
w	with
w/o	without
WFC	Wallops Flight Center
W/G	Waveguide
WGSA	Waveguide switching assembly
WWVB	National Bureau of Standards transmitter callsign
XMTR	Transmitter
ZLV	Z local vertical (spacecraft axis)
σ^o	Normalized backscatter coefficient

APPENDIX A

TECHNIQUES ADDENDUM

This appendix describes the techniques used to evaluate
S193 Radiometer/Scatterometer performance as presented in the
Sensor Performance Evaluation Report, MSC-05528, Volume IV,
dated October 30, 1974. These descriptions of the techniques
include both the theoretical approach and the mechanics of
application.

I. USE OF DEEP SPACE AND RELATIVELY UNIFORM TARGETS FOR DETERMINATION OF SYSTEM SENSITIVITY, NOISE LEVEL, CALIBRATION CONSTANTS, AND INTERFERENCE EFFECTS

S193 radiometer output data acquired from deep space and other relatively uniform targets were used to analyze system resolution, noise levels, calibration constants, and interference effects. Data from uniform targets were chosen to eliminate signal fluctuations like those that would result from changing terrain, etc. In this way, data recorded from a relatively constant source could be used to determine system sensitivity, noise level, and interference. In addition, "known" target temperature data could be used to provide large sample populations on which calculations of values for calibration constants could be made.

System calibration constants were verified using target temperature data and the derived system transfer equations. Radiometric temperatures of selected uniform targets were either calculated or measured using secondary standard measurement techniques, then the system transfer function was manipulated to determine the various constants and loss terms. For example, the antenna and antenna feed loss term, L_{ANT}, was recalculated and verified using deep space data and the following method.

Step 1 - The system transfer equation for antenna brightness temperature given sensor output data was

$$T_A = \frac{L_{ANT}L_K}{L_R}\left[T_R + \left(L_R-1\right)T_0-K_i\left[\frac{E_{OA}-E_{OB}}{E_{OC}-E_{OB}}\right]\left(T_1-T_2\right)\right]$$
$$- \left(L_{ANT}-1\right)T_{ANT} - L_{ANT}\left[L_K-1\right]T_K \qquad [A.I.1]$$

Step 2 - Rearranged to solve for L_{ANT}:

$$L_{ANT} = \frac{T_A - T_{ANT}}{\frac{L_K}{L_R}\left[T_R + \left(L_R-1\right)T_0-K_i\left(\frac{E_{OA}-E_{OB}}{E_{OC}-E_{OB}}\right)\left(T_1-T_2\right)\right] - T_{ANT} - \left(L_K-1\right)T_K}$$

$$[A.I.2]$$

Step 3 - Values for L_{ANT} were calculated using deep space data.

T_A = Antenna brightness temperature, assumed 4°K

T_{ANT} = Antenna physical temperature, a temperature sensor output

T_R = Reference temperature $\left(T_1 + T_2\right)/2$, a temperature sensor output

T_0 = WGSA temperature, a temperature sensor output

$\left(T_1 - T_2\right)$ = Reference temperature, a temperature sensor output

T_K = OMT, input W/G temperature, a temperature sensor output

L_K = OMT, input W/G and WSGA loss term

L_R = Reference path loss

K_i = Integrator equalization factor, mode dependent

$E_{OA} - E_{OB}$ = Rad output voltage minus Rad baseline voltage. Both voltages were sensor outputs, with Rad voltage a function of target brightness.

$E_{OC} - E_{OB}$ = Rad calibration voltage minus Rad baseline voltage. Both voltages were sensor outputs.

Manipulation of the system transfer equation could be carried out to solve for any calibration constant or loss term.

The sensitivity of radiometric receivers was expressed in terms of minimum detectable temperature ΔT °K. ΔT for the S193 Radiometer was

$$\Delta T_A = \left[\left[1 + \frac{\left[\dfrac{T_1 + T_0 - 2T_A}{T_1 - T_0}\right]^2}{1 + t_{AGC}/t_{SIG}}\right]\left[\left(T_1 + T_R\right)^2 + \left(T_0 + T_R\right)^2 + 2\left(T_A + T_R\right)^2\right]\left(2BT_{SIG}\right)^{-1}\right]^{\frac{1}{2}}$$

[A.I.3]

where

ΔT_A = apparent antenna temperature fluctuation (°K)

T_A = apparent antenna temperature (°K)

T_R = system noise temperature (°K)

T_1, T_0 = reference temperature (°K)

B = radiometer bandwidth (MHz)

t_{SIG} = signal integration time (ms)

t_{AGC} = AGC time constant (ms)

Uniform target data assigned values to T_A, and calculations for ΔT_A could then be made.

II. USE OF LAND-SEA BOUNDARY CROSSING TO EVALUTE ANTENNA
     PATTERN AND POINTING

The S193 antenna was designed to have a main beamwidth
of 1.5 degrees. At a nominal orbital altitude of 235 nautical
miles, this beamwidth corresponded to data cells approximately
6 nautical miles in diameter on the earth's surface at nadir.
These data cells were relatively small compared to scan
coverage, which sometimes swept a ground track 100 miles wide.
This scan motion permitted analysis of land-sea boundary
crossing data to evaluate the antenna pattern and instrument
pointing.

Figure A.II-1 illustrates the use of land-sea crossing
data to evaluate antenna pattern and pointing. The data
presented are two left-of-track scans from SL3, pass 31, CTC
Rad Only mode. Each circle represents a radiometer data cell
defined by the antenna pattern half-power beamwidth and contains
the radiometric temperature calculated from data recorded for
that particular cell. In this case, evaluation of the antenna
pattern was limited to verification that the data obtained were
reasonable, based on target and preflight antenna pattern
information, and hence that the preflight pattern had not
changed significantly. Particular attention was paid to
instrument response as the antenna scanned the land-sea
boundary. As is evident in the right data scan in Figure A.II-1,
the data cells swept from near nadir to the Michigan coast.
During this time, antenna temperatures, T_A, rose 93°K in two
measurement periods. This indicated that the antenna was
properly scanning; comparison of the target in each cell with
the related radiometric temperatures obtained indicated that
the 6-nautical-mile footprint representation of the antenna
pattern was valid within the accuracy of the model.

Antenna pointing was investigated by determining, from
data measurements, the location of each data cell as the
antenna scanned through a land-sea boundary (Figure A.II-1).
From the location of each data cell relative to nadir and the
altitude of the spacecraft at the time of the data measurement,
the antenna pointing angle was calculated. This angle was used
as a gross check of the accuracy of the roll or pitch antenna
position sensor readouts to determine whether proper antenna
pointing was achieved during selected radiometer modes. Also
by the use of this technique, it was apparent that some early
data reduction procedures had time-tagged data erroneously.

SL-3, PASS 31, DOY 253
S193 Rad Only CTC

LAKE SUPERIOR

137°K +   + 137°K

140°K +   + 136°K

148°K

224°K

209°K +

MICHIGAN

253°K +

+ 232°K

MICHIGAN

186°K

+ 150°K   LAKE SUPERIOR

144°K +

+ 139°K

NADIR

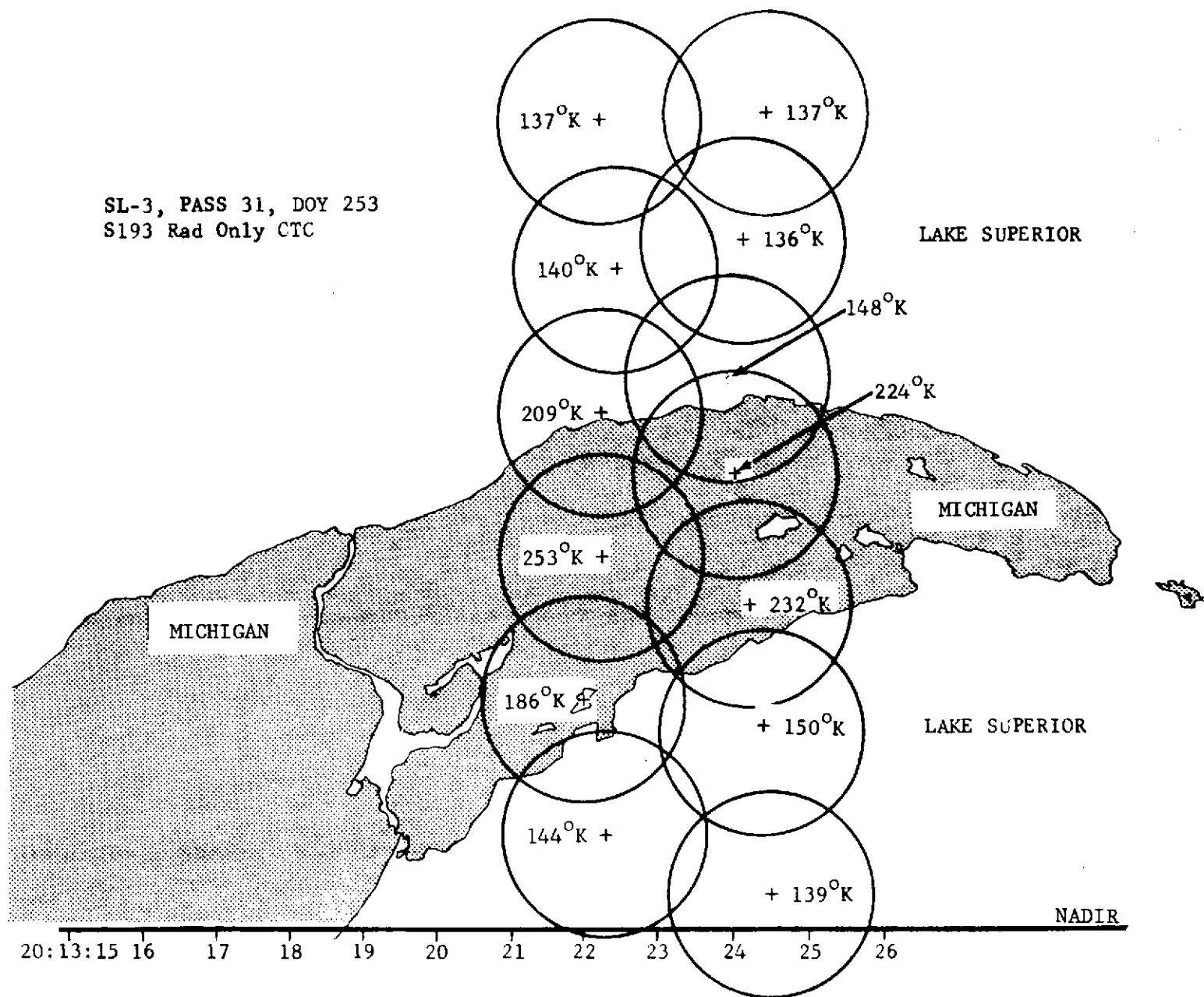20:13:15 16   17   18   19   20   21   22   23   24   25   26

Figure A.II-1   S193 Radiometric Data from Lake Superior

This procedure was especially useful in analyzing the SL4 data because there was a gross antenna pattern change between SL3 and SL4.
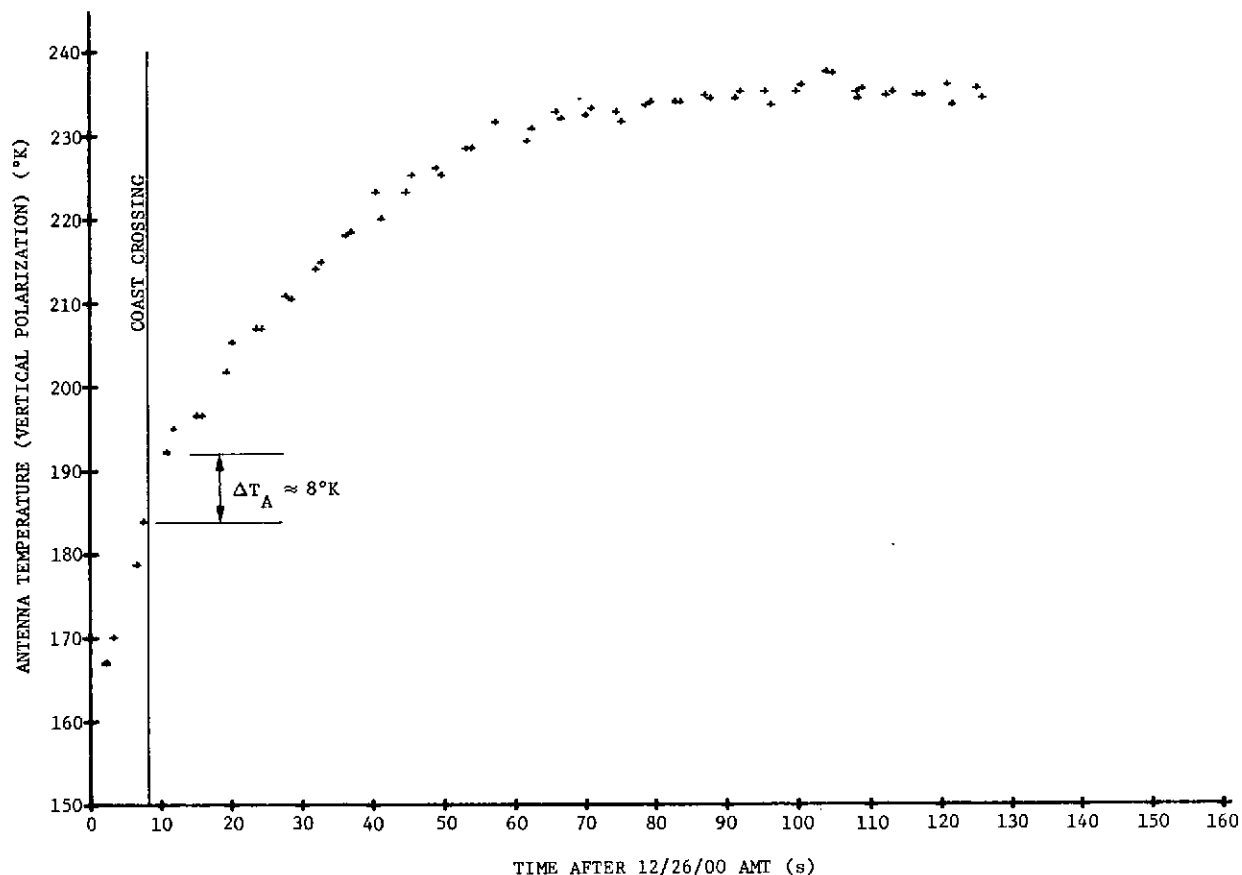

Figure A.II-2   SL4 Land-Sea Boundary Crossing

Figure A.II-2 is a plot of antenna temperature data during SL4 pass 92. The data are from an EREP pass over the California coast. Comparison of Figures A.II-1 and A.II-2 shows that for a land-sea boundary crossing during SL4, the instrument did not exhibit a step response equivalent in magnitude and nature to an SL3 land-sea crossing. The data in Figure A.II-2 show that a significant change took place in the S193 antenna pattern, which resulted in a larger signal contribution from the antenna side-lobes. This was evidenced by the gradual change in T_A as the antenna scanned from sea to land. However, the point of actual sea-to-land transition was still evident from a marked change in

the slope of the data. These characteristics of the data
verified antenna pattern testing at JSC, which suggested that
the S193 antenna pattern might have significant sidelobe
contributions to approximately 42° in addition to the main
beam signal.

III. USE OF GROUND-BASED RECEIVER ARRAYS FOR THE DETERMINATION
OF ANTENNA POINTING AND PATTERN CHARACTERISTICS, AND
SCATTEROMETER TRANSMITTER CHARACTERISTICS

To assist in evaluating the in-flight performance of the
S193, two ground instrumentation setups were used. These
are considered valid and useful techniques that should be
considered for use on similar programs in the
future. One setup was referred to as APEX (antenna pattern
exercise), the responsibility of the University of Kansas, and
the other was referred to as STAPE (surface test for altimeter
performance evaluation), primarily the responsibility of
Martin Marietta, operated with NASA/WFC personnel. The goals
and successes of each are briefly discussed in the following
paragraphs.

A. APEX*

1. Goals:

a) In-flight antenna pattern synthesis;

b) Verification of scatterometer transmitter operation;

c) Scatterometer radiated pulse shape and timing
verification;

d) Verification of antenna scan operation;

e) Verification of polarization switching.

2. Concept:

Five superhetrodyne receivers were located along the
Skylab ground track. Because of the high average output
power during the scatterometer mode, this transmitter mode of
the S193 was selected for the overflights. Because the antenna
always scanned in each scatterometer mode, a CTC mode was chosen
so the antenna pattern would be scanned through the line of
receivers to provide multiple antenna-pattern "cuts" from the
receiver power measurements. A Rad/Scat sequencing mode was
used in the overflights. Thus, bursts of pulses from the

---

* Also see paragraphs 5 and 9.3, 9.4, 9.5 of MSC-05528,
Volume IV.

scatterometer transmitter were separated by periods of S193 receiving only. To maximize the output from these data bursts and stagger the gaps in the pattern cuts, receiver locations were slightly staggered to each side of the actual ground track. Receiver locations relative to ground track are illustrated in Figure A.III-1.

All the measurements were synchronized in time so that data for the received power versus time from each receiver station could be combined for synthesizing the antenna pattern. Due to the many variables, computer data reduction was required. Data processing combined knowledge of the following variables:

1) Relative position of the receivers and S193 antenna;

2) Assumed scan motion of the S193 antenna;

3) Ground receiver and recorder characteristics;

4) Ground antenna pattern data and orientation;

5) RF link estimation;

6) OWS (Skylab) motion;

7) Estimates of processing procedure (interpolation) errors.

To synthesize the pattern once the data were translated into a common set of coordinates, a best fit estimation of the antenna pattern was used. This procedure was initialized based on the preflight pattern and used quadratic interpolation to fill gaps due to S193 radiometer periods in the measured data.

To increase the amount of data taken on the ground, CTC modes with roll offset biases were also scheduled so that data could be recorded when Skylab was on adjacent rather than overhead ground tracks. Also, on two passes, two sets of ground data were taken from the same pass by synchronizing the astronaut's switching of S193 pitch offset with a change in the ground receiver antenna pointing so that a forward pitched CTC scan mode was used before a nadir-centered CTC scan mode. S193 illuminated the same ground receiver station from two angles.
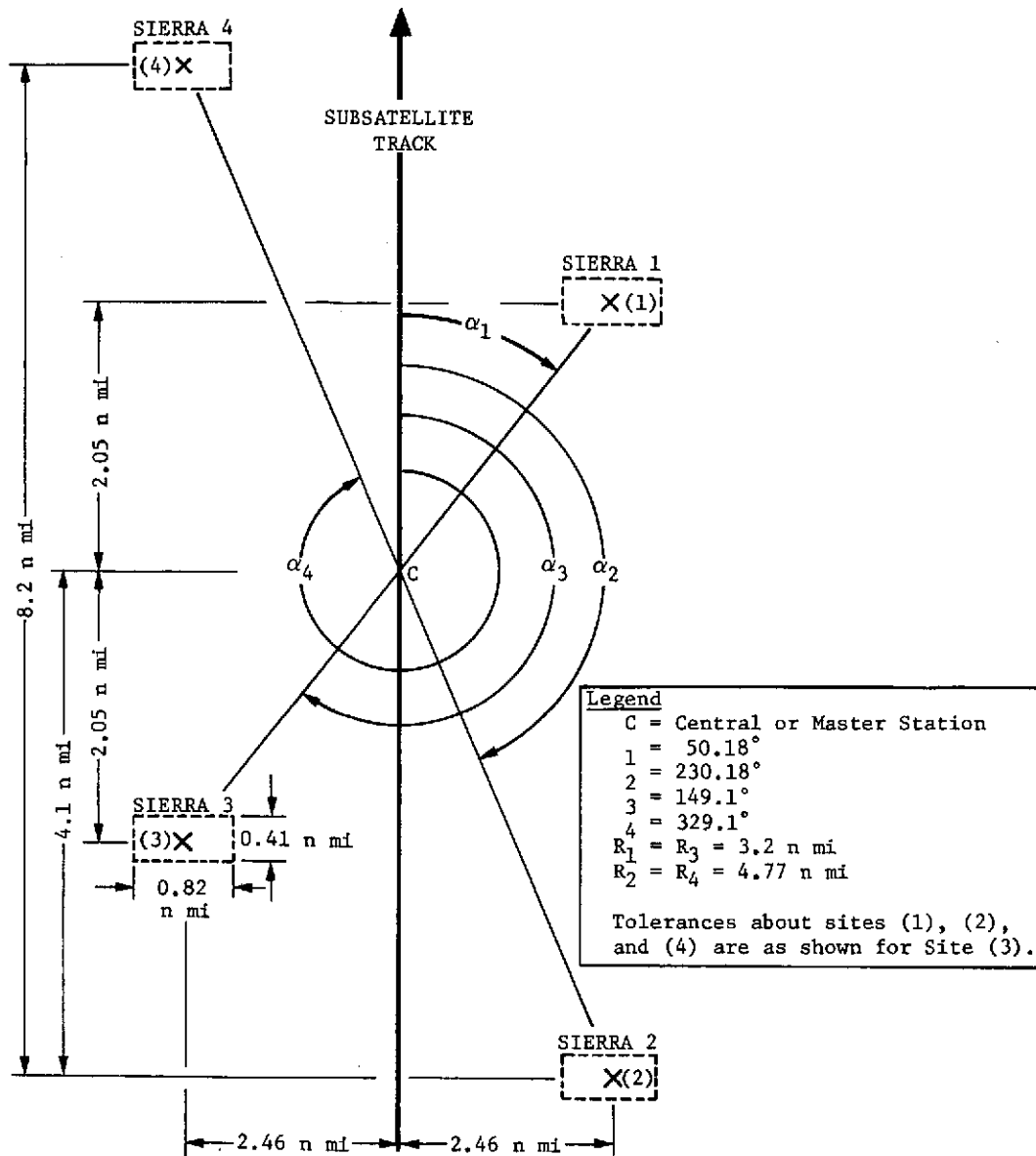
Figure A.III-1 Receiver Site Layout

The test setup used broad-beam antennas to minimize ground antenna pattern errors. The open breadboard receivers were tripod mounted and used log amplifiers to obtain signal measurements at least 35 dB down in the antenna pattern. A typical receiver block diagram is shown in Figure A.III-2. A measurement precision of 0.5 dB was sought. Data were recorded on FM tape recorders, which also recorded WWVB timing signals on AM channels and an IRIG B time code sent from a central-site transmitter via a VHF-FM transmitter for time synchronization of the data. The receiver bandwidths (approximately 1.25 MHz) were reduced to increase sensitivity but were still wide enough to encompass signal doppler and anticipated flight transmitter frequency drift. The bandwidth provided some verification that the S193 frequency was within 0.7 MHz of the design 13.9 GHz. Because the pattern was expected to be smooth, based on preflight measurements, a narrow postdetection bandwidth of 100 Hz was used.

In addition to the five receivers for pattern measurement, the test setup included a sixth receiver for recording a cross-polarization power measurement, and two of the receivers used a parallel linear IF amplifier channel for recording the received pulse shape. The 5-millisecond transmitted pulse and the narrow-bandwidth receivers, using a video bandwidth of approximately 7.5 kHz, were sufficient to permit photographic recording of the pulse by the use of an oscilloscope. The cross-polarized antenna pattern cuts assisted in verifying S193 polarization switching by comparison with preflight antenna pattern characteristics.

Although scan motion was assumed in the data reduction, scan timing could be confirmed when the preflight patterns were assumed valid. Also, the pulse on-off times were measured from the received power recording to show the scatterometer preprogramed timing to be operating in a repeatable manner and,, to within the limits of the measurement, at proper preprogramed time-interval values.
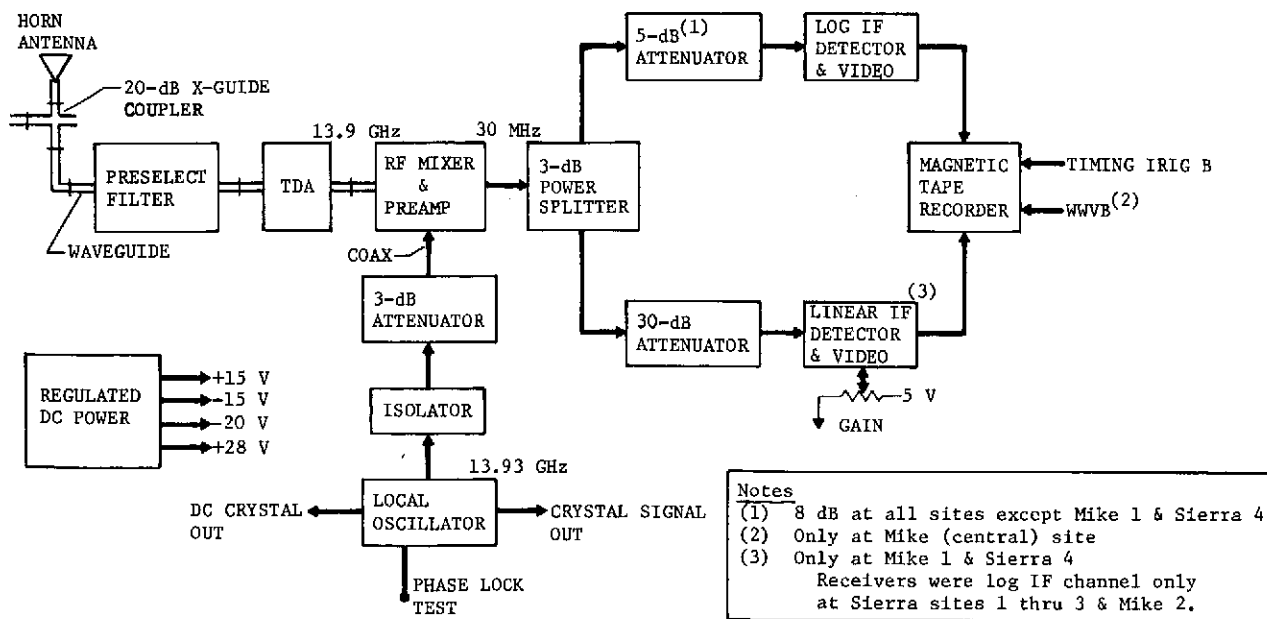
Figure A.III-2   13.9-GHz Microwave Receiver Block Diagram

3.   Partial Justifications:

a)   No antenna patterns were measured that included
     vehicle structure effects;

b)   Preflight antenna pattern questions were not
     resolved before launch;

c)   Verification of the antenna scans and pointing in
     zero gravity could only be simulated in preflight
     testing;

d)   Desirability of knowing transmitter power level
     and pulse shape at the surface of the earth;

e)   Diagnostic value of power, timing, and scan
     information should a failure occur (as it did);

f)   Special switching procedures were required to
     accomplish proper antenna polarization switching.

4. Successes/Accomplishments:

a) Verified scatterometer functioning in early flights;

b) Verified that scatterometer internal timing was within design expectations;

c) Provided information that the radiated power was decreased by approximately 12 dB during SL4;

d) Provided verification of scan motion;

e) Verified scatterometer pulse shape within expectations;

f) Provided pattern information for comparison with ground-measured patterns and the resolution of which pattern characteristics were valid;

g) Contributed inputs to the generation of antenna parameter values established for S193 data processing;

h) Assisted in verifying that proper S193 antenna polarization switching was being effected.

5. Problems:

a) S193 antenna scan motion was not linear nor completely repeatable, which meant that power measurements were not easily nor accurately positioned relative to the S193 antenna coordinates, degrading both pointing and pattern data;

b) Uncertainty of spacecraft location (point in space) and attitude compounded the ground-position and synchronization timing uncertainties to add to uncertainty of the relative positions of power measurements in the S193 antenna pattern;

c) Only a few directly overflown sites were surveyed, with only a limited number of data takes schedulable over these sites--data were thus limited;

d) Receivers were open breadboard designs and sites were open-field locations, thus weather was an important factor;

e) Failures of receivers deleted some cross-polarization power measurements;

f) Hoped-for precisions comparable to ground-based antenna measurements were not achieved;

g) Varactor chain multipliers from an L-band LO to K_u-band were trouble-prone in the field, requiring special power-supply corrections;

h) In-the-field absolute power-level calibrations of widely separated receivers were desired but only prelaboratory and postlaboratory calibrations, along with qualitative operation verification in the field, were possible, thereby reducing confidence in the absolute level of the data;

i) Postdata-take calibration revealed that a failed attenuator had resulted in saturation of the linear receivers on two data passes, causing a loss of some pulse shape data;

j) Many variables to be assimilated in the data reduction created computer programing problems and complexities not sufficiently resolved at this point to provide output pattern results.

B. STAPE*

The STAPE receiver site at NASA/WFC on the Virginia coastline could record received power versus time as Skylab passed overhead to provide single antenna pattern cuts. STAPE also has a transmitter that was used in a special antenna pointing test described in Section V of this appendix. Although antenna pattern (pulse power versus time) data were taken, orbit changes early in SL3 caused these pattern cuts to be made through insignificant sidelobes of the pattern. A high level of confidence in APEX capabilities resulted in a decision not to use the designed station mobility of the STAPE equipment to measure the beam width of the S193 antenna main beam.

The wide bandwidth (250 MHz) requirements imposed on the STAPE receiver due to the narrow altimeter pulse measurements

---

* Also see paragraph 5.1.2 of MSC-05528, Volume IV, and paragraphs 8.2.1 and 11.1.4.2 of MSC-05528, Volume V.

also meant that STAPE could, if required, back up APEX scatterometer pulse characteristics measurement. However, the ability to measure the scatterometer radiated pulse shape, RF frequency, sequence timing, and pulse repetition frequency was never used.

The STAPE transmitter was used in a special antenna pointing test of the radiometer section of the S193 instrument. This is described in Section V of this appendix.

IV. USE OF STATISTICAL PROCESSING TECHNIQUES TO DETERMINE CALIBRATION CONSTANTS

S193 radiometer gain was shown in the calibration data report* to be directly proportional to the difference between the radiometer calibration, R_C, and the radiometer baseline, R_B, voltages, and inversely proportional to the difference of the reference temperatures. Gain was stabilized by an automatic gain control (AGC) circuit with a 1-second time constant. Although the reference temperatures were found to be stable, individual values of R_C and R_B fluctuated about mean values. "Instantaneous" gain, calculated from consecutive values of R_C and R_B, showed similar fluctuations. When used to process the antenna (temperature) voltage, this "instantaneous" gain function increased the spread of the antenna temperature data. To ascertain the true uncertainty of radiometric temperature readings, statistical methods for smoothing the gain function were applied.

S193 radiometer data from lunar calibration were used to test the smoothing techniques. The deep-space target could be assumed to be homogeneous; variations in the measured radiometric temperature would be attributable to the S193 instrument, and the optimized processing algorithm, which yielded the least variation was determined.

In the first technique tested, the average of the last ten values of "instantaneous" gain was used to calculate antenna temperature, T_A. Both the running average gain, G_{RA}, and T_A were plotted with respect to time. The T_A points displayed moderate scatter about a mean curve that had the same shape as the G_{RA} curve. A long-term increasing trend was seen in both G_{RA} and T_A. This was in conflict with the assumed homogeneity of the target, and the conclusion was reached that the T_A calculations were biased by the gain algorithm.

---

* S193 Historical Logbook, S193 Vehicle 001, Vol 1A, Document No. 72 SD4234 Rev. A, 27 October 1972, General Electric Company, p 3-4.

Alternate Designation: S193 Calibration Data Report, Flight Hardware, Doc. No. 72 SD4207 Rev. D, 22 March 1973, Prime Unit 1A Volume 1A, SSO Contract NAS9-11195, General Electric.

The second technique involved fitting least-squares straight lines to the R_C and R_B data sets and obtaining a linear expression for $\left(R_C - R_B\right)$ versus time by subtraction. When this expression was used to calculate gain, a linear function with near zero slope resulted. T_A calculated using this straight-line gain, G_{SL}, was essentially constant. The standard deviation of T_A using this method was 1.10°K, whereas the G_{RA} method produced a T_A standard deviation of 1.79°K. The two favorable indications, constant temperature and low scatter, led to selection of the straight-line method as the preferred algorithm. Before June 1974, the running average method was used in the JSC production data processing; the straight-line technique was incorporated in all subsequent processing.

Gain stability was evaluated for selected modes in each mission by calculating the slope of the gain values for each mode. The straight-line slopes defined changes with time that were the same magnitude as the standard deviation of the data. A significance test was derived and applied to 26 cases from SL3 and SL4. In only four of the 26 cases were the slopes significant. In the other 22 cases, use of a single mean value would be as precise as the use of the straight-line function.

All of this work was documented in paragraph 12.5.1 of the interim sensor performance evaluation report, MSC-05528, Volume IV.

V. USE OF A GROUND-BASED TRANSMITTER FOR EVALUATION OF
    ANTENNA POINTING

Following the astronaut repair of the S193 antenna pitch
gimbal anomaly at the beginning of SL4, in which the pitch
gimbal was pinned at 0 degree (nadir or ZLV oriented), many
altimeter unlock indications occurred. These resulted from
weak return (echo) signal levels received by the S193. With
hindsight, they are known to have been the result of the missing
antenna feed cup during SL4 and the vehicle attitude with
respect to Z local vertical. However, before this was understood,
with the narrow preflight antenna beam assumed to still exist,
there was concern that the antenna might not have been properly
aligned with the ZLV to within 0.5 degree, which would have
required data passes with a planned biased alignment of the
Skylab attitude. Therefore, a measurements was conceived to
evaluate antenna pointing relative to vehicle orientation
provided by the SKYBET and field-of-view calculations. The
measurement used both the altimeter and radiometer portions
of the S193 sensor, as described in the following paragraphs.
Using the assumed preflight antenna pattern, the results
determined that the alignment was acceptable within the accuracy
of the measurement, approximately 0.3 degree. A recheck, using
the measured data and the SL4 antenna pattern associated with
the missing feed cup, was made after the pattern change was
confirmed for SL4, and it provided the same proper alignment
results.

A. Test Description

The test plan consisted of four parts:

1) A star check before and after the ZLV data pass to
    detect any gyro grift that might occur through the
    data pass;

2) An altimeter mode 1 operation over the North Pacific
    as the first data take of the pass to note whether
    S193 was aligned accurately enough not to abort.
    Return-pulse shape data were also obtained to
    determine the approximate magnitude of pointing
    offset from nadir.

3) A radiometer-only data-mode operation across a
    coastline to provide a land-sea interface measurement
    that would provide pointing information from the
    radiometric hot-cool edge in the scanned area.

4) A transmitter was set up inside the coastline on the
    flight path and radiometric data taken to record the
    "bright-spot" location on the ground.

A 13.9-GHz transmitter from the STAPE test setup was
relocated to be on the ground track near the sea coast. The S193
radiometer was operated in the cross-track contiguous mode
during its overpass of this transmitter (used on DOY 352, 1973,
EREP pass 68). SKYBET and EREP field-of-view data provided
predicted locations and times (GMT) for a ground track of the
center of the S193 field of view for this pass. This predicted
ground track was plotted on a 1:250,000-scale map. After
correction for known timing offsets in the reduced data, the
radiometer science data output was plotted at the appropriate
positions on the predicted ground track. The plot thus showed a
triangular scan progressing in the along-track direction on
which the observed radiometric temperatures were recorded in the
appropriate time cells. The temperatures showed a pattern of
instrument saturation and nonsaturation in the vicinity of the
transmitter.

To determine the pointing error from these data, a footprint
of the antenna pattern was made for both polarizations at the
level of sufficient gain to saturate the radiometer with the
given transmitter power. The boresight position on the antenna
footprint was placed over each data position on the predicted
ground track. If the transmitting site fell within the
saturation footprint, then the radiometric temperature at that
point on the ground track should have been saturated. By sliding
the footprint along the ground track, a consistent pattern of
position offsets was required to bring expected saturation and
nonsaturation points into correlation with the saturation
measurements indicated in the data. The results of this analysis
indicated the offsets of the actual pointing relative to the
SKYBET predicted boresight or center of the field of view. The
errors were primarily the uncertainty in the S193 antenna
patterns at the predicted saturation gain level.

The test setup consisted of a CW signal source, power
amplifier, standard gain horn, directional coupler, frequency
meter, and VSWR meter. A portable AC generator provided power
for equipment operation. Equipment setup for the test is shown
in Figure A.V-1. The transmitting antenna beam was adjusted
vertically and rotated approximately 45 degrees to the ground
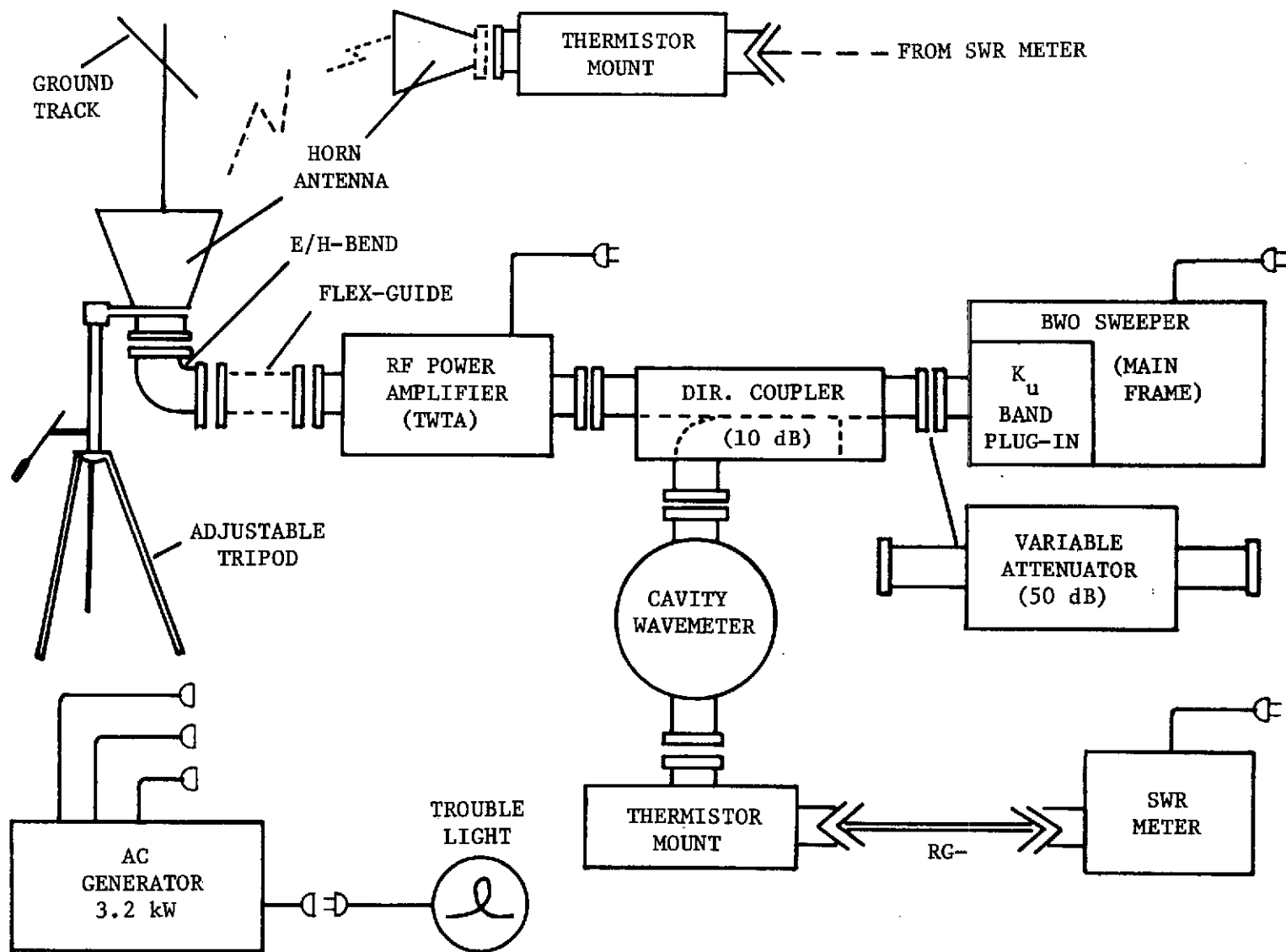track to provide power input for both S193 polarizations.

Figure A.V-1   Test Set Configuration for Ground-Site Transmission to S193 Radiometer

B. Test Results

1) The star check data, if taken, was not immediately available. Gyro drift problems had been noted during SL4 and aborts of the altimeter had been more numerous at the ends of data passes, suggesting an alignment drift error buildup during the data passes. Thus, vehicle alignment was assumed to have been good at the start of the pass.

2) The altimeter operated properly over the sea, indicating good alignment with nadir. The pulse shape data indicated a pointing error between S193 and true ZLV of less than 0.3 degree. (The method is discussed in paragraph 10.5 of MSC-05528, Volume V.)

3) The coastline was hidden in the measurement data, believed at first due to the power output of the transmitter located inland being too high, high enough to raise the measured sea brightness temperature through the preflight antenna side-lobe contributions. The angle of the ground track to the sea coast was such that roll angle data would have been expected but they were not easily extractable from the elevated temperatures. The elevated sea temperatures are now known to have been caused by the combination of the transmitter located just inland from the coast and the increased antenna pattern side-lobe levels that existed. These data thus confirm the SL4 antenna pattern change. However, the virtue of the coast location was lost, and this portion of the evaluation negated.

The transmitter site caused a number of ground spot radiometric measurements to saturate. These measurements were used to yield a pointing offset of S193 relative to the SKYBET sensor field-of-view locations of 0.28 ±0.3 degree in pitch forward. No significant or consistent roll offset could be determined in the data from this measurement, which led to the belief that 0 ±0.3 degree was a good estimate of the roll alignment offset at that time.

C. Test Conclusions

1) The misalignment, if any, of the S193 to ZLV as defined by SKYBET was not sufficient to warrant data passes with a bias offset to the nominally planned ZLV orientation.

2) Radiometric data from pass 68 (DOY 352) were
    artificially altered for engineering purposes
    and should not be used for scientific investigations.

3) Resultant radiometric data support the SL4 antenna
    pattern change.

VI. USE OF AIRCRAFT UNDERFLIGHT DATA AS A SECONDARY REFERENCE STANDARD TO ESTABLISH ABSOLUTE ACCURACY, DYNAMIC RANGE, AND SYSTEM LINEARITY

To establish a secondary reference source, a radiometer similar to the S193 instrument operating at 13.9 GHz was installed and operated in a NASA C130 aircraft. During selected Skylab EREP passes, a coordinated aircraft mission was planned over the same target. An effort was made to fly the aircraft mission at the same time as the Skylab pass but no later than 24 hours after it. In this way, data were acquired using similar instruments over similar targets and target conditions. Using the aircraft mounted sensor, comparison data were acquired over targets of varying but relatively uniform brightness temperatures. The aircraft data were analyzed to determine their usefulness in providing a means of evaluating Skylab S193 data for system accuracy, dynamic range, and linearity.

The method used to determine S193 radiometer accuracy consisted of calculating antenna temperatures, and determining a mean and standard deviation for the data from each instrument mode. If the standard deviation of S193 data was relatively small and, if antenna temperatures were repeatable for similar passes, S193 system accuracy could be estimated by comparison with aircraft data.

Dynamic range was evaluated by determining antenna mean temperatures from targets with large temperature differences, aircraft data again being used to verify Skylab data. A least-squares straight-line fit to the plot of sensor output voltage versus antenna temperature was extrapolated to the voltage limits of the instrument to determine the antenna temperature range of the instrument.

System linearity was primarily a function of antenna temperature (power) input versus instrument voltage output but was also affected by the instrument transfer function used to calculate T_A. Aircraft data were used to verify the correctness of the Skylab data used to evaluate linearity.

To establish a secondary reference for the scatterometer, the NASA aircraft also operated a 13.3-GHz scatterometer over some targets so that comparisons to its measurements could also be made. Unfortunately, the number of both radiometer and scatterometer aircraft underflight was limited and the targets selected for aircraft coverage did not meet sensor evaluation requirements.

Problems in the use of aircraft data are the difference in the ground-spot size sampled and differences in the angle at which both satellite and aircraft data were acquired, and the difference in the atmospheric perturbations affecting the two measurements. To reduce the first problem, the antenna pattern used for the satellite data was sometimes convolved with the variation in the target measured by the aircraft to establish comparison values or nearly homogeneous targets were used to avoid target variation. The second problem was inherent in sensor designs. The third problem was not as large a variable as it might have been because the moisture attentuation value at the frequencies used was not large. However, estimates or measurements of the humidity and/or standard atmosphere models were used to compensate the data for atmospheric effects. The aircraft data used must be regarded as potentially having bias errors as great as 5°K for the radiometer and several dB for the scatterometer, resulting from imperfections in the instruments and in data processing.